Impact of endoplasmic reticulum stress on lung tissue predisposition to pulmonary fibrosis and its development

Inauguraldissertation
zur Erlangung des Grades eines Doktors der Humanbiologie
des Fachbereichs Medizin
der Justus-Liebig-Universität Gießen

vorgelegt von
Irina Shalashova
Aus Almetjewsk, Russland

Gießen 2023

Aus dem Zentrum für interstitielle und seltene Lungenerkrankungen
Universitätsklinikum Gießen und Marburg GmbH

Betreuer: Prof. Dr. Andreas Günther
Gutachter: Prof. Dr. Saverio Bellusci

Prüfungsvorsitz: Prof. Dr. Gabriele A. Krombach
Prüfungsmitglied: Prof. Dr. Martin Berghoff

Tag der Disputation: 18.07.2023

Table of contents

Abbreviations

Bleo	Bleomycin
Dox	Doxycycline
ABCA3	ATP Binding Cassette Subfamily A Member 3
AECI	Alveolar epithelial cell type I
AECII	Alveolar epithelial cell type II
ATF4	Activating transcription factor 4
ATF6	Activating transcription factor 6
BiP	Immunoglobulin heavy-CCAAT/enhancer binding (EBP) homologouschain-bungibg protein
Bleo	Bleomycin
C_{cst}	Lung compliance
CD31	Cluster of differentiation 31, endothelial cells marker
CD45	Cluster of differentiation 45, hematopoietic cells marker
CK5	Cytokeratin 5
Col I	Collagen I
Col IV	Collagen IV
DAPI	4′,6′-diamidino-2-fenylindole
DMSO	Dimethyl sulfoxide
dNTP	Deoxynucleotide triphosphate

Dox	Doxycycline
eIF2	Eukaryotic translation initiation factor 2
EpCam	Epithelial cell adhesion molecule, epithelial cells marker
ER	Endoplasmic reticulum
ERAD	ER-associated protein degradation
ERS	Endoplasmic reticulum stress
FBS	Fetal bovine serum
FC	Flow cytometry
FITC	Fluorescein isothiocyanate
GOI	Gene of interest
H	Elastance
H&E	Hematoxylin and eosin
HSP70	Hot shock protein 70
IC	Inspiratory capacit
IF	Immunofluorescence
IPF	Idiopathic pulmonary fibrosis
IRE1	Inositol-requiring enzyme 1
MOI	Multiplicity of infection
NP	Nucleoprotein
PCLS	Precision cut lung slices

PCR	Polymerase chain reaction
PERK	Protein kinase RNA like ER kinase
PFU	Plaque forming units
PR8	Influenza virus A/PR/8/34 H1N1, mouse-adapted
RLU	Relative luciferase units
RNA	Ribonucleic acid
RT	Room temperature
rtTA	Reverse tetracycline-controlled activator protein
SDS	Sodium dodecyl sulphate
SDS-PAGE	SDS polyacrilamide gel electrophoresis
SFTPC	Surfactant protein C
SMA	Smooth muscle actin
SP-C	Surfactant protein C
TEMED	N,N,N′,N′-Tetramethyl-1-,-diaminomethane
TG	Thapsigargin
Trm	Thrombin
UPR	Unfolded protein response
WB	Western blotting
XBP1	X-box-binding protein 1

List of Figures

List of figures

1. Introduction

1.1. Idiopathic pulmonary fibrosis

1.1.1. Characteristics of idiopathic pulmonary fibrosis

Idiopathic pulmonary fibrosis (IPF) is a chronic lung disorder characterized by scarring of the lung tissue and a continuous decline in lung function. It belongs to a family of diffuse parenchymal lung diseases (DPLD) and is associated with the histopathologic and radiologic pattern of usual interstitial pneumonia (UIP) [Meltzer; Noble, 2008]. IPF occurs primarily in older adults and has a poor prognosis with a median survival time of 2–3 years [Kim et al., 2015a]. It can be considered in patients over 50 years old with unexplained chronic dyspnea, cough, bibasilar crackles, and finger clubbing. Additionally, IPF patients may have comorbid conditions including pulmonary hypertension, emphysema, sleep apnea, and obesity, which can complicate the diagnostic interpretation. In the latest S2K guideline, the diagnostic standards for IPF include clinical, radiological, and pathological assessments and exclusion of other known causes of DPLD (connective tissue disease, drug toxicity, environmental exposures, etc.) [Behr et al., 2021]. IPF progression is defined as increasing respiratory symptoms,

decline of pulmonary function tests, progressive fibrosis on high-resolution computed tomography (HRCT), and acute respiratory decline.

The natural history of IPF is variable. While some patients will develop symptoms gradually during the years, others can experience acute exacerbation (AE) and decline rapidly (Fig. 1). AE is defined as an acute, clinically significant respiratory deterioration resulting in acute lung injury (ALI) and histopathological diffuse alveolar damage. The median survival of IPF patients experiencing an acute exacerbation is approximately 3 to 4 months, annually incidence is ~13-15% of IPF patients, and the short-term mortality is ~50% [Ryerson et al., 2015]. Although the cause of AE is still unclear, several possible causes were proposed. Herold L. Collard and colleagues suggested three possible reasons for AE [Collard et al., 2007]: 1. pathobiological manifestation of the primary disease process, 2. other undiagnosed conditions (e.g., viral infection, aspiration), and 3. acute direct stress to the lung, with a subsequent acceleration of the already abnormal intrinsic fibroproliferative process of IPF. Analysis of pan-viral arrays, multiplex PCR, and assessment of post-mortem samples from patients who died from AE showed the presence of

viruses in some, but not all patients who experienced AE [Oda et al., 2014; Konishi et al., 2009; Ushiki et al., 2014]. Other interesting results came from a post hoc analysis of the placebo arms from three clinical trials. It showed that AE of IPF occurred only in those subjects that have not received anti-acid therapy. This could be explained by the fact that anti-acid treatment reduces the potential for microaspiration-related lung injury [Lee et al., 2013]. Additionally, it was reported that patients after surgical lung biopsy and bronchoscopy have a higher risk of AE development [Bando et al., 2009; Ghatol et al., 2012; Sakamoto et al., 2012]. Thus, it seems that IPF lungs are very vulnerable to additional stress, which can be caused by intrinsic acceleration of the underlying fibrotic condition and response to occult external events.

1.1.2. IPF etiology

Although the etiology is unknown, several potential risk factors, like smoking [Baumgartner et al., 1997], environmental exposure [Miyake et al., 2005; Hubbard et al., 1996; Hubbard et al., 2000], microbial agents [Qiao et al., 2009; Tang et al., 2003; Kuwano et al., 1997; Egan et al., 1995; Irving et al., 1993], gastroesophageal reflux [Gribbin et al., 2009] were described. Moreover, it was also shown that genetic susceptibility plays a role in IPF development. For example, familial forms of lung fibrosis are associated with

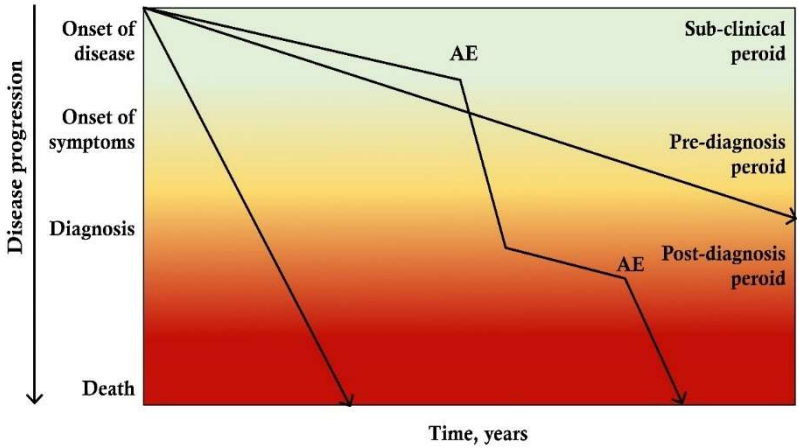

Figure 1. Schematic representation of potential clinical courses of IPF

The disease progression leading to patient's death may be rapid, slow, or mixed with acute exacerbations (AE) associated with acute decline. Adapted from [Ley et al., 2011].

mutations in surfactant proteins [Campo et al., 2014; Lawson et al., 2004; Nogee et al., 2001], mutations in genes of the telomere protein complex [Alder et al., 2008; Molina-Molina et al., 2018] and MUC5B promoter polymorphism [Seibold et al., 2011]. Nine percent of the European population carry the common variant rs35705950 in the promoter region of MUC5B. This variant is considered to be the strongest risk factor for IPF development (30–35%) and predicts asymptomatic mild fibrosis development [Seibold et al., 2011; Hunninghake et al., 2013; Peljto et al., 2013]. Interestingly, there is also evidence from animal experiments that some mutations (e.g. Δexon-4 SFTPC) develop spontaneous lung fibrosis [Bridges et al., 2003], whereas others, (e.g. L188Q SFTPC) only develop the fibrosis when exposed to the second hit, like a low dose of bleomycin [Lawson et al., 2011]. Besides, in several studies, IPF-associated genetic loci were found to be connected to the different cell mechanisms like a host-defense response [Noth et al., 2013; Fingerlin et al., 2013; Seibold et al., 2011] and cell-cell senescence [Minagawa et al., 2011].

1.1.3. Histopathological changes in IPF

The histopathological pattern of IPF is known as usual interstitial pneumonia (UIP). UIP is characterized by

changes in the lung architecture with patchy areas of parenchymal fibrosis. It markedly affects the subpleural and paraseptal parenchyma and is featured by alveolar septal thickening and areas of collagen deposition. Often in the lungs of patients with UIP, cystic structures known as microscopic honeycombs can be observed (Fig. 2C). They are frequently lined by bronchiolized epithelium and filled with mucus and inflammatory cells. The scarred lung tissue contains characteristic structures known as fibroblast foci containing loose extracellular matrix molecules and proliferating fibroblasts and myofibroblasts (Fig. 2 A, B) [Meltzer; Noble, 2008].

Inflammation is usually mild and consists of a patchy interstitial infiltrate of lymphocytes and plasma cells associated with hyperplasia of alveolar epithelial cells type 2 (AECII) and bronchiolar epithelium [Raghu et al., 2011].

An extensive amount of research has shown that all lung compartments are involved in or affected by IPF. The initial epithelial injury affects all cellular and histological compartments and leads to heterogeneous histopathological changes (Fig 2).

1.1.4. Pathogenesis of IPF

According to the current paradigm of IPF pathogenesis, there is a continuous epithelial injury in the IPF lung that is accompanied by an aberrant repair process. As mentioned in chapter 1.1.1., several factors can cause cell injury, and they can be direct (radiation, drugs) or indirect (gene mutations).

Under normal conditions, tissue damage leads to inflammation followed by repair. These processes serve to restore lung architecture and function. However, in IPF lungs, this process is impaired because of either constant injury or disrupted repair, or a combination of both [Coward et al., 2010].

For instance, in the case of some surfactant and surfactant production-related gene mutations, at least two events can be a cause of alveolar epithelial injury. The first one is related to the surfactant's function and manifests on a tissue level. A lack of surfactant leads to an increase in alveolar surface tension, inducing alveolar collapse and AECI and AECII injury. The second event is intracellular. Due to their mutations, surfactant proteins cannot be correctly folded, and they accumulate in the endoplasmic reticulum, which results in endoplasmic reticulum stress

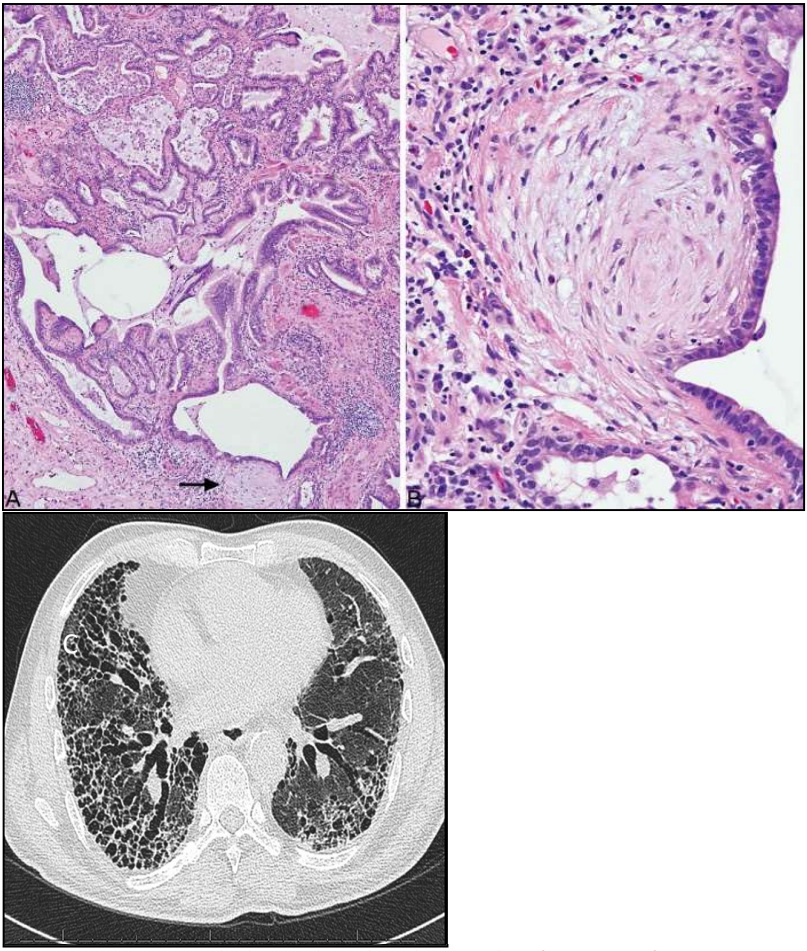

Figure 2. Histopathological and radiographic features of UIP

A. *Low magnification showing prominent fibroblast focus (arrow) in an area of typical honeycomb change.* ***B.*** *Higher magnification of fibroblast focus showing low columnar epithelium covering the characteristic spindle cells.* ***C.*** *An HRCT of the lungs showing reticulation, traction bronchiectasis, honeycombing, "in a sub-pleural distribution. HRCT, high resolution computed tomography; UIP, usual interstitial pneumonia.Pictures adapted from Koegelenberg et al. (Koegelenberg et al. 2016) and Thoracic Key (https://thoracickey.com/).*

(ERS) and the unfolded protein response (UPR) pathway activation.

Prolonged ER stress can lead to AECII apoptosis induction [Bridges et al., 2003; Thomas et al., 2002; Young et al., 2008]. Thus, continuous epithelial injury and cell death become so extensive and overwhelming over time, that the repair capacity of the epithelium is exhausted, causing irreversible pathological tissue changes, which affect the lung structure-function relationship.

Besides epithelial cells, other cell types like macrophages and fibroblasts are involved in a reactive manner in IPF pathogenesis. Following epithelial injury in healthy tissue, macrophages are first activated towards a pro-inflammatory M1 state. Once inflammation recedes, M2 macrophages are activated for wound repair [Venosa et al., 2016; Wynn; Vannella, 2016; Allden et al., 2019]. After the repair process is finished, the M2 macrophages are cleared through apoptosis. In IPF, due to the constant epithelial injury, macrophage recruitment and activation continue and most likely, become deregulated.

Both epithelial cells and macrophages secret mediators promoting fibroblast recruitment and proliferation [Murray et al., 2011; Yang et al., 2013]. Fibroblasts, in return, produce extracellular matrix (ECM) proteins like collagen and fibronectin, thus increasing scar tissue in the lungs [Zhang et al., 1994; Phan, 2002]. Moreover, it was reported that there is a positive feedback loop between fibroblasts and aberrant ECM in IPF lung tissue resulting in more fibroblast production and enhancing pathological ECM remodeling [Parker et al., 2014]. Furthermore, epithelial cells also can produce ECM after they undergo epithelial-mesenchymal transition (EMT). EMT is a biological process that occurs during embryonic development, injury, carcinogenesis, and

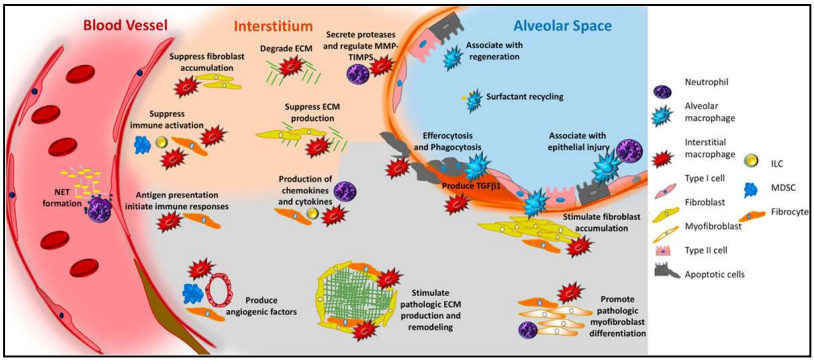

Figure 3. Unifying schematic of mechanisms of idiopathic pulmonary fibrosis

Adapted from (Desai et al. 2018)

fibrosis. During this transition, epithelial cells lose contact adhesions and apical-basal polarity, change their cytoskeleton, and alter their shape. They also acquire some mesenchymal features of invasion, migration, and, as mentioned before, production of ECM [Acloque et al., 2009; Pain et al., 2014; Bucala et al., 1994; Hinz et al., 2007; Maharaj et al., 2013].

On a molecular level, multiple reports showed that in IPF there is increased production of reactive oxygen species and activation of autophagy, UPR, cell proliferation and cell senescence [Hawkins et al., 2015]. Also, several development pathways such as TGFβ and Wnt are activated and play a central role in fibrosis development and progression. TGFβ ligands are produced by various cell types (immune cells, epithelial cells, and fibroblasts). Their activation promotes collagen synthesis, fibroblast proliferation, and differentiation into myofibroblasts [Scotton; Chambers, 2007], and induces epithelial apoptosis [Yoo et al., 2003; Hagimoto et al., 2002]. Additionally, TGFβ activation can upregulate angiogenic factors like connective tissue growth factor (CTGF), vascular endothelial growth factor (VEGF) [Sánchez-Elsner et al., 2001], and expression, secretion, and activation of matrix metalloproteinases (MMP) [Derynck et

al., 2001; Ishikawa et al., 2010; Hsieh et al., 2010].

At the same time, it was reported that the Wnt pathway is activated in bronchiolar and alveolar epithelial cells type II (AECII) of IPF patients, as well as in AECII isolated from the fibrotic lungs from bleomycin treated mice [Königshoff et al., 2008; Königshoff et al., 2009; Königshoff; Eickelberg, 2010]. Additionally, Chilosi et al. showed that β-catenin, the central transducer of canonical Wnt signaling, translocates from the membrane to the nucleus of fibroblasts in fibrotic foci in the lung tissue of IPF patients [Chilosi et al., 2003]. It suggests that the Wnt pathway is activated not only in epithelial cells but also in fibroblasts in IPF lungs, which probably can be expected since Wnt signaling is essential for cell proliferation and differentiation. Moreover, the evidence shows a strong interaction between Wnt and TGFβ pathways [Xu et al., 2017; Vallée et al., 2017; Tian et al., 2013], and the α3β1 integrin-dependent TGFβ activated interaction between Smad2 and β-catenin was reported to be important for EMT [Kim et al., 2009]. Thus, IPF shows a complex pathogenesis, which involves the activation and communication between different pathways and cell types.

1.1.5. Role of virus infections in IPF

Though the precise role of virus infections in IPF

pathogenesis is unknown, it is widely accepted that they may have a possible impact on disease development and progression. On one side, chronic infections caused by viruses like hepatitis C, Transfusion Transmitted virus, and Epstein-Barr virus were linked to the pathogenesis of lung fibrosis [Naik; Moore, 2010; Wootton et al., 2011] and are considered to lead to susceptibility or predisposition to lung fibrosis. On the other side, respiratory viruses like influenza (IV) or rhinovirus may provoke an acute decline in lung function in IPF patients and lead to acute exacerbations of the disease (AE) [Nguyen-Van-Tam et al., 2010]. In recent publications, human herpesvirus and influenza A have been reported as the most prominent viruses in the AE-IPF group by testing viral sequences from nasopharyngeal swabs of IPF patients [Weng et al., 2019]. Interestingly, AE has also been reported after influenza A vaccination [Umeda et al., 2010]. In several animal studies, IV-infected mice were also shown to develop typical pulmonary fibrosis during the restoration period, with promoted collagen deposition via αvβ6 integrin-mediated TGFβ activation [Qiao et al., 2009; Jolly et al., 2014].

Influenza virus (IV) is an enveloped negative-strand RNA virus with a segmented genome containing seven to

eight gene segments [Fields et al., 2001]. There are three subtypes: influenza A, B, and C. They differ in pathogenicity and host range. The majority of IV B and C are isolated from humans, and IV A infects a variety of animals, including humans. IV A viruses have been further subdivided by antigenic characterization of the hemagglutinin (HA) and neuraminidase (NA) surface glycoproteins that project from the virion. Influenza A is one of the main causes of seasonal epidemics and has a high mutation rate.

IV preferably infects and replicates in the respiratory epithelium, which results in lung inflammation caused by the immune response. Influenza is associated with frequent induction of acute respiratory distress syndrome (ARDS), and about 30–40% of the hospitalized patients with laboratory-confirmed influenza are diagnosed with acute pneumonia. Moreover, IV can affect other organs (heart, brain) and the course of different respiratory diseases [Koul et al., 2017; Weng et al., 2019]

1.1.6. IPF treatment

Despite the therapeutic advances in the past few years, IPF remains an incurable disease. The currently available treatment is focused on symptom relief and slowing down disease progression. Two common drugs that are in use are

nintedanib and pirfenidone. Pirfenidone showed anti-inflammatory, anti-oxidant, and anti-fibrotic effects in animal studies and clinical trials [Taniguchi et al., 2010; Azuma et al., 2005]. It regulates the expression of TGF-β and inhibits fibroblast and collagen synthesis. However, the precise mechanism of action remains unknown.

Nintedanib inhibits tyrosine kinase receptors, including PDGF receptors α and β, VEGF receptors 1, 2, and 3, and FGF receptors 1, 2, and 3 [Hilberg et al., 2008]. Nintedanib demonstrated the ability to prevent the development of lung fibrosis in the bleomycin treated mice [Chaudhary et al., 2007], and it successfully reduced the rate of functional loss in phase 2 and 3 clinical trials [Richeldi et al., 2011; Richeldi et al., 2014; Ryerson et al., 2019].

Both treatments prolonged the patient's survival in clinical trials, but neither stopped nor reversed disease progression [Richeldi et al., 2011; Costabel et al., 2015; Albera et al., 2016]. Thus, the only curative therapeutic intervention at the moment is lung transplantation, but this is limited to a small minority of patients due to limited organ availability and the fact that most patients do not fulfill the transplantation criteria [Kapnadak; Raghu, 2021; Laporta Hernandez et al., 2018].

Besides already approved IPF treatment, there are several therapies in the experimental phase. Among them is cell transplantation therapy, where healthy epithelial lung cells are delivered into the lungs to replace the sick ones and restore the normal tissue regeneration process. For this purpose, a variety of cells can be used, including lung AEC II [Serrano-Mollar et al., 2007], mixed lung epithelial cells [Tanaka et al., 2014], and different stem cell types, including lung stem cells, induced pluripotent stem cells (iPSCs), embryonic stem cells (ESCs), mesenchymal stem cells (MSCs), and adipose stem cells (ADSCs) [Banerjee et al., 2012; Zhou et al., 2014; Lee et al., 2014]. From all, AECII is probably more effective and safer since they seem to have the lowest tumor-forming potential. Several animal experiments showed promising results of such therapy [Serrano-Mollar et al., 2007; Guillamat-Prats et al., 2014]. Nevertheless, this method has to be further developed and optimized before entering clinical testing in the IPF patients.

There are also chemical agents going through different phases of clinical trials, such as N-acetylcysteine (NCT02707640*), PRM-151 (NCT01254409*), valganciclovir (NCT02871401*), tipelukast (NCT02503657*), fentanyl citrate (NCT03018756*). They have various targets and can be used for patients with different clinical features. Fibrosis treatment evolution has a long history with many promising drugs and treatments, as well as with many failures (Fig. 4). Nevertheless, the search for a curative treatment is still going on.

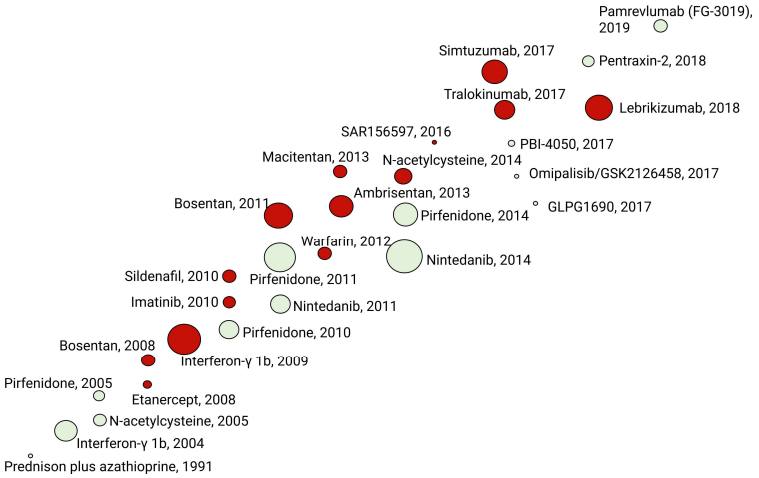

Figure 4. Clinical trials of IPF therapy performed in the past three decade.

Circle sizes are an approximate representation of the sample sizes of the clinical trials. Green: study ended with a positive outcome; red: study ended with a negative outcome. Adapted and modified from (Somogyi et al. 2019).

1.1.7. Bleomycin model of pulmonary fibrosis

Though there are several animal models of lung fibrosis (radiation, silica, asbestos-induced), bleomycin (BLM) induced fibrosis is considered as the golden standard in preclinical testing [Moore; Hogaboam, 2008]. BLM was initially identified as a pro-fibrotic agent when patients developed fibrosis as a side effect after intravenous administration for lymphoma treatment. The mechanism of action is based on the induction of double and single DNA breaks that interrupt the cell cycle, followed by apoptosis. Interestingly, different tissue types produce BLM hydrolase, an enzyme that inactivates the drug, but its expression is low in the lungs. Thus, the lung is more susceptible to BLM-induced fibrosis. Nevertheless, BLM causes systemic sclerosis when administered intravenously. To avoid the systemic effects in the mouse model of lung fibrosis, BLM can be administered intratracheally. After the drug is applied, mice rapidly develop fibrosis, with massive cell death on days 1-3, followed by an inflammatory response between days 3-9. A fibrotic phase is observed between day 10 till day 20 characterized by fibroblast proliferation and ECM deposition. Finally, a resolution phase appears between days 21-28 [Tashiro et al., 2017; Walters; Kleeberger, 2008;

Moeller et al., 2008]. Unlike human IPF, which takes years or even decades to develop, BLM-induced fibrosis is very fast, self-limited, and reversible. There are also differences between IPF and the BLM model in histopathology: lack of honeycomb cyst formation and bronchiolization and central localization of the fibrotic lesions. Nevertheless, the BLM model is the best-characterized model and is widely accepted as clinically relevant [Liu et al., 2017].

1.2. Endoplasmic reticulum stress and UPR

1.2.1. Endoplasmic reticulum function and ER stress

The endoplasmic reticulum (ER) is an organelle that is responsible for several functions. The first is associated with protein synthesis, folding, maturation, quality control, and secretion [Stefan et al., 2011]. The purpose of protein processing in the ER is the production of active, correctly folded and functioning proteins. To reach this goal, proteins usually maturate via post-translational modifications, such as signal sequence cleavage, N-linked glycosylation, isomerization or reduction of disulfide bonds and isomerization of proline or lipid conjugation [Braakman; Bulleid, 2011; Hebert; Molinari, 2007]. Defects in these processes constantly happen in living cells, and if not strongly controlled, they can lead to cellular damage and death. This

control is handled by the quality control machinery that detects misfolded or damaged proteins and ensures their degradation by ER-associated degradation machinery (ERAD) [Meusser et al., 2005].

The second ER function is related to lipid synthesis, lipid droplet/vesicle formation, and fat accumulation for energy storage [Yen et al., 2008]. To support this function, ER contains cholesterol sensors ensuring cholesterol homeostasis [Brown; Goldstein, 1999].

The third important function of the ER is the transport of proteins and lipids. As the process of synthesis is constant, providing non-stop delivery of these molecules to the place of use and prevention of their accumulation in ER are extremely important. It can be done by the coat protein complex II (COPII) vesicle transport, termed chylomicron transport vesicles or accumulating in lipid droplets [Amodio et al., 2017; Siddiqi et al., 2010].

Thus, the ER has many important functions, and its homeostasis is vital for cellular homeostasis. Different factors may affect it. Extrinsic factors include temperature, reactive oxygen species, or chemicals like tunicamycin (inhibitor of N-linked glycosylation) and thapsigargin (non-competitive inhibitor of the sarco/endoplasmic reticulum Ca^{2+} ATPase)

[Lepock, 2005; Schultz; Oroszlan, 1979; Sehgal et al., 2017; Zeeshan et al., 2016]. Intrinsic factors are represented by activation of oncogenes like Myc, RAS, and BRAF [Nagy et al., 2013; Qing et al., 2012; Horiguchi et al., 2012; Croft et al., 2014; Corazzari et al., 2015]. When cells are affected by one or more of these factors, regular protein synthesis and transport is disturbed, leading to the accumulation of unfolded and misfolded proteins in ER and induction of ER stress.

1.2.2. Unfolded protein response

When cells experience ER stress, they activate the unfolded protein response (UPR), which enables them to cope with misfolded protein accumulation. ER stress is detected via the three transmembrane sensors IRE1/XBP1, ATF6, and PERK/ATF4, each of which has its own pathway of response and downstream targets (Fig. 5). There is a constant cross-talk amongst these three pathways, and its outcome most probably depends on the inducing stimulus [Guo et al., 2014; Tsuru et al., 2016; Yoshida et al., 2001; Yoshida et al., 2009]. Unfortunately, this complicates the understanding of the precise mechanism of ER stress. UPR activation has three main aims: 1) producing new chaperons to increase protein folding capacity, 2) translational

attenuation to prevent newly synthesized proteins accumulation in the ER, 3) activation of ER-associated degradation (ERAD) to remove misfolded proteins and restore homeostasis.

1.2.2.1. IRE1/XBP1 pathway

In humans, there are two paralogues of IRE1, IRE1α and β [Tirasophon et al., 1998; Iwawaki et al., 2001]. IRE1α is ubiquitously expressed, and its genetic knockout is embryonically lethal due to growth retardation and

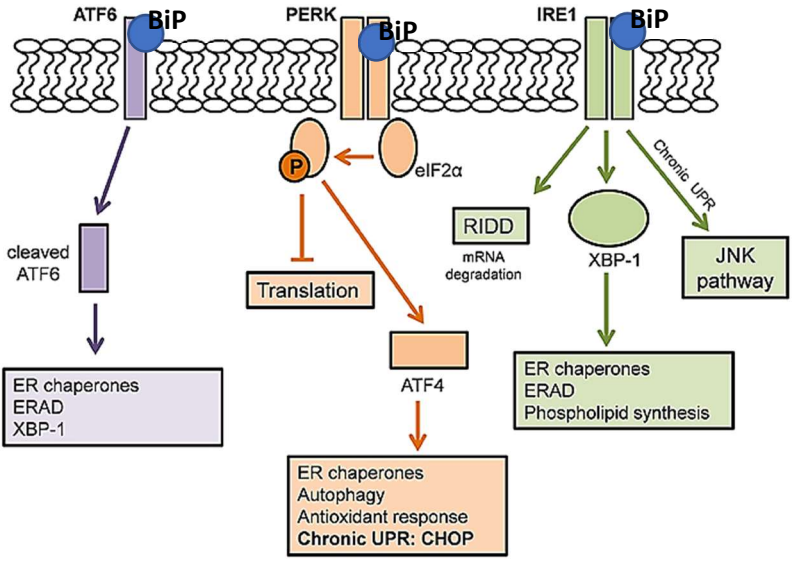

Figure 5. Overview on the three arms of the UPR

Modified from Emma R. Perri et al, Cell Dev. Biol., 2015 (Perri et al.

defects in liver organogenesis and placenta development [Iwawaki et al., 2009]. Expression of IREβ, on the other hand, is restricted mainly to the gastrointestinal tract and the pulmonary mucosal epithelium, and its knockout leads to severe colitis [Bertolotti et al., 2001]. The functional differences of IRE1α and IRE1β are explained by different substrate specificities of their RNAse domain. IRE1α has higher activity in XBP1 splicing and IRE1β in 28sRNA cleavage [Imagawa et al., 2008]. Since IRE1α plays the most crucial role in ER stress, all further descriptions will refer to this paralogue.

Under normal conditions, IRE1 presents as a dimer, and its activity is blocked by binding to the ATPase domain of chaperon GRP78/BiP. When unfolded proteins appear in ER, they bind to the active site of the BiP substrate-binding domain that leads to BiP-IRE1 dissociation and IRE1 oligomerization [Kopp et al., 2018]. Oligomerized IRE1 undergoes self-phosphorylation, which activates its nuclease activity [Prischi et al., 2014] and JNK pathway activation by recruiting tumor necrosis factor receptor-associated factor 2 (TRAF2) [Urano et al., 2000]. The RNAse domain of IRE1 can digest different mRNA and reduce new protein synthesis by a mechanism called regulated IRE1-dependent mRNA

decay (RIDD) [Hollien; Weissman, 2006]. Also, the nuclease activity of IRE1 can support alternative splicing. The most studied example is the IRE1 cleavage of the two introns from X-box binding protein 1 (XBP1) mRNA in a spliceosome-independent manner. It leads to a frameshift and translation of a nuclear transcription factor XBP1s containing C-terminal transactivation domain that does not exist in the unspliced form [Yoshida et al., 2001; Calfon et al., 2002]. During ER stress, XBP1s binds to a cis-acting unfolded protein response element (UPRE) [Yamamoto et al., 2004]. This binding activates the expression of chaperons (BiP, p58IPK, ERdj4, PDI-P5, and HEDJ) and components of the ER-associated degradation pathway (ERAD) such as EDEM, HRD1, Derlin-2, and Derlin-3 to relieve ER stress and restore homeostasis [Lee et al., 2003; Travers et al., 2000; Oda et al., 2006].

Besides UPR, the IRE1-XBP1 pathway also plays an essential role in very-low-density lipoprotein assembly, lipid biosynthesis and controls rough ER volume enlargement to increase ER functionality [Sriburi et al., 2004; Wang et al., 2012]. It regulates glucose metabolism, insulin, and glucagon secretion [Lee et al., 2011; Park et al., 2014; Zhou et al., 2011; Akiyama et al., 2013]. It was reported that IRE1 signaling is

involved in insulin resistance and obesity through JNK activation which can act in four different ways: 1. inhibition of insulin receptors phosphorylation [Aguirre et al., 2000; Sabio et al., 2010b], 2. promotion of metabolic inflammation [Solinas et al., 2007; Han et al., 2012], 3. promotion of metabolic efficiency and adiposity via inhibition of the TSH-thyroid hormone axis [Sabio et al., 2010a], and 4. negative regulation of the PPARα-FGF21 axis [Vernia et al., 2014]. IRE1 also is involved in the differentiation and maturation of plasma cells, gastric zymogenic cells, Paneth cells, and adiposities [Acosta-Alvear et al., 2007; Lee et al., 2005; Sha et al., 2009; Reimold et al., 2001; Todd et al., 2009; Huh et al., 2010]. Moreover, the IRE1-XBP1 pathway can regulate apoptosis, and its role depends on cell type. For instance, XBP1 plays a protective role in hematopoietic cells and fibroblasts treated with cyclopiazonic acid [Allagnat et al., 2010; Kurata et al., 2011], but induces cell death in pancreatic beta-cells and endothelial cells [Allagnat et al., 2010; Zeng et al., 2009].

Unspliced XBP1 RNA can, as well, be translated and form XBP1u protein, which has different functions than XBP1s. During the recovery stage after ER stress, XBP1u acts as a negative regulator of XBP1s and ATF6 [Yoshida et

al., 2006; Yoshida et al., 2009]. On the other hand, under normal conditions, it is associated with the ribosomal tunnel and reduces the speed of translation [Yanagitani et al., 2011].

1.2.2.2. ATF6 pathway

ATF6 is another sensor of ER stress. It has two paralogs ATF6α and ATF6β, which seem to have an overlap in functions, but the nature of their interaction is not clear [Yamamoto et al., 2007; Thuerauf et al., 2007]. Since ATF6α plays a more significant role, all further discussion will be related to this paralog. Non-active ATF6 (ATF6p90) exists as a type II transmembrane protein with the C-terminal binding to BiP and being located in the ER lumen, while the N-terminus faces the cytosol. When misfolded proteins accumulate in the ER, BiP dissociates from ATF6. This dissociation unmasks two Golgi-localization sequences, and ATF6p90 traffics to the Golgi by COPII vesicles for processing [Shen et al., 2005; Shen et al., 2002]. For successful transport, ATF6 needs to be underglycosylated (Hong et al. 2004) and oligomerized by protein disulfide isomerase A5 (PDIA5) [Nadanaka et al., 2007; Nadanaka et al., 2006; Higa et al., 2014]. When ATF6p90 arrives in Golgi, S1P and S2P proteases remove the luminal and transmembrane anchors to form transcription factor

ATF6p50. This transcriptional factor contains a basic leucine zipper (bZIP) DNA binding domain, transcriptional activation domains, and nuclear localization signals. When localized in the nucleus, ATF6p50 binds to cis-acting elements ERSE and ERSEII [Morishima et al., 2011; Yamamoto et al., 2004; Yoshida et al., 1998]. This binding activates transcription of chaperons GRP94, GRP78/BiP, and calreticulin [Mao et al., 2006; Haze et al., 1999; Blackwood et al., 2019; Yoshida et al., 1998; Yamamoto et al., 2007]. Other known targets of ATF6 are ER degradation-enhancing α-mannosidase-like protein 1 (EDEM1) and protein disulfide isomerase associated 6 (PDIA6), which can promote correct protein folding as well as degradation of misfolded proteins [Vekich et al., 2012]. EDEM plays an essential role in ERAD by pulling misfolded proteins out of the calnexin cycle for further degradation [Oda et al., 2003; Molinari et al., 2003]. Thus, ATF6p50 can control protein folding as well as the protein degradation process. Another significant function of ATF6 during ER stress and cell differentiation is regulation of ER expansion together with XBP1 or in XBP1 independent manner [Bommiasamy et al., 2009; Maiuolo et al., 2011]. During prolonged and exaggerated ER stress, ATF6p50 can induce apoptosis

through upregulation of CHOP and the mitochondrial apoptotic pathway [Huang et al., 2018].

During ER stress, UPR can also activate the autophagy pathway. One way to achieve it is by ATF6p50 binding to the DAPK1 promoter, which results in autophagosome formation followed by autophagic cell death [Gade et al., 2012; Inbal et al., 2002; Zalckvar et al., 2009; Eisenberg-Lerner; Kimchi, 2012]. Another way is by GRP78 suppressing the mTOR pathway with the help of AMPK and TSC2 [Cook et al., 2012]. UPR and autophagy are closely related, functioning together to eliminate unfolded/misfolded proteins or dysfunctional organelles.

Besides UPR, ATF6 is crucial in a variety of physiological processes in different types of cells. It was reported that ATF6 expression is essential for stem cell function. To demonstrate this, Kroeger et al. used primary human fibroblast cells to generate iPSCs and showed that specific activation of the ATF6 pathway led to pluripotency suppression and cell differentiation. Interestingly, the cells with activated ATF6 were directed towards mesodermal fate and developed into functional vascular endothelial cells. One of the proposed mechanisms by which ATF6 may affect cell pluripotency was ER expansion and changes in protein

homeostasis [Kroeger et al., 2018]. In another paper, mouse embryonic stem cells were used to demonstrate ATF6 binding to the myocardin promoter resulting in its activation, which leads to upregulation of smooth muscle lineage markers [Wang et al., 2015a]. Additionally, it was reported that knockout of both ATF6 α and β in mice leads to embryonic lethality, which also confirms an essential role of ATF6 in early development [Yamamoto et al., 2007].

ATF6 is also crucial for chondrogenesis and osteogenesis. It positively regulates chondrocyte growth and differentiation and endochondral bone formation in a Runx2-dependent manner [Xiong et al., 2015; Jang et al., 2012]. Xiong et al. also demonstrated that ATF6 overexpression leads to the hypertrophy and mineralization of chondrocytes, most likely through osteocalcin upregulation, which is recognized as a marker of cartilage pathological changes [Xiong et al., 2015]. Additionally, several studies suggested that ATF6 is essential for adipogenesis and lipogenesis [Bou et al., 2017; Lowe et al., 2012; Zeng et al., 2004].

1.2.2.3. PERK pathway

The third transmembrane ER stress sensor is the protein kinase RNA-activated (PKR)-like ER kinase

(PERK). Like IRE1, PERK is ubiquitously expressed and has a cytoplasmic kinase domain and an ER luminal domain bound to BiP. During ER stress, BiP detaches from PERK, and it leads to PERK oligomerization, trans-autophosphorylation, and activation. Activated PERK phosphorylates the α subunit of eukaryotic translation initiation factor 2 (eIF2α) [Shi et al., 1998; Harding et al., 1999]. eIF2 acts as a heterotrimeric GTPase (eIF2α/β/γ) and recruits the initiator methionyl tRNA (Met-tRNAi) to form eIF2-GTP-Met-tRNAi ternary complex (TC). TC binds to the 40S ribosomal subunit and then attaches to the mRNA [Hinnebusch, 2014; Jackson et al., 2010]. After the complex finds the AUG start codon, eIF2 hydrolases GTP and dissociates. eIF2 is reactivated by exchanging GDP to GTP and binds again to a new Met-tRNAi. For binding and reactivation, eIF2 needs the guanine nucleotide exchange factor eIF2B. When PERK phosphorylates eIF2α, it inhibits eIF2B activity, leads to translational attenuation, and alleviates ER protein overload [Bertolotti et al., 2000; Bogorad et al., 2017; Kulalert et al., 2017; Harding et al., 2000b]. Interestingly, some transcripts are translated more efficiently after elF2 phosphorylation. The best-studied example is the activating transcription factor 4 (ATF4),

which contains short upstream open reading frames (uORFs). PERK translational attenuation initiates a shift toward uORF, which leads to the synthesis of ATF4 protein [Harding et al., 2000a; Vattem; Wek, 2004]. Elevated ATF4 signaling can result in ATP depletion, oxidative stress, and cell death [Hiramatsu et al., 2014]. The PERK/ATF4 pathway also regulates apoptosis through upregulation of C/EBP-homologous (CHOP) protein. CHOP can act either through the mitochondria-dependent pathway (inhibition BCL2 proteins family, upregulation of BH-3 only proteins, release cytochrome C, activation of the caspase cascade) [McCullough et al., 2001; Puthalakath et al., 2007; Bromati et al., 2011] or through the death-receptor pathway (DR4, DR5 genes expression, caspase 8 mediated cascade) [Chen et al., 2016; Lu et al., 2014; Yamaguchi; Wang, 2004]. Additionally, CHOP can regulate apoptosis by promoting the expression of ER oxidoreductin-1α (ERO1α). In physiological conditions, ERO1 α catalyzes the oxidation of protein disulfide isomerase (PDI), but in conditions of prolonged stress this can result in the production of H_2O_2 in the ER, its leakage into the cytoplasm, production of ROS, and consecutive apoptosis [Rao et al., 2015; Ramming et al., 2015; Li et al., 2009; Chen et al., 2015; Sevier et al., 2007].

Another important role of CHOP is supporting ATF4-induced transcription of growth arrest and DNA-damage-inducible 34 (GADD34). GADD34 is a subunit of the phosphatase PP1, which facilitates the dephosphorylation of phospho-eIF2α, restoring normal protein synthesis [Choy et al., 2015; Connor et al., 2001; Novoa et al., 2001; Rojas et al., 2015]. Additionally, Han et al. showed that restored protein synthesis in stressful conditions increases ROS production and induces cell death through oxidative stress and ATP depletion [Han et al., 2013].

Besides the role of PERK and elF2 in UPR, they play a crucial role in the function and survival of β pancreatic cells under physiological conditions. Harding *et al.* demonstrated that $PERK^{-/-}$ pups had a similar phenotype as patients with Wolcott-Rallison syndrome, which is characterized by permanent neonatal diabetes mellitus and acute liver failure. The animals also developed early diabetes mellitus and showed early mortality [Harding et al., 2001]. In another recent publication, Sowers *et al.* proposed a possible mechanism of how PERK can control insulin production in β cells by orchestrating the activity of chaperones like BiP, ERp 72, Pdi [Sowers et al., 2018]. Likewise, transgenic mice that cannot phosphorylate eIF2α, had a phenotype similar to

type II diabetes. Interestingly, the homozygous mice were born with severe β cells deficiency. At the same time, heterozygous mice had standard pancreatic islets under the normal conditions, but developed obesity with features of type II diabetes on a high-fat diet (hyperleptinemia, hyperinsulinemia, high glucose rate) [Scheuner et al., 2005].

The PERK–eIF2a-ATF4 pathway is also involved in the regulation of lipid metabolism. It was reported that ATF4 can activate genes involved in fatty acid and lipid production and, thus, in lipid metabolism in hepatocytes in response to nutritional stimuli [Li et al., 2011; Xiao et al., 2013]. Additionally, Oyadomari *et al.* showed that dephosphorylation of eIFα by GADD34 reduces hepatic steatosis upon a high-fat diet [Oyadomari et al., 2008].

1.2.3. UPR stress in diseases

ER stress is involved in the pathology of several different groups of diseases amongst which cancer, diabetes, degenerative and cardiovascular diseases, have been widely studied. Of particular interest to my research is its activation during viral or bacterial infections where it may play a dual role. In the infected cells, the UPR cascade enhances the host defense response, but at the same time, microorganisms can use the host UPR to support or enhance their own protein

production and folding, and multiplication process. Other diseases, where ER stress plays an important role, are protein conformational diseases or proteopathies (proteinopathies). This group involves more than forty disorders caused by the accumulation of the unfolded or misfolded proteins. Conformational diseases can be inherited (cystic fibrosis, familial hypercholesterolemia, Huntington, sickle cell disease) or induced (diabetes type 2, Alzheimer, prions). Many conformational diseases are, however, of unknown etiology. Besides, ER stress and UPR are involved in the pathogenesis of many acute and chronic disorders, some of which are discussed in the following sections.

1.2.3.1. Neuronal diseases

There are several classes of neurodegenerative diseases characterized by the accumulation of misfolded proteins in the brain tissue. For instance, tauopathies, which include Alzheimer's disease (AD) and subtypes of frontotemporal dementia. This group of diseases is described as the aggregation of hyperphosphorylated Tau proteins. Although Tau is not localized in the ER, there is strong evidence that an increase of BiP and the activation of PERK and IRE1 arms of the UPR represent early events in AD [Hoozemans et al., 2009; Nijholt et al., 2012; Hoozemans et al., 2005;

Hamos et al., 1991].

Another group of neurodegenerative disorders characterized by the accumulation of misfolded proteins are the synucleinopathies. This group includes Parkinson's disease (PD), dementia with Lewy bodies (DLB), and multiple system atrophy (MSA). In these diseases, α-synuclein proteins accumulate intracellularly, inducing ER stress. It was reported that different UPR mediators were increased in the brain tissue affected by these diseases [Baek et al., 2016; Hoozemans et al., 2007; Makioka et al., 2010].

1.2.3.2. Diabetes

In the pathogenesis of diabetes, functional disturbances of pancreatic β-cells play a central role, leading to decreased insulin production. Similar to the alveolar epithelial cells type (AECII), they have an innate fragility and are susceptible to secretory pathway overload. This sensitivity is caused by the intensified synthesis and secretion of insulin, which is needed to control blood glucose fluxes. This balance can be disturbed by aberrations in the translation or posttranslational modifications of proteins, which lead to ER stress. The problems in protein production, in turn, can be caused by gene mutations in insulin or UPR genes [Støy et al., 2007; Meur et al., 2010; Boesgaard et al., 2010]. It was reported that

maladaptive ER stress leads to β-cell degeneration, apoptosis, and diabetes development [Tersey et al., 2012; Scheuner; Kaufman, 2008; Papa, 2012; Ozcan et al., 2004; Chan et al., 2015]. Recent research also showed that the IRE1 arm of UPR plays a crucial role in switching ER stress to the apoptotic pathway leading to β-cells death. Because of this finding, IRE1 blockers were proposed as potential drugs for patients with diabetes [Ghosh et al., 2019].

1.2.3.3. Cancer

Cancer cells are fast-growing and proliferating cells that constantly face rapid environmental changes such as hypoxia, glucose deprivation, inadequate vascularization, and metabolic challenges. Thus, to continuously respond to these changes, they require an increased ER function. This is also supported by various data showing increased expression of ER stress markers in different kinds of cancer, such as breast cancer, multiple myeloma, colorectal cancer, and gliomas [Chen et al., 2014; Moenner et al., 2007; Segawa et al., 2002; Carrasco et al., 2007]. IRE1α activation in tumor cells was linked to an increased ER protein folding capacity, ERAD activity, enhanced production of angiogenic factors (VEGF), and restored protein homeostasis [Harnoss et al., 2020]. Additionally, the expression of chaperones rendered

cancer cells resistant to the pro-apoptotic signals, and their upregulation correlated to the degree of malignancy of the tumor and poor survival in patients [Zheng et al., 2014; Lee, 2007].

1.2.3.4. ER stress and infection

Bacteria and viruses induce UPR activation during infection. In particular, the Lipopolysaccharides (LPS) of Gram-negative bacteria promote Grp90 expression to increase protein folding, which is also associated with increased virulence [Coope et al., 2012]. The cytotoxin of *Escherichia coli* induces cell cycle arrest and apoptosis via BiP cleavage and following DNA-fragmentation and UPR associated apoptosis [Morinaga et al., 2008] or, in some cells, through Ca^{+2} release from ER and following PERK-CHOP-mediated DR5 apoptosis [Lee et al., 2008; Lee et al., 2009]. On the other hand, *Mycobacterium tuberculosis* (*Mtb*) does not produce a toxin but still activates ER stress. In this case, host cells use UPR to suppress the intracellular growth of *Mtb* by activating caspase-12 in the outer membrane of the ER [Choi et al., 2013]. It also was reported that ROS-mediated ER stress in *Mtb*-infected macrophages leads to activation of the RIDD pathway and following apoptosis [Go et al., 2019].

Viruses also use UPR and ER stress to promote their

replication and escape host defense [Gao et al., 2019; Hinte et al., 2020]. For instance, the herpes simplex virus (HSV) uses phosphorylation of eIF2α and promotes ERAD to reduce the level of MHC-I to suppress the immune response [Mulvey et al., 2007; Wang et al., 2006; Wang et al., 2007]. Similarly, the HIV-1 virus downregulates CD4 expression on the surface of T-cells by manipulating the ERAD [Magadán et al., 2010]. RNA viruses also use the UPR machinery to serve their needs. For example, hepatitis virus B and C activates ATF6 and IRE1 to support their replication [Li et al., 2007; Wang et al., 2014a]. In multiple publications, it was shown that the influenza virus (IV) uses calnexin and calreticulin chaperones to glycosylate hemagglutinin (HA), a transmembrane glycoprotein that determines viral antigenicity [Hebert et al., 1996; Hebert et al., 1997]. Moreover, IV activates the IRE1-XBP1 branch, and blocking of IRE1 prevents virus replication in alveolar epithelial cells [Hassan et al., 2012; Schmoldt et al., 2019].

1.2.3.5. UPR and Cardiovascular Diseases

ER stress is also involved in the pathogenesis of heart diseases such as myocardial ischemia/infarction and cardiomyopathies. Research on cellular models showed that high ventricular pressure induces ER stress and apoptosis in

cardiac myocytes [Okada et al., 2004]. Additionally, enhanced cardiac dysfunction, fibrosis, and apoptosis were observed in inducible cardiac-specific PERK knockout mice after transverse aortic constriction (TAC) [Liu et al., 2014]. Interestingly, despite PERK knockout, the level of CHOP expression was elevated in response to TAC. It indicates that CHOP-induced apoptosis may contribute to heart failure but not through the PERK branch of UPR. At the same time, less cardiac hypertrophy, fibrosis, and cardiac dysfunction were observed in CHOP knockout mice compared with wild-type mice after TAC, confirming that CHOP indeed contributes to the development of heart failure in mice [Fu et al., 2010]. UPR induction (Bip/GRP78 and XBP1 splicing) was also described in the heart tissue of human patients with heart failure [Minamino et al., 2010; Sawada et al., 2010; Okada et al., 2004].

Besides cardiomyopathies, activation of UPR was also reported under ischemic conditions [Glembotski, 2008; Azfer et al., 2006]. It was shown that the XBP1 branch plays a protective role in ischemia. Mice with cardiomyocyte-specific deletion of XBP1 showed an increase in myocardial infarct size, impairment in cardiac function, and hypertrophic remodeling after ischemia/reperfusion (I/R)

injury. Conversely, XBP1s and GRP94 overexpressing transgenic mice showed reduced infarct size and significant improvement of cardiac function after I/R injury, which further indicates the protective role of the XBP1 branch in cardiomyocytes [Wang et al., 2014b; Vitadello et al., 2003]. Similarly, it was reported in several publications that ATF6 and PERK also played a short-term protective role in cardiomyocytes under stress conditions [Lu et al., 2004; Doroudgar et al., 2009; Jin et al., 2017]. Nevertheless, when ER stress was prolonged, PERK activation led to cell apoptosis through CHOP activation [Mughal; Kirshenbaum, 2011].

1.2.3.6. UPR in lung disease

ER stress and UPR are activated and play an essential role in many different acute and chronic lung disorders [Khan et al., 2017; Zeng et al., 2017]. For instance, acute lung injury (ALI) and its most severe form, acute respiratory distress syndrome (ARDS), are characterized by massive tissue destruction and inflammation that is often a result of bacterial or viral pneumonia, systemic infections, lung ventilation, or trauma [Mizgerd, 2008; Darwish et al., 2011; Rajdev et al., 2021; Rubenfeld et al., 2005; Bernard et al., 1994; Steinvall et al., 2008]. Exposure to LPS and other Toll-

like receptor ligands is a classic model of ALI in mice. Thus, several publications reported that LPS induced ER stress and UPR in mouse lung tissue and was associated with inflammatory cytokines and neutrophil activation [Kim et al., 2013; Kim et al., 2015b; Zeng et al., 2017]. One of the latest discoveries in ALI research demonstrated that in a mouse model of LPS-induced ARDS, circulating exosomes (CE), which are considered a novel cross-communication mechanism in critical diseases (Xumao Tang *et al.*) activated ER stress and resulted in GRP78 and CHOP expression in lung tissue [Tang et al., 2020]. Another finding connects UPR and its IRE1/XBP1 arm to macrophage modulation in ALI. It was shown that thapsigargin, an ER stress inducer, promoted the polarization of pro-inflammatory macrophages M1 and the switch from anti-inflammatory macrophages M2 to M1. At the same time, non-targeted inhibition of ER stress, as well as selective inhibition of XBP1 splicing suppressed the M1 fate, but did not promote the M2 fate in *in vivo* and *ex vivo* experiments [Zhao et al., 2020]. Besides epithelial cells and macrophages, lung vascular endothelial cells are also affected by ER stress. Interestingly, mild ER stress has a protective role in endothelial cells [Esposito et al., 2013; Barabutis, 2019], whereas robust and prolonged ER stress was

associated with inflammatory response and apoptosis. This inflammation led to an alteration in alveolar endothelial and epithelial permeability followed by accumulation of protein-rich edema fluid in the alveoli and hypoxemia [Leonard et al., 2014; Wang et al., 2015b; Li et al., 2016].

Another example of an acute respiratory condition is pulmonary arterial hypertension (PAH), which results in chronic hypoxia, inflammation, and consequently oxidative stress and ER stress [Federti et al., 2017]. Recent research showed a connection between the IRE1α-XBP1 arm of UPR with hypoxia-induced pulmonary vascular remodeling. At the same time, inhibition of XBP1 splicing could restrain hypoxia-induced cell proliferation and migration and reverse the hypoxia-induced apoptosis arrest. Therefore, suppression of UPR was proposed as a new potential therapy in PAH [Cao et al., 2019].

Bronchopulmonary dysplasia (BPD) is another pulmonary disorder in which ER stress plays an important role. BPD is a chronic lung disease caused by hyperoxia during lung ventilation in premature neonates. Increased ROS production, ER stress, and apoptosis were observed in the alveolar epithelium in BPD animal models [Lu et al., 2015; Teng et al., 2017]. Moreover, it was shown that

prolonged ER stress suppresses the survival IRE1/XBP1 pathway and activates apoptosis via the IRE1α/c-Jun N-terminal kinase pathway [Tong et al., 2021].

Besides acute respiratory syndrome, ER stress and UPR play an essential role in chronic inflammatory and mucopurulent diseases. Although there is a lack of evidence about the precise role of ER stress in cystic fibrosis (CF), research showed that XBP1 splicing is activated in patients with F508del-CFTR mutation [Bartoszewski et al., 2008], which is to be expected since this mutation leads to elevated levels of misfolded CFTR in ER. Additionally, Martino *et al.* showed that the mucopurulent secretions from CF patients stimulate ER stress in healthy cultured human bronchial epithelial cells with consequent XBP1-dependent expansion of the ER [Martino et al., 2009]. Moreover, CF lungs are characterized by chronic infections, neutrophil release, macrophage accumulation, and the appearance of a broad array of inflammatory cytokines in the mucosa and lung secretions. All these factors also stimulate ROS formation and oxidative and ER stress. Thus, the CF lung is constantly exposed to injury and stress, which in the long run leads to pathological changes in the tissue and fibrosis development [Tiringer et al., 2013; Tiringer et al., 2014].

Chronic obstructive pulmonary disorder (COPD) also belongs to the group of chronic lung diseases. Cigarette smoke is considered to be the primary cause of COPD where it was shown that smoking induces ER stress leading to bronchial and alveolar epithelial cell apoptosis [Min et al., 2011]. In support of this, several experiments showed the protective role of ER stress inhibition against apoptosis in bronchial and alveolar epithelial cells in COPD lungs [Liu et al., 2018; Lin et al., 2017; He et al., 2019].

The last, but most important to discuss is the known role of ER-stress in idiopathic pulmonary fibrosis (IPF). Maladaptive ER stress induces apoptosis in the alveolar epithelial type II cells (AECII), thus, presumably playing a crucial role in the triggering fibrosis. In support of this theory, it was shown that all branches of UPR (ATF6, XBP1s, ATF4, PERK, Grp78), as well as apoptotic markers (CHOP, caspases), were activated in the lung tissue of IPF patients and particularly in AECII [Korfei et al., 2008; Lawson et al., 2008]. Similarly, in a mouse model of lung fibrosis, bleomycin administration also activated the UPR markers in the lung epithelium [Hsu et al., 2017; Thamsen et al., 2019].

AECIIs are the most complex and metabolically active cells in the lung and have two important functions: surfactant

production and the generation of AECII and AECI under homeostatic conditions as well as during the repair process following alveolar injury [Nabhan et al., 2018; Fehrenbach, 2001]. Surfactant synthesis is a continuous and complex process, prone to mistakes, which leads to the accumulation of misfolded and unfolded proteins in the ER. However, under physiological conditions, UPR can manage the misfolded protein load in a healthy manner, without consequences on the cell's function. ER stress becomes maladaptive and induces cell death when additional stressors like mutated proteins (SFTPA2, SFTPC, MUC5), viruses, aging, or chemical agents come into play. Cumulatively these factors dramatically increase ER stress and apoptosis in AECIIs resulting in chronic extensive AECIIs injury [Lawson et al., 2011; Lawson et al., 2008; Maitra et al., 2010; Katzen et al., 2019; Hsu et al., 2017; Thamsen et al., 2019; Beri et al., 2010]. Presumably, malfunctioning AECIIs and their massive and continuous loss results in an injury-repair imbalance in the fibrotic lungs, which causes a decrease in epithelium regeneration capacity and an increase in scar tissue production. As a result, profound lung structure alterations and lung function decline occur.

The role of ER stress in AECIIs in IPF pathogenesis

was demonstrated in *in vivo* experiments involving the expression of the L188Q SFTPC mutation, which in humans leads to familial forms of IPF, and experiments with tunicamycin-treated mice [Lawson et al., 2011]. In both cases, ER stress was not enough to cause spontaneous fibrosis, but the lungs of these mice were already vulnerable, which led to lung fibrosis worsening compared to control mice after bleomycin treatment. Thus, activated and continuous ER stress affects lung epithelial cell health and potentially triggers fibrosis development.

Another cell-type that plays an essential role in lung fibrosis development is the macrophage (Mφ). Macrophages have a dual role in any injury-repair process, where they first take over a pro-inflammatory M1 fate, and later a pro-repair M2 fate. Both M1 and M2 macrophages infiltrate the fibrotic lung and influence IPF disease progression, although their precise role in this process remains unknown. Nevertheless, it was shown that in both IPF lung tissue and animal models, there is a predominant infiltration of M2 Mφ [Pechkovsky et al., 2010; Hancock et al., 1998; Murray et al., 2010; Venosa et al., 2016] that can secrete growth factors (PDGF, TGF-β, IGF-1), extracellular matrix components (collagen, fibronectin) and mediators recruiting and stimulating

fibroblasts to differentiate into myofibroblasts [Rappolee et al., 1988; Shimokado, 1985; Chujo et al., 2009]. Macrophages differentiate from monocytes and change their metabolism to M1 or M2 depending on their environmental stimuli. It was shown that UPR is associated with macrophage polarization [Soto-Pantoja et al., 2017; Díaz-Bulnes et al., 2019; Lara-Reyna et al., 2019], and although the precise mechanism is unknown, it was reported that the IRE1-XBP1 and PERK arms of UPR associated with M1 Mφ polarization, and TUDCA and 4μ8c ER stress inhibitors downregulate M1 markers [Shan et al., 2017; Batista et al., 2020; Lara-Reyna et al., 2019; Zhao et al., 2020; Yang et al., 2019]. At the same time, mice with CHOP deficiency were protected from bleomycin-induced fibrosis and had decreased levels of TGFβ and pSTAT6 compared to wild-type mice [Yao et al., 2016; Oh et al., 2012]. The macrophages from $CHOP^{-/-}$ mice were found to not express M2 markers and had an increased level of cytokine signaling 1/3, which is a known suppressor of the STAT6/PPAR-γ pathway. Interestingly, the adoptive transfer of activated M2 macrophages from wild-type mice into $CHOP^{-/-}$ mice lungs reversed this protective effect. Data from liver fibrosis research also support the connection between CHOP

expression and Mφ polarization into M2. Mouse experiments demonstrated increased colocalization of CHOP and CD206, an M2 marker, in the fibrotic liver. Moreover, direct induction of ER stress with thapsigargin in M-CSF stimulated macrophages increased M2 surface markers and cholesterol uptake [Oh et al., 2012]. Thus, UPR mediators are involved in macrophage polarization, and its regulation is probably associated with different UPR branches or/and stages: early UPR mediators IRE1-XBP1 and PERK seems to induce M1 phenotype, and late UPR mediator CHOP associated with M2 phenotype.

Fibroblasts are the third cell type involved in fibrosis pathogenesis [Ghavami et al., 2018]. Multiple studies showed that UPR plays an important role also in the activation of this cell type. Particularly, activation of fibroblasts by TGFβ upregulated UPR proteins in these cells (Baek et al. 2012; Ghavami et al. 2018), and suppression of UPR in fibroblasts reduced ECM proteins expression [Ghavami et al., 2018; Hsu et al., 2017]. Moreover, it was reported that the IRE1-XBP1 pathway was essential for ECM proteins expression upregulation in fibroblast cells. For instance, IRE1 was required for collagen 1α2 and fibronectin production, and an IRE1 inhibitor decreased TGF-β1-

induced ECM protein synthesis in IPF lung fibroblasts, but not in non-IPF donor fibroblasts [Ghavami et al., 2018]. This mechanism is poorly understood, but both the endonuclease and kinase domains of IRE1 have the potential for pro-fibrotic response regulation. The IRE1 endonuclease domain was involved in MiR-150 cleavage that suppressed c-Myc upregulation of αSMA gene expression. Furthermore, XBP1 splicing induces ER expansion to support ECM proteins expression [Heindryckx et al., 2016]. At the same time, Liu and colleagues demonstrated upregulation of ECM proteins in hepatic stellate cells by pIRE1 in ASK1/JNK related manner [Liu et al., 2019]. Interestingly, in cardiac fibroblasts, ATF6 overexpression had a protective role in permanent occlusion myocardial infarction in mice and let to decreased collagen and fibronectin expression [Stauffer et al., 2020]. Therefore, different UPR arms seem to have positive or negative regulation of the pro-fibrotic response depending on the cell type and their environment.

Besides intracellular regulation, cells can interact and affect each other by the extracellular release of different active molecules, called cytokines. For example, it was shown that co-culturing fibroblasts with macrophages from IPF patients, but not from the donor lungs, activated fibroblasts, of note

also in a cell-to-cell contact independent way [Shruthi Sethuraman, April 2019]. Adding the apoptotic cells to this equation showed interesting results. In *in vitro* experiments, growth medium from macrophages co-cultured with apoptotic Jurkat cells abolished fibroblast TGFβ-induced migration and activation [Kim et al., 2017]. Such an effect was not observed with control or necrotic cells. Also, exposure of fibroblasts to media from only apoptotic cells did not inhibit their activation. The same results were obtained in *in vivo* experiments. Intratracheal application of apoptotic Jurkat cells decreased fibroblast activation, ECM deposition, and mitigated lung fibrosis [Kim et al., 2017; Lee et al., 2012]. Thus, these data suggest that apoptotic cells activate an anti-fibrotic program in macrophages for controlling fibroblast activation. In these experiments, researchers used Jurkat cells (immortalized T cells) as a source of apoptotic cells. Recent work of Zhang et al. brought some light on how apoptotic T cells can affect fibrosis. The authors demonstrated induction of Tregs (functional regulatory T lymphocytes) by apoptotic thymocytes. Tregs reduced immune response and enhanced the resolution of acute lung inflammation through αv integrin-mediated mechanisms [Zhang et al., 2020]. It, in turn, mitigated tissue damage and subsequently the fibrotic

response.

Thus, fibrosis development requires the activation and communication of multiple cell types. All mentioned cells were shown to experience ER stress markers in various manners, which probably has a different regulatory meaning. Nevertheless, more experiments are required to understand the precise role of all UPR members in this communication and fibrosis development and progression.

2. Aims and Objectives

There is a lack of deep understanding of the precise mechanism of fibrosis development, its initial stages, and trigger mechanisms. While induction of all UPR branches following extensive ER stress in AECIIs has been demonstrated, it is still not fully understood if these changes are causing fibrosis or if they are a consequence of lung fibrosis. The UPR is a very complex pathway with three branches, which can be differently activated depending on environmental signals and cell types. It can lead to different outcomes. Moreover, the crosstalk amongst different UPR branches and effectors enables an understanding of their individual roles in cell injury and fibrogenesis. Additionally, the UPR may play an essential role in acute exacerbation (AE). It is considered that AE can be caused by viral infections, which also can activate the UPR.

Therefore, this thesis aimed to decipher the role of different UPR branches in AECIIs in the development of lung fibrosis. To that end, three UPR mediators, XBP1s, ATF6p50, and CHOP, were overexpressed in the AECIIs of mouse lungs, and the following aspects were analyzed in each case:

1. Impact of the overexpression of a key UPR mediator

on the AECII proliferation and survival status, which can influence the predisposition of mouse lung tissue to injury.

2. Impact of the expression of a key UPR mediator on the morphology and function of the mouse lungs in the model of bleomycin-induced fibrosis.
3. Impact of the overexpression of a key UPR mediator on the level of influenza virus infection and murine lung epithelial cell survival.

3. Materials and Methods

3.1. Animal work

3.1.1. Mice strains

Animal studies were performed following the Helsinki convention for the use and care of animals and were approved by the local authorities at Regierungspräsidium Giessen V 54 – 19 c 20 15 h 01 GI20/10 Nr. 19/2015 (ER-Stress Effektormoleküle - Lungenfibrose). The animal proposal had also approved changes for experiments with bleomycin from 02.06.2017 with the supplement from 14.06.2017. All animals used in the experiments were between 10 and 16 weeks old at the beginning of the experiment.

All mouse lines were created in our laboratory by Dr. M. Hühn (ATF6 and XBP1), Dr. O. Klymenko, and Dr. M. Korfei (CHOP), and the detailed description of the generation process was published in their doctoral theses [Klymenko, 2016b; Hühn, 2013]. For all mouse lines, a two component Tet-on system (Clontech Laboratories Inc.) was used. The first component was the doxycycline-inducible transcriptional activator (rtTA) expressed under the human SP-C promoter, which allows targeted transgene expression

exclusively in AECIIs. The second element is the Tetracycline Response Element. It carried the gene of interest (GOI) and luciferase on either side of a bidirectional promoter, which allows the co-expression of GOI and luciferase. Thus, following doxycycline treatment, luciferase expression reports GOI transgene expression. Three GOIs were used throughout the work: ATF6p50, sXBP1 and CHOP.

Previously in our laboratory, it was determined that at least four days of doxycycline treatment was necessary to achieve detectable levels of transgene induction. Based on this, mice were exposed to doxycycline (625 mg/kg food, Altromin) for four days before all experiments, after which the count of the transgene expression time began. The number of mice per group was three to five.

3.1.2. Bleomycin model

On day 0, mice (n=3-6) were anesthetized and intubated, and bleomycin (Hexal, 2.5U/Kg body weight in 0.9% saline) or saline was aerosolized using a Microsprayer (Penncentury). All mice were weighed and scored every day. On day 28, the lung mechanical parameters were measured by Flexi Vent, after which mice were sacrificed, and lung tissue was used for further analysis.

3.1.3. Lung function

Mouse lung function was evaluated by the forced oscillation technique, which measures flow-volume relationships in the respiratory system. Evaluations were performed according to the manufacturer's instructions.

Figure 6. Overview of experiments with bleomycin treatment

Briefly, the mice were anesthetized (xylazine/heparin/ketamine 2:1:2, 200 µl total), intubated, and connected to the animal ventilator FlexiVent (SciReq, Montreal, QC, Canada). Ventilation was performed at a respiratory rate of 150 breaths/min, a tidal volume of 10 mL/kg, and a PEEP set at three cmH2O. The procedure was performed until three acceptable measurements (coefficient of determination > 0.95) were recorded for each subject, from which an average was calculated. Additionally,

two types of techniques were used to perform forced oscillation. The first one, the single-FOT maneuver ("Snapshot-150"), belongs to the single-compartment model and describes respiratory system resistance (Rrs) and respiratory system compliance (Crs). The second maneuver, the multi-frequency FOT maneuver ("Quick Prime-3"), belongs to the constant phase model and describes Newtonian resistance (Rn), tissue damping (G), and tissue elastance (H). Additionally, PV loops were generated to obtain dynamic compliance (Cst) of the respiratory system, inspiratory capacity (A), and the area enclosed by the PV loop (Area). A, H, Crs, and PV loops were used to present data.

3.1.4. Lung tissue collection

After evaluation of the lung function, mice were exsanguinated via the abdominal aorta. The lung was removed from the thoracic cavity and the lung lobes were divided for several of analyses as follows: left lobe for IHC, right superior either for flow cytometry or protein analysis, right middle and inferior lobes for protein, and RNA analysis, post-caval lobe either for IV infection or protein analysis.

3.2. PCLS

3.2.1. PCLS preparation and culturing

The right superior lung lobes from dox-induced mice and respective non-induced control mice were used to make precision-cut lung slices (PCLS). The number of mice per group was three to five. Lungs were inflated with a warm (37^0C) 1.5% Low Melt Agarose solution and allowed to solidify on ice for 30 min. The lung tissue was sliced by McIlwain Tissue Chopper at 200µm thickness. During the cutting process, ready PCLS were kept on ice in CO_2-independent based medium (see below). After PCLS from all mice were ready, they were transferred to 24-well plates with DMEM based medium (see below) for further doxycycline treatment or infection with influenza virus (IV).

Medium for keeping PCLS during preparation:	**Medium for PCLS culturing:**
CO_2-independent medium 1% (V/V) Pen/Strep	DMEM medium 1% (V/V) Pen/Strep 1% (V/V) L-Glutamine Doxycycline 2µg/ml (if needed)

3.2.2. Infection of PCLS with influenza virus

Comparably sized PCLS were chosen for infection to keep a similar value of multiplicity of infection (MOI). For the infection procedure, the influenza virus (A/PR/8/34 H1N1, mouse-adapted) was resuspended in DMEM medium without FBS to reach a final concentration of virus particles of 10^7 pfu/ml. After that, 100 µl of the virus-containing medium or virus-free medium for non-infected control were transferred to each well of a 24 well plate. Thus, the final concentration of the virus was 10^6 pfu/well. The PCLS were incubated for 1 hour in the infection medium, after which the medium was replaced with respective post infection (p.i.) medium (see below). PCLS were dissociated into single cell suspension 48 hours p.i. and analyzed by flow cytometry. Titrated influenza virus stock was kindly provided by the research group of Dr. Susanne Herold.

Medium for PCLS p.i. culturing:
DMEM medium
1% (V/V) Pen/Strep
1% L-Glutamine
2µg/ml Doxycycline (if needed)
0.5% (V/V) Trypsin
0.1% (W/V) BSA

3.3 Cell culture

3.3.1. Cell culture of lung epithelial cell lines

The mouse lung epithelial cell line, MLE12, was obtained from ATCC, Manassas, USA. Cells were grown in 10 cm^2 tissue plates in DMEM-F12 based medium with the following ingredients:

DMEM-F12 medium
10 nM Hydrocortisone
10 nM Hydrobeta estradiole
5% (V/V) ITS
10 nM HEPES
2 nM L-Glutamine
2% (V/V) FBS
1% (V/V) Pen/Strep

Cells were passaged whenever they reached 80-90% of confluence. To detache cells from the culture plates, they were incubated in trypsin solution (0.025% in PBS) for 1-2 min at 37^0C. To neutralize the trypsin activity, FCS containing medium was added to the culture plates. After washing, cells were diluted (1:10) and plated into new dishes with fresh medium.

3.3.2. Generation of stably transfected epithelial cell line

To create the conditional ATF6 overexpressing MLE12 cell line, Tet-on advanced inducible gene expression system was used (Clontech). All procedures were performed following the manufacturer's instructions. Shortly, two vectors were used, regulatory-plasmid pTet-On (Clontech) and the response-plasmid pBI-L-ATF6 (Hühn 2013). MLE12 cells were transfected with two μg of the linearized pTet-On vector (HindIII, New England BioLabs). After 48h the MLE12 growth medium was replaced with 500 μg/ml geneticin (G418, Roche) containing medium for positive selection. Cells were kept for an additional 48 hours for positive selection. Surviving cells were transfected with the linearized pBI-L-ATF6 plasmid (AatII, New England BioLabs) together with the linear hygromycin marker (Clontech). After 48 hours, the medium was replaced for the fresh one containing 100 μg/ml of G418 and 100 μg/ml of hygromycin (InvivoGen) for further positive cell selection. Clones were analyzed using luciferase assay, and clone #3 was chosen for the experiments. For both transfection procedures, TurboFect™ Transfection Reagent (Thermo Scientific™) was used following the manufacturer's guidelines.

3.4. Assays

3.4.1. Luciferase assay

Analysis of luciferase expression in lung tissue and transgenic MLE12 cells was made using luciferase assay (Promega). All procedures were done following the manufacturer's guideline. Each measurement was repeated three times, and the mean values were used for data representation.

3.4.2. Cell proliferation assay

Cell proliferation ELISA BrdU assay (Roche) and Cell Proliferation Reagent WST-1 assay were used to analyze the influence of ATF6 overexpressing MLE12 cells on fibroblasts proliferation. First, ATF6 overexpressing cells were activated with dox (1μg/ml) for 24 and 48 hours, and their culture medium as well as medium from non-induced cells control were transferred to Mlg fibroblast cells (ATCC #CCL-206). Mlg cells were incubated in these media for 24 h and processed for proliferation analysis. Thrombin (Trm) (1μg/ml), a pro-coagulant factor, was used as a positive control for proliferation. It was chosen as its ability to induce a pro-fibrotic phenotype in fibroblasts has been well described in several publications [Bogatkevich et al., 2001; Ludwicka-Bradley et al., 2004]. Both cell proliferation assays were used

following the manufacturer's guideline. The obtained results were presented as a mean of three repeated independent experiments.

3.5. Microscopy

Lung tissue was embedded in paraffin and sectioned at 3 μm thickness. Tissue sections were mounted on positively charged glass slides. At least three sections from one mouse were stained and analyzed. The number of biological replicates varied from three to seven, depending on the experiment settings and the animal study protocol.

3.5.1. Immunofluorescence staining protocol

1. Deparaffinize lung tissue in Xylene for 10 min.
2. Use ethanol in various concentrations to wash away xylene and rehydrate the tissue. Start with 100% ethanol and keep slides in each solution for 2 min.
3. 100% ethanol → 99% ethanol → 96% ethanol → 70% ethanol → 40% ethanol → distilled water
4. Use freshly prepared citrate buffer for antigen retrieval. For this, 0.1 M citric acid monohydrate was mixed with 0.1 M Sodium citrate tribasic dihydrate in ratio 9:41. Bring the mix to the final volume by diluting it with distilled water in a ratio of 1:9. Place slides with tissue into the buffer and microwave at 900 watts for 10 minutes two times. Add water

for volume replacement if needed during boiling. Cooldown the slides in buffer and wash with PBS. Circle each section with hydrophobic PAP-pen.

5. Use donkey serum (5% in PBS) to block nonspecific binding of secondary antibodies to the tissue proteins. Apply about 50-100 µl of blocking solution to each tissue sample and incubate for 30 minutes at room temperature. Rinse slides in PBS.

6. Apply 50-100 µl of the primary antibodies mix to each tissue sample and incubate overnight at 4°C. Wash the slides in PBS for 5 min 3 times.

7. Apply 50-100 µl of the secondary antibodies mix to each section and incubate for 60 min at room temperature. Wash the slides in PBS for 5 min 3 times.

8. Apply 50-100 µl of DAPI solution to each tissue sample and incubate for 1 min at room temperature. Rinse slides in PBS.

9. Apply 50-100 µl of Sudan Black solution (3m% g/v in 70Vol% Ethanol) to each tissue sample and incubate for 1 min at room temperature. Rinse slides in PBS.

10. Cover tissue with cover glass using DAKO fluorescence mounting medium for mounting and preserving slide specimens.

11. Store slide in a dark place at 4°C.

Stained tissue was fully scanned using the Evos FL2 Imaging system (Thermo Fisher Scientific). Additionally, the pictures of the region of interest (ROI) were taken using Axio Observer Z1 fluorescence microscope (Carl Zeiss, Micro Imaging). Before quantification, a channel of interest was extracted from an RGB color image, after which it was converted into an 8-bit gray image. The signal of anti-ECM proteins antibodies was estimated using the Mean Intensity of gray values. The cytokeratin 5 positive patches were quantified using Integrated Density as this parameter also considers the Area of the signal. Image quantification was done in FIJI [Rueden et al., 2017] software.

3.5.2. Masson-Goldner's trichrome staining protocol

1. Deparaffinize lung tissue in Xylene for 10 min.
2. Use ethanol in various concentrations to wash away xylene and rehydrate the tissue. Start with 100% ethanol and keep slides in each solution for 2 min.
3. 100% ethanol → 99% ethanol → 96% ethanol → 70% ethanol → 40% ethanol → distilled water
4. To color nuclei, keep tissue in Weigert's hematoxylin for 5 min and rinse in warm tap water until water becomes clear.
5. Keep tissue in warm tap water for 10 min.

6. Keep tissue in Xylidine Ponceau acidic solution 5 min to stain cytoplasm. Wash 2-3 times with 1% acetic acid.
7. Keep tissue in Orange G solution for 1 min to stain keratin and muscle fibers. Wash 2-3 times with 1% acetic acid.
8. Keep tissue in Light Green SF yellowish solution for 8 min to stain collagen. Wash 2-3 times with 1% acetic acid.
9. Dehydrate tissue using ethanol in various concentrations. 70% ethanol → 96 % ethanol → 2 times 100% ethanol → 2-3 time in xylene
10. Cover tissue with cover glass using a rapid drying medium (Pertex) for mounting and preserving slide specimens.

All slides were scanned using NanoZoomer 2.0 RS Imaging System (Hamamatsu).

3.5.3. H&E staining protocol

1. Deparaffinize lung tissue in Xylene for 10 min.
2. Use ethanol in various concentrations to wash away xylene and rehydrate the tissue. Start with 100% ethanol and keep slides in each solution for 2 min.
3. 100% ethanol → 99% ethanol → 96% ethanol → 70% ethanol → 40% ethanol → distilled water

4. Keep tissue in Mayer's hemalum solution for 20 min to stain nuclei. Rinse in tap water for 5 min.
5. Keep tissue in 96% ethanol for 1 min
6. Keep tissue with eosin solution for 4 min to stain cytoplasm and intercellular substances. Rinse in tap water.
7. Dehydrate tissue using ethanol in various concentrations. 70% ethanol → 96 % ethanol → 2 times 100% ethanol → 2-3 time in xylene
8. Cover section with cover glass using a rapid drying medium (Pertex) for mounting and preserving slide specimens.

3.5.4. Microscopes and scanners.

Slides were fully scanned at 40x magnification using three different scanners:

- Evos FL2 Imaging system (Thermo Fisher Scientific) to scan immunofluorescent staining
- Nano Zoomer 2.0 RS Imaging System (Hamamatsu) to scan slides with Masson-Goldner's trichrome staining
- MIRAX DESK (Carl Zeiss) to scan H&E staining

Additionally, pictures of the different regions were taken by using Axio Observer.Z1 fluorescence microscope (Carl Zeiss, Micro Imaging). The intensity of the fluorescent

signal was quantified as integrated density in FIJI [Rueden et al., 2017] software.

3.6. Tissue morphometric analysis

Morphometric analysis was performed using the mean linear intercept (MLI) and alveolar septal wall thickness. MLI was determined on a transparent overlay consisting of horizontal and vertical lines superimposed overall area of parenchymal tissue with discrimination of bronchioles and vessels. All intercepts with alveolar septal walls were counted at the intersection point of the two lines. The length of all lines was summarized and divided by the total number of intercepts to obtain the MLI parameter that characterizes the entire acinar air space complex (not just alveoli). Alveolar septal wall thickness was measured using lines drawn at 90° angles across the narrowest section of alveolar walls. The length of all the lines was summarized and divided by the total number to obtain the mean value. The calculations were done in Visiopharm NewCast computer-assisted stereology system software (Visiopharm, Hoersholm, Denmark). Additionally, kernel density estimation was applied to see the distribution of septal thickness and alveolar size values. The plots were generated in R software with an advanced package.

3.7. Flow cytometry

3.7.1. Cell isolation

Flow cytometry was used to analyze the level of transgene positive AECIIs in mice and IV infection in PCLS. In both cases, the tissue was chopped with small scissors, followed by incubation in a dispase solution (see below) for 20 min (PCLS) or 30 min (lung tissue). Additionally, to achieve better cell dissociation, the suspension was gently pipetted up and down, after which DMEM medium with 10% FBS was added to neutralize the dispase. The obtained cell suspension was filtered through a 100 and 40 µm cell strainer, centrifuged at 450 g for 5 min, and resuspended in 100 µl of FACS buffer containing antibodies mix.

Dispase solution	**Medium for cell washing**	**FACS buffer**
DMEM	DMEM	
5 Units/ml dispase (Corning)	30 µg/ml DNase	HBSS
30 µg/ml DNase	1% (V/V) Pen/Strep	2% (V/V) FBS
	1% (V/V) L-Glutamine	10 µg/ml DNase
	10% (V/V) FBS	0.1 mM HEPES

3.7.2. Staining protocol for flow cytometry

1. Resuspend cells after isolation in 100 µl/10^6 cells master mix containing following ingredients:

Set 1 for AECII number quantification

Anti-EpCam antibody APC-Cy7 (mouse)	1:100	Biolegend (118218)
Anti-CD45 antibody Pe-Cy7 (mouse)	1:100	Biolegend (103114)
Anti-CD31 antibody Pe-Cy7 (mouse)	1:100	Biolegend (102418)
Zombie Violet™ Fixable dye	1:500	Biolegend (423113)

Set 2 for IV infection analysis

Anti-EpCam antibody APC-Cy7 (mouse)	1:100	Biolegend (118218)
Anti-CD45 antibody Pe-Cy7 (mouse)	1:100	Biolegend (103114)
Anti-CD31 antibody Pe-Cy7 (mouse)	1:100	Biolegend (102418)
Zombie Violet™ Fixable dye	1:500	Biolegend (423113)

1. Incubate cells at 37^0C degrees for 1 hour and wash after with 1ml PBS buffer.

2. Use cell fixation/permeabilization kit according to manufacture protocol to fix and permeabilize cells.
3. Resuspend washed cells in 100 µl/10^6 cells staining buffer containing:

Set 1	Set 2
Anti-SPC antibody (1:100, Santa-Cruz, sc-7706)	Anti-Nucleoprotein FITC (rabbit, 1:100, abcam ab20921) Anti-cleaved Caspase-3 PE (rabbit, 1:100, Cell signaling (9978)

4. Incubate for 1 hour at room temperature in a dark place. After incubation, wash cells with PBS, centrifuge at 450 g for 5 min, and discard the supernatant.
5. Resuspend washed cells in 100 µl/10^6 cells staining buffer containing secondary antibody. Incubate for 30 min at room temperature in a dark place. After incubation, wash cells with PBS, centrifuge at 450 g 5 min, discard the supernatant and resuspend in 200-300 µl PBS buffer. Cells are ready to analyze by flow cytometry.

Set 1	Set 2
Donkey F(ab´)2 anti-goat IgG Alexa Fluor® 488, Abcam (ab150138), 1:500	No secondary needed

3.7.3. Controls

For precise flow cytometry analysis, three types of controls were used. The first one was negative control without antibodies to determine a signal-free area and cells´ autofluorescence in a particular channel (Fig. 7A). The second type of control was single color controls to compensate for spectral overlap. If the cell number after tissue dissociation was enough, the third type of control, fluorescence minus one (FMO), was used for FITC, PE, and APC colors (Fig. 7 C, D, E). FMO controls are samples containing all fluorescent antibodies except the one of interest and they were applied to set the background boundary for the omitted channel and thus to identify and gate positive populations more precisely. Additionally, secondary antibodies only control was used to exclude non-specific binding of secondary antibody in indirect staining with anti-SP-C antibody (Fig. 7B).

3.7.4. Gaiting strategies

The following two hierarchy was created to gate the events for analysis (Fig. 8):

A Gating strategy to analyze AEC from infected PCLS

1. Selecting a population of cells based on their forward and side scatter properties (SSA-A vs. FCS-A), removing debris and other events of non-interest.
2. Excluding the doublets by pulse geometry gating (FCS-H vs. FCS-A).
3. Selecting the whole epithelial cells as $EpCam^{pos}$, $CD45^{neg}$, and $CD31^{neg}$ population (CD45/CD31 vs. EpCam).

a. Analysis of the number of infected cells (FSC-A vs. Nucleoprotein).

b. Analysis of the cell death (Cleaved caspase 3 vs. Zombie). To this end, the following four populations were analyzed: early apoptotic cells ($Zombie^{neg}$ cl. $casp3^{pos}$), late apoptotic cells ($Zombie^{pos}$ cl. $casp3^{pos}$), necrotic cells ($Zombie^{pos}$ cl. $casp3^{neg}$), and living cells ($Zombie^{neg}$ cl. $casp3^{neg}$).

B Gating strategy to analyze number of AECII and BiP^{pos} AECII

1. Selecting a population of cells based on their forward and side scatter properties (SSA-A vs. FCS-A), removing debris and other events of non-interest.
2. Excluding the doublets by pulse geometry gating (FCS-H vs. FCS-A).
3. Selecting living cells as Zombieneg population (SSC-A vs. Zombie).
4. Selecting the whole epithelial cells as EpCam^{pos}, CD45^{neg}, and CD31^{neg} population (CD45/CD31 vs. EpCam).
5. Analysis of the number of AECII by selecting SP-Cpos population (SP-C vs. EpCam).
6. Analysis of the number of Grp78/BiPhigh AECII (FCS-H vs. Grp78/BiP). This gating was applied only to analyze cells from the ATF6 overexpressing mouse lungs.

3.7.5. Flow cytometer

BD FACS Canto II (BD Bioscience, Franklin Lakes, USA) was used to quantify the number of transgene positive AECII in mice and LSR Fortessa (BD Bioscience, Franklin Lakes, USA) for IV infection and cell death

analysis in PCLS. All data were analyzed in FlowJo software [BD Life Sciences].

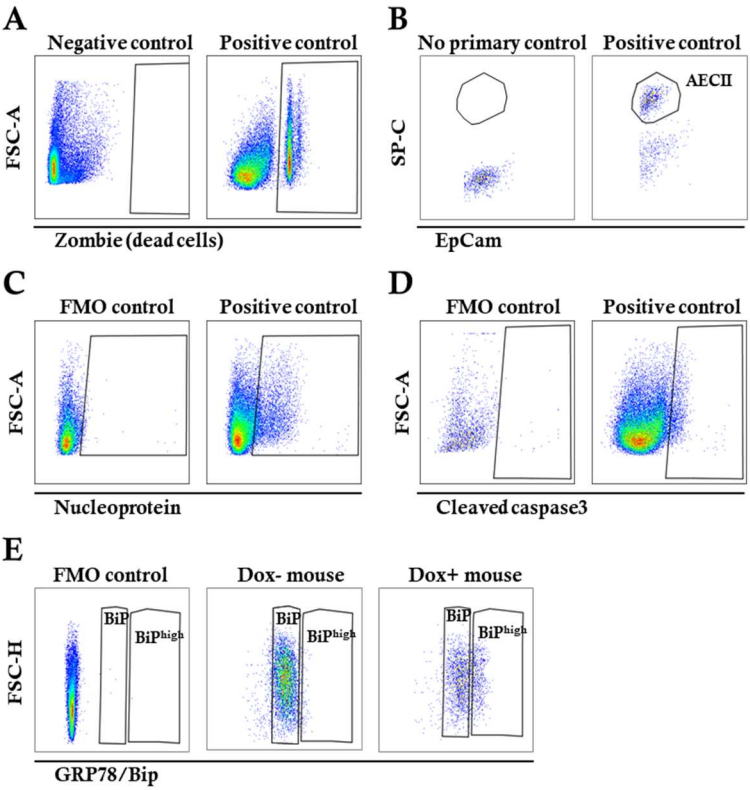

Figure 7. Overview of controls for flow cytometry analysis

A. *An example of a single-color control, Zombie dye to mark dead cells.* ***B.*** *No primary anti-SP-C antibody control (only secondary antibody control) to exclude non-specific binding of secondary antibody in indirect staining.* ***C and D*** *FMO controls for anti-Nucleoprotein and anti-Cleaved Caspase 3 to set the background boundary for the omitted channel for more precise targeted population gating.* ***E.*** *FMO control for anti-GRP78/BiP antibodies and GRP78/BiP staining for dox-induced and non-induced mice.*

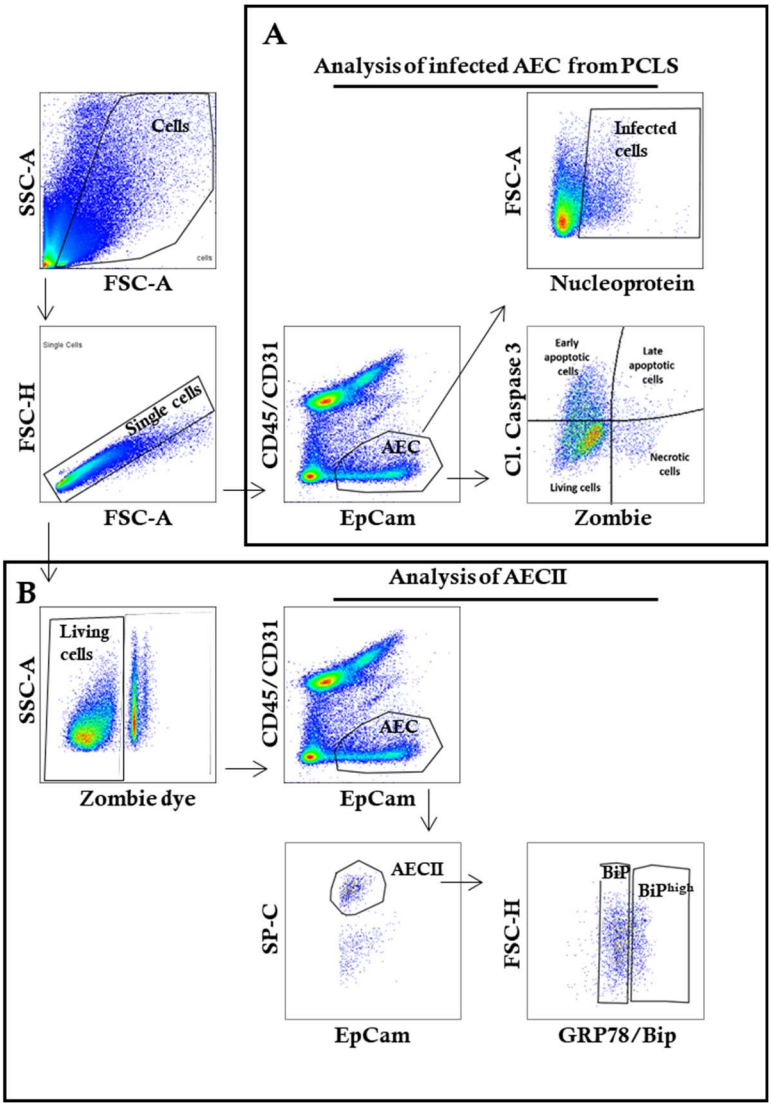

Figure 8 Gaiting strategy for flow cytometry analysis

Two types of gating were used. ***A.*** *Analysis of AEC from infected PCLS.* ***B.*** *Analysis of the number of AECII and Grp78/BiP^{pos} AECII (B).*

3.8. Western blotting

Cells or tissue were lysed or homogenized (Precellys homogenizer, PrgLab) and kept on ice for one hour. Pierce BCA Protein assay kit (Thermo Scientific) was used to determine protein concentration, after which the samples were accordingly diluted to obtain the same protein concentration in all samples.

Lysis buffer	**Loading buffer (4x)**
50 mM Tris-HCl/pH 8.0	5% (W/V) SDS
5 mM EDTA	156mM Thris/HCl, pH 6,8
150 mM NaCl	40% (V/V) Glycerol
1% (V/V) Triton-X-100	0,01% (W/V) bromophenol blue
0.5% (W/V) Na-deoxycholate	5 % (V/V) 2-mercaptoethanol
1 mM PMSF	Water

The proteins in ready samples were separated using SDS-PAGE and transferred to PVDF membranes (Roth) in a wet blotting chamber according to the manufacturer´s protocol (Bio-Rad). Obtained blots were incubated in a blocking buffer (5% w/v dried milk in TBST) for 30 min at room temperature and used for immunostaining with primary antibodies overnight at 40C. After incubation, the blots were washed in the TBST buffer for 15 min 3 times and incubated in a solution with secondary HRP antibodies for 1 hour at room

temperature. After this, blots were washed for 15 min 3 times. The signal was developed using Immobilon Western Chemiluminescent HRP Substrate (Millipore) and imaged on a Chemostar imager (Intas). HRP signal was analyzed in FIJI software [Rueden et al., 2017]. Afterward, blots were

SDS-PAGE	Running gel 10%	Stacking gel 4%
Acylamide/Bisacrilamide (30%/0,8%)	3,33 ml	1,33 ml
Distilled water	3,2 ml	6,57 ml
10% SDS	100 µm	100 µm
1,125M Tris, pH 8,8	3,33 ml	-
0,625M Tris, pH6,8	-	2 ml
10%APC	50 µm	100 µm
TEMED	10um	10 µm
SDS Running buffer	Transfer buffer	
25mM Tris	20mM Tris	
192mM Glycine	159mM Glycine	
0,1% (W/V) SDS	20% (V/V) Methanol	
Water	Water	
TBST buffer, pH 7,5	Stripping buffer pH 2.5	
50 mM Tris	1:10 Glycine 7%: dist. water	
50 mM NaCl		
0,1% (V/V) Tween-20		
Water		

washed for 15 min in a glycine stripping buffer to remove antibodies and used again to test another antibody against a protein of interest or loading control. The list of all antibodies used for western blotting is listed at the end of the Material & Method chapter.

3.9. Real Time PCR

RNeasy Plus Mini Kit (Qiagen) was used following the manufacturer's instruction to extract RNA from MLE12 cells. From each sample, 1.5 µg of RNA was reverse-transcribed to cDNA using Omniscript Reverse Transcription Kit (Qiagen) and Oligo-dT primers (Applied Biosystem). Real-time PCR was performed by using PowerUpTM SYBR Green Master Mix (Thermo Fisher) and Mx3000P PCR instrument (Agilent). Relative mRNA expression levels were calculated using the ΔCT and ΔΔCT methods, accordingly to which ΔCT is defined by

$$CT_{\text{gene of interest}} - CT_{\text{housekeeping gene}}.$$

List of used primers

Mouse ATF6 for	AATGCCAGTGTC CCAGCAA	[Hühn, 2013]
Mouse ATF6 rev	GCGCAGGCTGT ATGCTGA	[Hühn, 2013]
Mouse β-actin for	CTACAGCTTCAC CACCACAG	[Korfei et al., 2008]

Mouse β-actin rev	CTCGTTGCCAATAGTGATGAC	[Korfei et al., 2008]

3.10. Statistical analysis

All data are given as mean ± SD that were calculated from at least three independent measurements. Statistical significance between two groups was estimated using the unpaired two-sided Student's t-test. For comparison of more than two groups, ANOVA with Bonferroni's multiple comparison test was performed. Data were checked for normal distribution by Shapiro–Wilk test. Calculations were done with GraphPad Prism version 8.0.0 and OriginPro. p-value 0.05 and lower was considered as significant.

3.11. Lists of used reagents and equipment

3.11.1. List of used reagents

2-(4-(2-Hydroxyethyl)-1-piperazinyl)-ethansulfonsäure (HEPES)	Carl Roth, Karlsruhe, Germany
2-(4,2-Hydroxyethyl)-piperazinyl-1-2-amino-2hydroxymethyl-1,3-propanediol (Tris)	Carl Roth, Karlsruhe, Germany
2-Mercapto-ethanol	Sigma Aldrich, Germany
4′,6-diamidino-2-phenylindole (DAPI)	Sigma-Aldrich, München, Germany
Acetic acid	Sigma-Aldrich, München, Germany
acrilamide solution, Rotophorese Gel 30	Roth, Germany

Ammonium Persulfate (APS)	Roth, Germany
Bromphenol blue	Sigma Aldrich, Germany
BSA (Bovine-serum-albumin)	Carl Roth, Karlsruhe, Germany
Cell Strainer 100µm, 70µm	BD Bioscience, Franklin Lakes, USA
Citric-acid-monohydrate	Carl Roth, Karlsruhe, Germany
CO_2 independent medium	Gibco, Germany
Culture plates: 12 and 24 wells	Greiner Bio, Kremsmünster, Austria
D-(+)-Glucose	Roth, Germany
DAKO Fluorescence mounting medium	Agilent, Santa Clara, USA
Disodium Phosphate Dihydrate (Na_2HPO_4 x $_2H_2O$)	Merck, Darmstadt, Germany
Dispase	BD Bioscience, USA
DMEM-F12 Medium	Gibco, Germany
DNAse (Powder)	Sigma-Aldrich, München, Germany
Dneasy blood and tissue kit	Qiagen, Germany
Dulbecco's Phosphate Buffered Saline (PBS)	Sigma-Aldrich, München, Germany
Ethanol 100 Vol%	Carl Roth, Karlsruhe, Germany
Ethanol 70 Vol%	Carl Roth, Karlsruhe, Germany
Ethanol 96 Vol%	Carl Roth, Karlsruhe, Germany

Ethanol 99 Vol%	Carl Roth, Karlsruhe, Germany
Ethylendiamintetraacetate (EDTA)	Merck, Darmstadt, Germany
Falcon Tubes 10ml, 50ml	Thermo-Fischer-Scientific, Waltham, USA
Fetal Bovine Serum (FBS)	Sigma-Aldrich, München, Germany
Genecetin/G418	Roth, Germany
Glycerol	Roth, Germany
Glycine	Roth, Germany
Hank's balanced salt solution (HBSS)	PAN Biotech, Aidenbach, Germany
HindIII	New England BioLabs
Hydrobeta-estradiol	Sigma Aldrich, Germany
Hydrochloric acid (HCl) 32%	Sigma Aldrich, Germany
Hydrocortison	Sigma Aldrich, Germany
Hygromycin	Roth, Germany
Immobilon Western Chemiluminescent HRP Substrate, Millipore	Millipore, Germany
L-Glutamine	Gibco, Germany
Low melt Agarose (3 Vol%)	Carl Roth, Karlsruhe, Germany
Luciferase assay kit	Promega, Germany
Methanol 99,9%	Roth, Germany

Milk Powder	Roth, Germany
Monopotassium phosphate (KH_2PO_4)	Merck, Darmstadt, Germany
N,N,N´,N´-tetramethyl-1-1,2-diaminomethane (TEMED)	Sigma Aldrich, Germany
Na-deoxyholate	Merck, Darmstadt, Germany
Natriumcitrate-dihydrate	Carl Roth, Karlsruhe, Germany
Normal donkey serum (NDS)	Jackson Immunoresearch, West Grove, USA
NP-40	Sigma Aldrich, Germany
Nucleotide Mix (dNTP)	Qiagen, Germany
Oligo(dT) Primers	Roth, Germany
Omniscript RT Kit	Qiagen, Germany
PageRuler™ Prestained Protein Ladder	Thermo Scientific, USA
Paraffine, Paraolast Plus	Sigma Aldrich, Germany
Penicillin-Streptomycin	Sigma-Aldrich, München, Germany
Phenyl-methyl-sulfonil fluoride) PMSF	Thermo Scientific, USA
Phosphatase Inhibitor Cocktail Set III™	Thermo Scientific, USA
Pierce BCA Protein Assay Kit	Thermo Scientific, USA
Potassium chloride (KCl)	Merck, Darmstadt, Germany
PowerUp™ SYBR Green Master mix	(Thermo Fisher)

RNeasy Plus Mini Kit	Qiagen, Germany
Sodium Chloride (NaCl)	Sigma Aldrich, Germany
Sodium Citrate Tribasic Dihydrate	Sigma Aldrich, Germany
Sodium Dodecyl Sulfate (SDS)	Carl Roth, Karlsruhe, Germany
Sodium Hydroxid (NaOH)	Sigma Aldrich, Germany
Sodium Phosphate (monobasic, anhydrous)	Sigma Aldrich, Germany
Sudan Black	Sigma-Aldrich, München, Germany
Triton-X 100 (Tr-X)	Sigma-Aldrich, München, Germany
Trypsin/EDTA	PAA, Austria
TurboFect	Thermo Scientific, USA
Tween 20	Sigma-Aldrich, München, Germany
Western Chemiluminescent HRP Substrate	Millipore, Germany
Xylene (Dimethylbenzen)	Carl Roth, Karlsruhe, Germany

3.11.2. List of used equipment

Analytocal Balance	Mettler Toledo, Switzerland
BD FACSCanto II	BD Bioscience, Franklin Lakes, USA
Cell culture bench MSC Advantage	Heraeus, Hanau, Germany
Cell culture incubator, HERAcell 150i	Thermo Scientific, germany

Cell Scrapers	Costar, USA
Centrifuges Rotina 380, Rotina 46R	Hettich, Tuttlingen, Germany
Ceramic beads	PeqLab, Germany
Chemostar imager	Intas
Evos FL2 Imaging system	Thermo Fisher Scientific
Falcon Roller	CAT, Germany
Falcon tubes	Greiner, Germany
Freezer, -20°C -80°C	Bosch, Germany
Fridge +4°C	Bosch, Germany
Glass bottles	Roth, Germany
Glass pipettes	Gtreiner, Germany
Heating block VLM EC2	VLM, Bielefeld, Germany
Heracell Vios 160i CO2 incubator	Thermo-Fischer-Scientific, Waltham, USA
Leica RM 2235 Microtome	Leica Biosystems, Nussloch, Germany
Leica VT1000S Vibratome	Leica Biosystems, Nussloch, Germany
Light microscope, Axiovert 25	Carl Zeiss, Jena, Germany
Mini spin centrifuge	Eppendorf, Hamburg, Germany
MIRAX DESK	Carl Zeiss Micro Imaging, Jena, Germany

Multifuge centrifuge	Eppendorf, Hamburg, Germany
Mx3000P PCR machine	Agilent, Germany
NanoDrop	PeqLab, Germany
NanoZoomer 2.0 RS Slidescanner	Hamamatsu, Japan
PAP Pen for Immunostaining	Kisker Biotech GmbH & Co. KG
Petri Dishes	Sarstedt, Germany
Ph meter	MettlerToledo, Germany
Pipet tips	Eppendorf, Hamburg, Germany
Pipettes, Pipetboy	Eppendorf, Hamburg, Germany
Pipetting aid	Eppendorf, Hamburg, Germany
Precellys Homogeniser	PeqLab, Germany
PVDF Transfer Membran, Hybond™-P	GE Heathcare, UK
SpectralFluorophore Plus	Tecan, Germany
SuperFrost Ultra Plus™ Adhesion Slides	Menzel Glaser GmbH & Co. KG / Thermo Scientific Germany
Vortex-Genie 2	Scientific Industries, New York, USA
Waterbath	Leica Biosystems, Nussloch, Germany
Western blot chambers	Bio-Rad, USA
Wet blot transfer	Bio-Rad, USA

Whatmann paper	GE Heathcare, UK
Zeiss Axiovert 25	Zeiss, Oberkochen, Germany

3.11.3. List of used software

Axio Observer ZEN software, version 1	Carl Zeiss MicroImaging
EVOS FL Auto 2 Imaging System Software	Thermo Fischer Scientific
FIJI	BMC Bioinformatics
FlexiWare Version 7.6, Service Pack 4	EMKA Technologies, France
FlowJo™ v10.8	BD Life Sciences, Ashland
GraphPad Prism version 8.0.0	GraphPad Software, San Diego, California USA, www.graphpad.com
Microsoft Office	Microsoft Corporation (2018) www.office.microsoft.com
NDP.view2 Viewing software	Hamamatsu, Germany
OriginPro	OriginLab Co., Northampton, MA, USA
R Core Team (2020). R: A language and environment for statistical computing.	R Foundation for Statistical Computing, Vienna, Austria. www.R-project.org
Visiopharm NewCast computer-assisted stereology system	Visiopharm, Hoersholm, Denmark

3.11.4. List of used antibodies and dyes

Anti-ABCA3 (mouse polyclonal)	Seven Hills (WMAB-17-H5-24)	1:200 IF
Anti-α SMA (rabbit polyclonal)	Abcam (ab5694)	1:500 IF
Anti-ATF4 (goat polyclonal)	Abcam (ab1371)	1:200 IF
Anti-ATF6 (rabbit polyclonal)	Abcam (ab37149)	1:200 IF
Anti-beta actin (rabbit polyclonal)	Abcam (ab8227)	1:5000 WB
Anti-Calnexin (rabbit polyclonal)	Abcam ab22595	1:100 IF
Anti-Calreticulin (rabbit polyclonal)	Abcam (ab2907)	1:200 IF
Anti-CD31 PE/Cy7 (mouse)	Biolegend (102418)	1:400 FC
Anti-CD326 / EPCAM APC/Cy7 (mouse)	Biolegend (118218)	1:400 FC
Anti-CD45 PE/Cy7 (mouse)	Biolegend (103114)	1:400 FC
Anti-CHOP (mouse monoclonal)	Cell signaling (2895)	1:100 IF
Anti-Cleave PARP (rabbit polyclonal)	Abcam (ab32064)	1:100 WB
Anti-Cleaved caspase-3 PE (rabbit)	Cell signaling (9978)	1:100 FC
Anti-Collagen I (rabbit polyclonal)	Rockland, 600-401-103	1:500 IF
Anti-Collagen IV (rabbit polyclonal)	Abcam (ab6586)	1:200 IF

Anti-Cytokeratin 5 (rabbit)	Abcam (ab53121)	1:200 IF
Anti-Fibronectin (mouse polyclonal)	BD Biosciences (BD610077)	1:500 IF
Anti-GAPDH (rabbit monoclonal)	Abcam (ab181602)	1:5000 WB
Anti-GRP78/BiP (chicken polyclonal)	Abcam (ab89789)	1:200 IF, FC
Anti-HSP70 (rabbit monoclonal)	Abcam (ab79852)	1:100 IF
Anti-Influenza A Virus Nucleoprotein FITC (mouse)	Abcam (ab20921)	1:100 FC
Anti-Ki67 (rabbit polyclonal)	Abcam (ab15580)	1:500 IF
Anti-SPC (goat polyclonal)	Santa-Cruz (sc-7706)	1:500 IF,1:100 FC
Anti-XBP1s (rabbit monoclonal)	Cell signaling (12782)	1:100 IF
DAPI	Sigma (D9542)	0.5 mg/ml IF
Donkey F(ab´)2 anti-goat IgG Alexa Fluor® 488	Abcam (ab150138)	1:500 IF, FC
Donkey F(ab´)2 anti-goat IgG Alexa Fluor® 647	Abcam (150139)	1:500 IF
Donkey F(ab´)2 anti-mouse IgG Alexa Fluor® 488	Abcam (ab181289)	1:500 IF

Donkey F(ab´)2 anti-rabbit IgG Alexa Fluor® 488	Abcam ab181346	1:500 IF
Donkey F(ab´)2 anti-rabbit IgG Alexa Fluor® 555	Abcam (ab150070)	1:500 IF
Goat Anti-Chicken IgY Alexa Fluor® 488	Abcam (ab150173)	1:500 IF, FC
Zombie Violet™ Fixable dye	Biolegend (423113)	1:500 IF

4. Results

4.1. ATF6 branch of UPR

4.1.1. Stable transfected ATF6p50 overexpressing MLE12 cells

To investigate the ATF6 branch of UPR and its potential role in lung fibrosis, a stable transfected inducible ATF6p50 (referred to as ATF6 from here on) overexpressing MLE12 cell line was created. For this purpose, I used a Tet-on system that consists of two components; (1) a doxycycline-inducible transcriptional activator rtTA expressed under the SP-C promoter, and (2) a Tetracycline Response Element carrying the gene of interest (GOI) and luciferase on either side of a bidirectional CMV promoter. This system allows simultaneous doxycycline (dox)-regulated expression of the GOI and the reporter gene (luciferase). Thus, several clones were created and screened (see material and methods chapter 3). Clone # 3 had the highest level of luciferase activity after one day of induction with 1 mg/ml dox (Fig. 9A). Therefore, it was used for Figure 9, the transgene was detected in all days of dox treatment on protein and RNA levels (Fig. 9 B, C, D). Further analysis and experiments. ATF6 expression in this clone was analyzed by western blot, RT-PCR, and luciferase assay on days 1, 2, and 3 after dox induction. As shown in Figure 9, the transgene

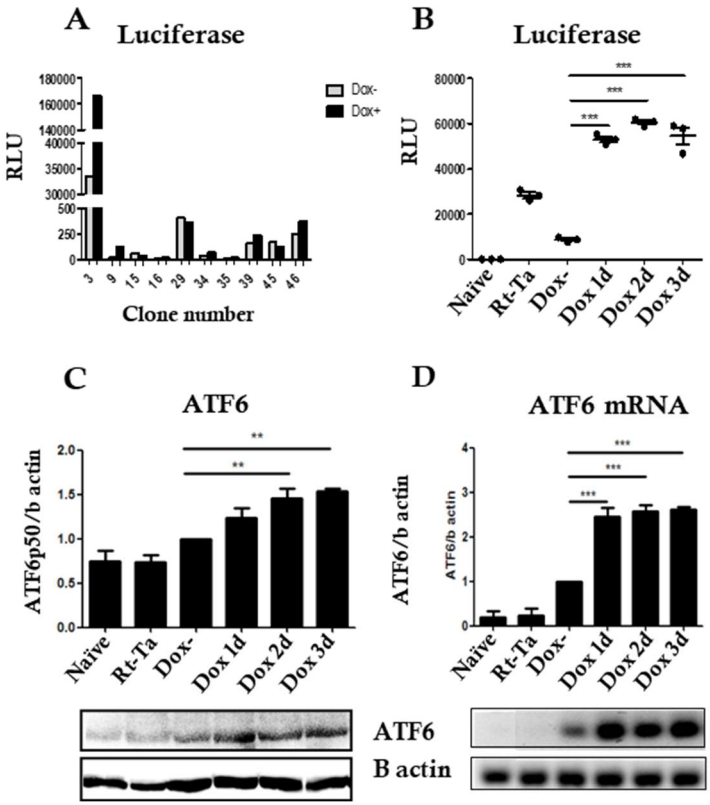

Figure 9. Analysis of inducible ATF6p50 overexpressing MLE12 cells

A. *Screening of inducible ATF6p50 overexpressing MLE12 cell populations for stable, high producing clones using luciferase assay.* ***B.*** *Luciferase activity of selected clone # 3 in different time points.* ***C.*** *Protein level of ATF6 p50 in selected clone # 3 in different time points.* ***D.*** *ATF6 mRNA expression level in selected clone # 3 in different time points. Data for B, C and D are normalized to dox- control and expressed as means ± SD from n=3 independent experiments, with analysis by unpaired Student's t test. * p<0.05, ** p<0.01, *** p<0.001*

was detected in all days of dox treatment on protein and RNA level (Fig. B,C,D).

4.1.1.1. Crosstalk of ATF6 with other UPR mediators

The cross-talk among UPR branches has been previously described [Nishitoh, 2012; Pobre et al., 2019; Tsuru et al., 2016; Yoshida et al., 2001], but the mechanism behind this it is still not fully understood. In this regard, I investigated whether overexpression of the activated form of ATF6, named ATF6p50, affects the two other UPR pathways ATF4 and XBP1. Western blot analysis showed upregulation of XBP1 and GRP78/BiP in induced, compared to non-induced, cells after 24 and 48h of dox treatment (Fig. 10). At the same time, ATF4 and its downstream target CHOP were not affected (Fig. 10A, B). Consistent with the lack of upregulation of the pro-apoptotic factor CHOP, there was no significant difference in the apoptosis level, as determined by the expression of the cleaved (activated) caspase 3 in dox treated cells compared to non-treated cells (Figure 10A). These data suggest that ATF6 overexpression impacts the XBP1, but not the ATF4 branch of the ER stress in MLE12 cells.

4.1.1.2. Impact of ATF6p50 overexpression on fibroblasts activation

Abundant ECM protein expression and proliferation of fibroblasts are considered as hallmarks of lung fibrosis. To determine if ATF6 overexpression in epithelial cells is sufficient to induce a pro-fibrotic phenotype of lung fibroblasts, the murine fibroblast MLg cell line (ATCC CCL206) was treated with conditioned media from induced or non-induced ATF6 overexpressing MLE12 cells. Thrombin (Trm), a procoagulant factor, was used as a positive control. It was chosen as its ability to induce a pro-fibrotic phenotype in fibroblasts was well described in several publications [Bogatkevich et al., 2001; Ludwicka-Bradley et al., 2004]. Thus, ATF6 overexpressing MLE12 cells were induced with dox for 24 and 48 h, after which their culture medium was transferred to MLg cells. MLg were incubated for additional 24 hours and processed for proliferation analysis by WST1 and BrdU ELISA assay. As expected, thrombin effectively induced cell proliferation, but there was no significant difference between treatments with conditioned medium from ATF6 induced and non-induced MLE12 cells (Fig. 11A, B). Additionally, the production of ECM proteins collagen I and collagen IV were analyzed by

western blotting. As shown in Figure 11C, there was a non-significant increase in collagen I level in MLg cells incubated in the culture medium after 48h of ATF6 induction. At the same time, there was no difference in collagen IV expression between all experimental samples. Positive control thrombin, in its turn, effectively induced the expression of both proteins. Put together, this data suggests that ATF6 overexpression does not seem to promote a pro-fibrotic phenotype *in vitro*.

4.1.2. Inducible ATF6p50 overexpressing transgenic mice

To assess the consequences of ATF6 activation *in vivo*, I used the AECII-specific inducible transgenic mouse line SP-C rtTA/tetO7-ATF6p50 (termed ATF6 overexpressing mice), developed in our laboratory by Dr. Martin Hühn. Generation of the transgenic mouse line and validation of transgene expression in alveolar epithelial type II (AECII) cells was performed by Dr. Hühn and has been published in his dissertation [Martin Hühn, 2012]. Briefly, the transgenic system used to induce ATF6 was identical to the one used in the stably transfected MLE12 cells in the previous section. Transgenic mice expressing ATF6 and luciferase under the bi-directional Tet-On promoter were crossed with driver mice expressing rtTA transgene under the SP-C promoter [Perl et al., 2009].

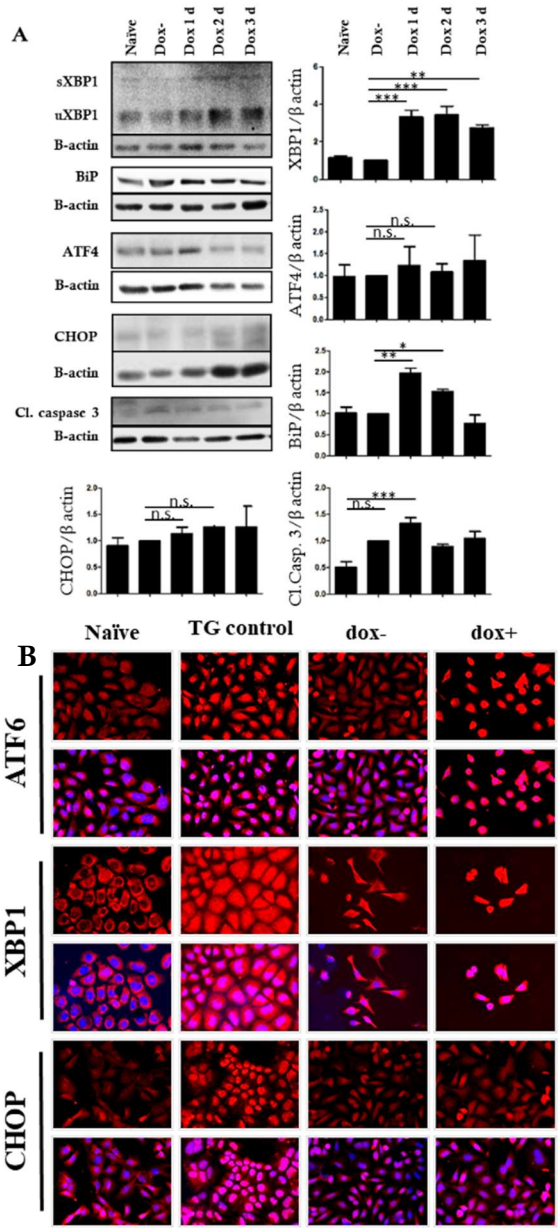

Figure 10. Impact of ATF6p50 overexpression on its downstream targets in MLE12 cells

A. *Western blots and densitometry quantification. Data are normalized to dox- control, expressed as means ±SD from n= 3 independent experiments and analyzed by unpaired Student's t test. *p< 0.05, ** p<0.01, *** p<0.001.* ***B.*** *Representative pictures of immunofluorescence staining of inducible ATF6p50 overexpressing MLE12 cells after 24h dox treatment. Cells treated with 1μM thapsigargin (TG) were used as a positive control.*

4.1.2.1 Efficiency of ATF6 overexpression

To determine the short- and long-term consequences of ATF6 overexpression *in vivo*, ATF6 overexpressing mice were exposed to dox for 2 days, 28 days, 6 months, and 12 months. At each time point, mouse lungs (n=3-5) were analyzed for ATF6 protein expression and luciferase activity (Fig. 12A and 13A). Maximal luciferase expression was noted at day two and was followed by a consistent decrease in expression level. Analysis of immunofluorescent staining with anti-ATF6 antibody showed similar results. The transgene expression was highly activated on day two and slowly decreasing on other analyzed time points.

To further quantify the number of transgene-overexpressing cells, I took advantage of the strong upregulation of BiP (a downstream target of ATF6) in ATF6 overexpressing mice [Haze et al., 1999; Morishima et al., 2011] (Fig. 12B). The reason for switching to BiP analysis was an anti-ATF6 antibody limitation and obtaining much more precise results by using an anti-BiP antibody. Thus, I performed immunofluorescence co-staining for BiP and proSP-C (an AECII specific marker).

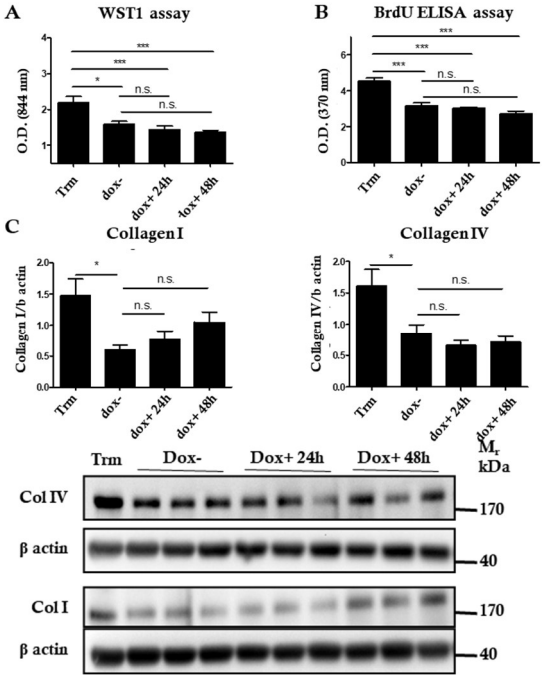

Figure 11. Impact of ATF6 expression in epithelial cell on fibroblast activation

A. *WST1 proliferation assay. After 24 and 48 h of transgene induction in ATF6 p50 overexpressing MLE12 cells, cell culture medium was transferred to MLg fibroblasts. After another 24 h of incubation, WST1 assay was performed. Fibroblasts treated with 1μg/ml thrombin (Trm) were used as positive control.* ***B.*** *BrdU assays. After 24 and 48 h of transgene induction in ATF6 p50 overexpressing MLE12 cells, cell culture medium was transferred to MLg fibroblasts. After another 24 h of incubation BrdU ELISA assay was performed. Fibroblasts treated with 1μg/ml thrombin (Trm) were used as a positive control.* ***C.*** *Western blots and densitometry quantification. Analysis of MLg fibroblasts for Collagen I and Collagen IV expression. All data are expressed as means ± SD, from n= 3 independent experiments and analyzed by unpaired Student's t test, *p< 0.05, ** p<0.01, *** p<0.001.*

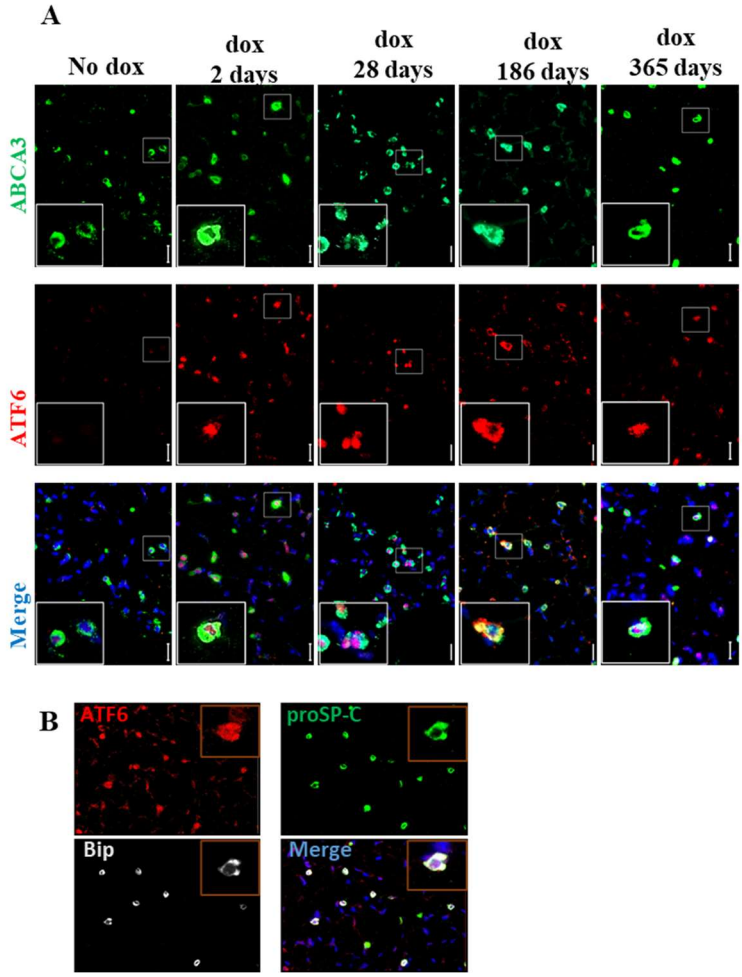

Figure 12. Transgene expression in lungs of SP-C rtTA/tetO7-ATF6p50 transgenic mice over one year

A. *IF staining of mouse lung tissue in different time points of dox feeding. ABCA3 was used as a marker of AECII.* ***B.*** *Representative picture of colocalization of ATF6, BiP and proSP-C in dox-induced mouse lung The number of biological replicates was 3-5 in each treatment group, the number of technical replicates was 3 per a mouse (whole sections).*

The number of BiP^{high} expressing AECIIs was quantified by using the following formula:

$$\textit{\% of transgene overexpressing AECII} = (N_{BiP^{high}\,SP\text{-}C^{pos}\,cells} * 100) / N_{SP\text{-}C^{pos}}\ \textit{cells}$$

These data followed the trend of the luciferase assay data with efficient protein expression at day two and downregulation at later time points (Fig. 13). The only difference was that BiP was still highly upregulated at day 28 when the reporter activity was already downregulated. Since

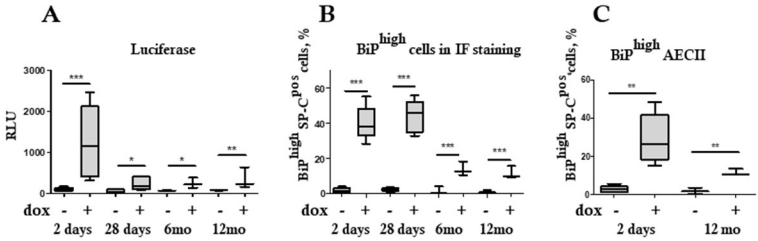

Figure 13. Transgene expression efficiency in lungs of SP-C rtTA/tetO7-ATF6p50 transgenic mice

A. *Luciferase activity in response to dox food.* ***B.*** *Quantification of BiP^{high} AECII cells in IF staining of lung tissue.* ***C.*** *Flow cytometry. Number of BiP^{high} AECII in mouse lungs after 2 days and 12 moths of transgene induction. Data are expressed as box plots where the horizontal lines represent 25th ,50th and 90th percentiles and the vertical lines represent min and max values, analyzed by unpaired Student's t test. The number of biological replicates was 3-5 in each treatment group, the number of technical replicates was 3 per a mouse (whole sections or probes). *p< 0.05, ** p<0.01, *** p<0.001.*

BiP is a downstream target of ATF6, it probably could explain its prolonged expression.

To further consolidate the transgene expression data, I turned to flow cytometry evaluation of BiP expression. Mouse lungs from day 2 and day 365 (12 months) were dissociated into single cells, and the proportion of BiP^{pos} cells was determined within the living, $CD45^{neg}$, $CD31^{neg}$, $EpCAM^{pos}$, $proSPC^{pos}$ cells (Fig. 13C). Thus, the flow cytometry data confirmed the robust transgene expression at day two and its marked decrease at day 365.

The time-dependent decrease in transgene expression suggests the presence of compensatory mechanisms either at the intra-cellular level (increase in protein degradation or promoter-inactivation) or at the tissue level (culling of ATF6 pos cells and replacement by the proliferation of AECII progenitors). To distinguish between these possibilities, the number of AECII and the level of proliferation and apoptosis were determined on days 2 and 28. Flow cytometry was used to quantify the number of AECII ($CD45^{neg}$ $CD31^{neg}$ $EpCAM^{pos}$ $proSPC^{pos}$) (Fig. 14A). The level of proliferation was analyzed by immunofluorescence staining for Ki67, and the apoptosis level was examined using western blotting for cleaved PARP1 (Fig. 14B, C). Neither apoptosis,

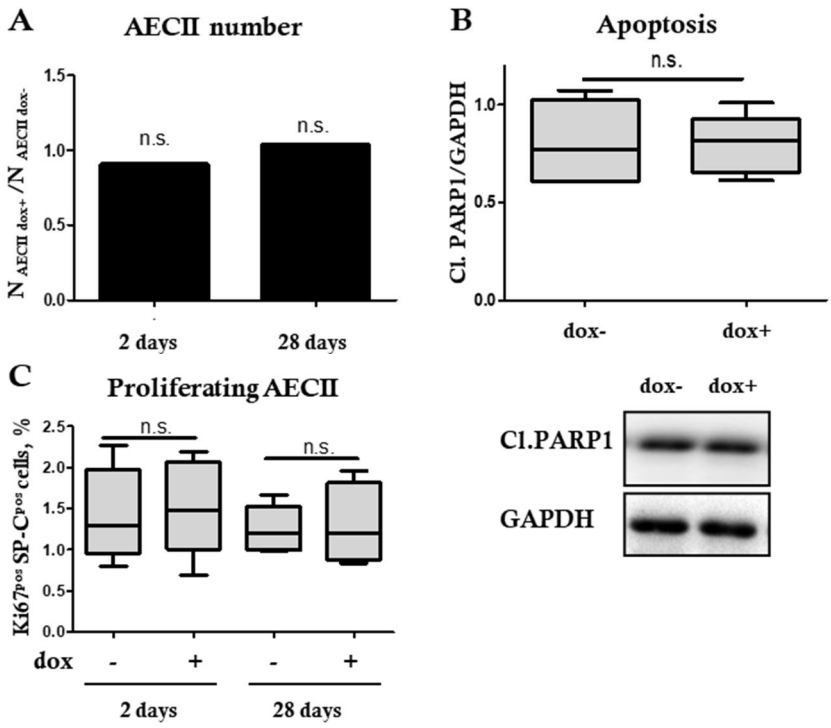

Figure 14. Analysis of AECIIs in lungs of SP-C rtTA / tetO7-ATF6p50 overexpressing mice

A. *Flow cytometry analysis of the number of AECIIs (CD45^{neg} CD31^{neg} EpCAM^{pos} proSP-C^{pos}) in the mouse lungs of 2 days and 28 days induced compared to non-induced controls (n=3-5).* ***B.*** *Western blotting and densitometry quantification of expression of cleaved PARP 1 in lung tissue from mice after 28 days of dox feeding.* ***C.*** *IF staining. Quantification of number of Ki67^{pos} AECII cells in the mouse lungs at day 2 and day 28 of transgene expression. For B and C data are expressed as box plots where the horizontal lines represent 25th ,50th and 90th percentiles and the vertical lines represent min and max values. All data were analyzed by unpaired Student's t test. The number of biological replicates was 3-5 in each treatment group, the number of technical replicates was 3 per a mouse (whole sections).*

proliferation, nor AECII number were increased at any of the studied time points, suggesting that most probably the decrease in transgene expression was the result of activation of cell-intrinsic mechanisms like epigenetic changes at the promoter level.

4.1.2.2 Expression of ATF6 downstream targets

The previously described BiP data suggested that the maximum expression of ATF6 downstream target genes was attained by day 28 of dox treatment. Therefore, I focused my analysis on this time point to determine other downstream targets of ATF6. As expected, ATF6 overexpression led to chaperone upregulation (GRP78/BiP, Calreticulin, and Calnexin) and the transcription factor XBP1 (Fig. 15). Thus, *in vivo* and *in vitro* data correspond with existing knowledge about ATF6 downstream targets.

4.1.2.3 Pro-fibrotic markers in the lungs of ATF6 overexpressing mice

To determine the tissue-level consequences of ATF6 overexpression, Masson-Goldner's staining of mouse lung tissue was performed. No obvious fibrotic phenotype was observed at all-time points of dox-treatment (Fig. 16C).

These data come along with the results from Dr. M. Hühn and confirm that ATF6p50 overexpression *in vivo* was

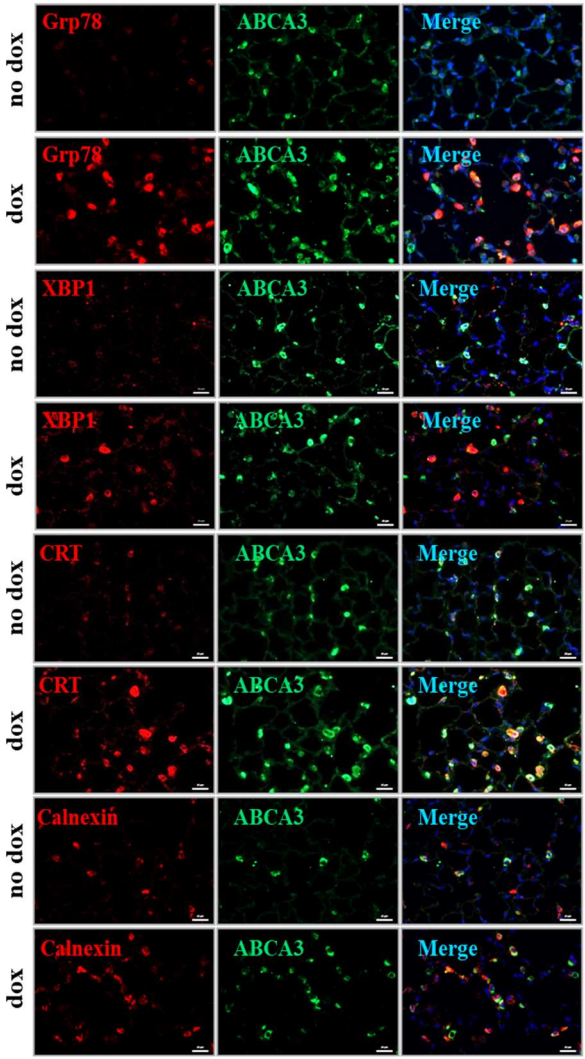

Figure 15. Representative pictures of IF staining of lung tissue from inducible rtTA/tetO7-ATF6p50 transgenic mice for downstream targets of ATF6 at day 28 of transgene expression

The whole stained lung sections were analyzed. The number of biological replicates 3-5 in each treatment group, the number of technical replicates 3 per a mouse (whole sections).

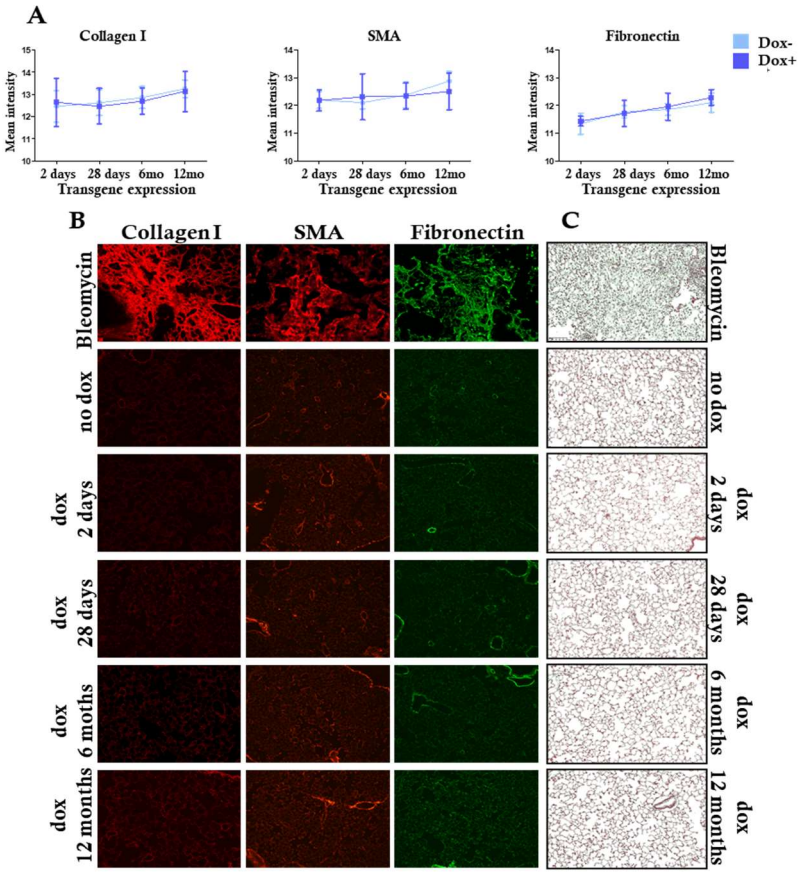

Figure 16. Dynamics of ECM protein expression in the lungs of SP-C rtTA/tetO7-ATF6p50 transgenic mice over one year

A. *Quantification of IF staining as integrated density. Data are expressed as mean values of groups ± SD with analysis by Student's t test, the number of biological replicates 3-5 in each treatment group, the number of technical replicates 3 per a mouse (whole sections).* ***B.*** *Representative images of IF staining for fibrotic markers at various time points of transgene expression.* ***C.*** *Representative images of Masson-Goldner's trichrome staining at various time points of transgene expression. Lung tissue from a bleomycin treated mouse was used as a positive control.*

not sufficient to induce epithelial apoptosis and lung fibrosis. Although ATF6 overexpression did not result in overt fibrosis, it still could promote a pro-fibrotic phenotype. To determine this, I performed immunofluorescence analysis of collagen I, alpha-smooth muscle actin (SMA), and fibronectin in mouse lungs after 2 days, 28 days, 6 months, and 12 months of dox treatment and compared it to the results from relevant untreated (n=3-5) control mice. From each mouse, three whole sections of lung tissue were used to quantify the immunofluorescence signal. Results revealed no significant changes in any of the analyzed markers (Fig. 16A, B). Therefore, the data demonstrate that AECII specific ATF6 overexpression is not sufficient to provoke the pro-fibrotic phenotype of murine lungs.

4.1.3. Impact of ATF6p50 expression on bleomycin induced lung fibrosis

The impact of ATF6 overexpression on lung fibrosis development was evaluated using the bleomycin mouse model. At first, ATF6 was induced for four days, after which dox-induced and non-induced mice were treated with bleomycin or NaCl and sacrificed on day 28 for analysis (Fig. 17). Since ATF6 has apoptotic potential, it was expected that its overexpression could exacerbate bleomycin-induced lung

Figure 17. Experiment overview

Briefly, 4 days dox treated and dox untreated mice were additionally treated with bleomycin or NaCl and sacrificed on day 28 for analysis.

fibrosis. Therefore, a mild dose of bleomycin was chosen for this experiment (2.5U/kg). The number of mice per group was three to six.

4.1.3.1 Evaluation of lung injury

To evaluate the level of injury after bleomycin treatment, mice were scored and weighed every day of the experiment. No differences were observed between Bleo dox- and Bleo dox+ groups. At the same time, one mouse in the NaCl dox- group spontaneously and dramatically lost weight during the experiment, which drastically affected the dynamics of the whole control group (Fig. 18C).

Several publications showed that patches of cytokeratin 5 positive ($CK5^{pos}$) epithelial cells arise in the lung parenchyma during tissue regeneration and re-epithelization after injury. Moreover, the size of $CK5^{pos}$ patches is

proportional to the level of injury [Bruen et al., 2004; Kanegai et al., 2016; Vaughan et al., 2015; Zuo et al., 2015]. Based on this knowledge, I determined CK5 expression by immunofluorescence staining to evaluate the bleomycin-induced injury level. While $CK5^{pos}$ cell pods were observed in the lungs from all bleomycin treated mice, no significant differences were observed between dox induced and non-induced groups (Fig. 18A, B).

Also, western blotting analysis with late apoptotic marker PARP showed no difference in apoptosis level between Bleo dox+ and Bleo dox- mice (Fig. 21B). These data suggested that ATF6 overexpression does not induce cell or tissue sensitivity to bleomycin injury in mice.

4.1.3.2. Evaluation of morphological and structural changes in lung tissue

Fibroblast accumulation, changes in alveolar size, and septal thickness are typically seen in fibrotic lungs. Therefore, Masson-Goldner's trichrome staining was performed to evaluate mouse lung tissue alterations together with extracellular matrix deposition. Although fibrotic areas were observed in most samples from Bleo dox- and Bleo dox+ groups, there was no difference between these groups evaluating the lung tissue by light microscopy (Fig. 19).

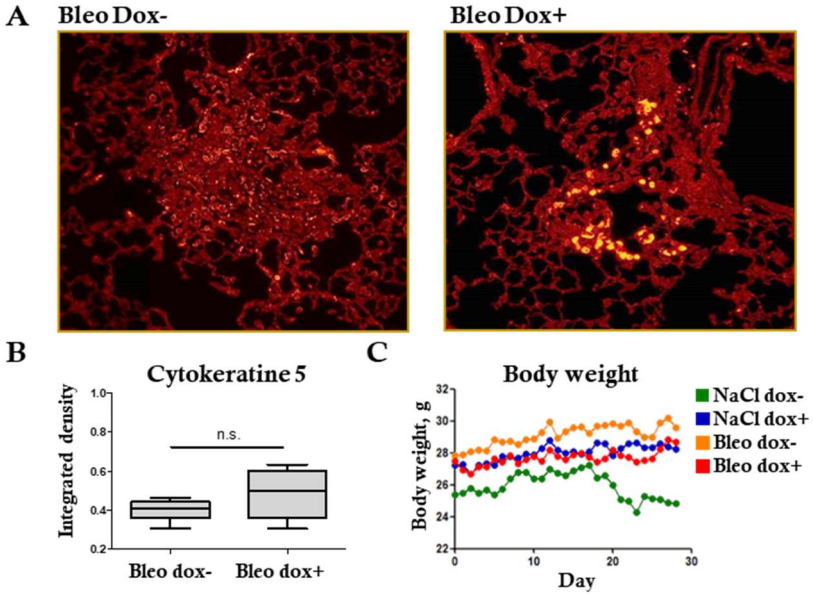

Figure 18. Evaluation of injury in lung tissue from inducible rtTA/tetO7-ATF6p50 transgenic mice after bleomycin treatment

A. *Representative pictures of IF staining of lung tissue with anti-CK5 antibodies.* ***B.*** *Quantification of anti-CK5 antibodies fluorescence signal as integrated density. Data are expressed as box plots where the horizontal lines represent 25th ,50th and 90th percentiles and the vertical lines represent min and max values, analyzed by unpaired Student's t test. The number of biological replicates 3-6 in each treatment group, the number of technical replicates 3 per a mouse (whole sections).* ***C.*** *Dynamic of mice body weight after bleomycin treatment. Data are expressed as a mean of a group, n=3-6.*

In the next step, morphometric analysis was performed using the mean linear intercept method. It showed a significant decrease in septal thickness and alveolar diameter in Bleo dox+ group compared to Bleo dox- but not in NaCl dox+ compared to NaCl dox- (Fig. 20A, B). Additionally, kernel density estimation was applied to see the distribution of the septal thickness and alveolar size values. In support of the previous data, there was a shift in the distribution in favor of smaller alveolar size in the Bleo dox+ group compared to Bleo dox- (Fig. 20C). At the same time, there was almost no difference in septal thickness values distribution between the groups.

Thus, ATF6 overexpression only marginally affected the lung tissue morphometry of Bleo dox+ mice compared to Bleo dox- mice.

4.1.3.3. Evaluation of pro-fibrotic markers in lung tissue

Immunofluorescence (IF) staining and western blotting were used to detect the level of ECM proteins in the lungs of ATF6 induced and non-induced mice after bleomycin administration. For this, whole three lung tissue sections from each mouse were analyzed using IF staining for collagen I, SMA, and fibronectin. The slides were scanned

using the EVOS imaging system, and staining intensity was quantified by ImageJ software. As shown in Figure 21a, there is an increase of collagen I, fibronectin, and SMA in all Bleo treated mice, but no significant difference between Bleo dox- and Bleo dox+ mice. Although, the level of ECM proteins in the Bleo dox+ group tended to be higher.

Additionally, the western blotting analysis showed a significant increase of Collagen I in the lungs of Bleo dox+ mice compared to Bleo dox- mice, but no difference in Collagen IV level (Fig. 21b). Thus, ATF6 overexpression seems not to have profound additional effect to increase pro-fibrotic markers in bleomycin-treated lungs. Nevertheless, probably the dose of bleomycin was not high enough to induce a more pronounced effect. This idea is also supported by the fact that all bleomycin-treated mice developed only mild fibrosis.

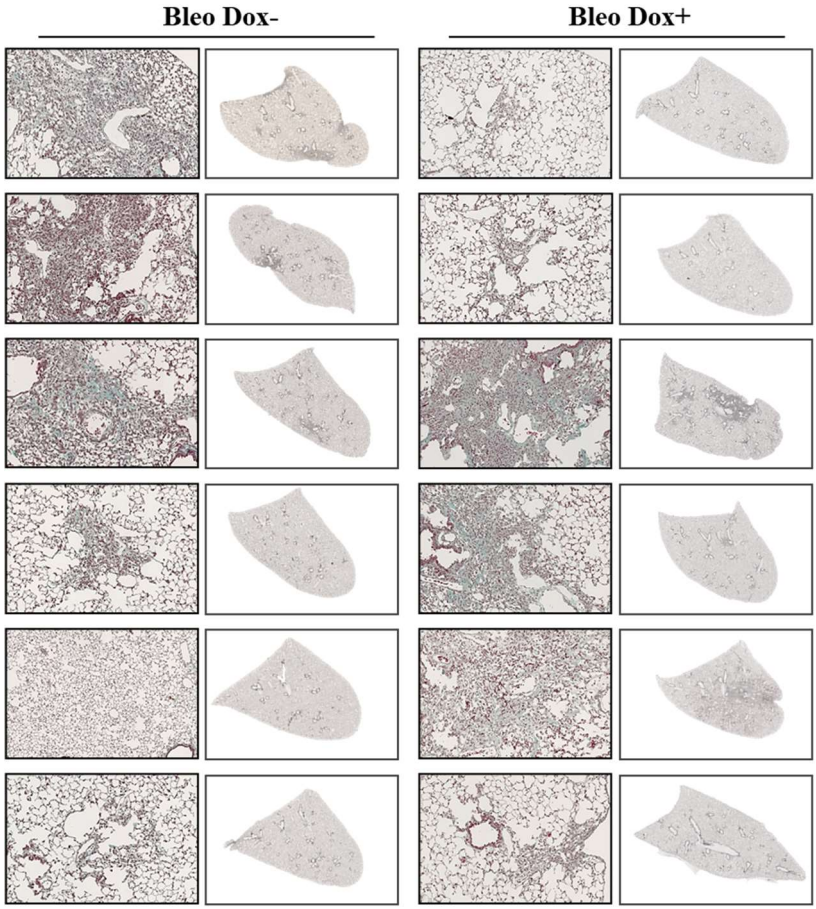

Figure 19. Representative pictures of Masson-Goldner's trichrome staining of lung tissue from inducible rtTA/tetO7-ATF6p50 transgenic mice after bleomycin treatment (N=6)

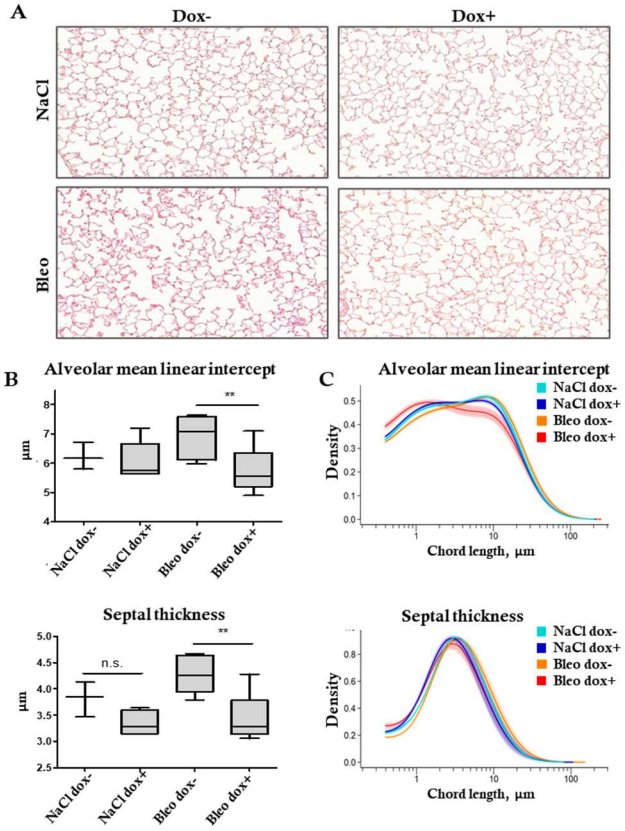

Figure 20. Morphometry of lungs from inducible rtTA/tetO7-ATF6p50 transgenic mice after bleomycin treatment

A. *Representative pictures of H&E staining of alveolar regions of lung tissue.* ***B.*** *Morphometric analysis of septal thickness and alveolar mean linear intercept. Data are expressed as box plots where the horizontal lines represent 25th ,50th and 90th percentiles and the vertical lines represent min and max values, analyzed by Bonferroni's multiple comparison test. The number of biological replicates was 3-6 in each treatment group, the number of technical replicates was 3 per a mouse (whole sections). **p< 0.01.* ***C.*** *Morphometric analysis of septal thickness and alveolar mean linear intercept. Data are shown as a probability density estimate function. The displayed curves represent point-wise mean values from individual densities within a group, and the shaded area indicates the standard errors.*

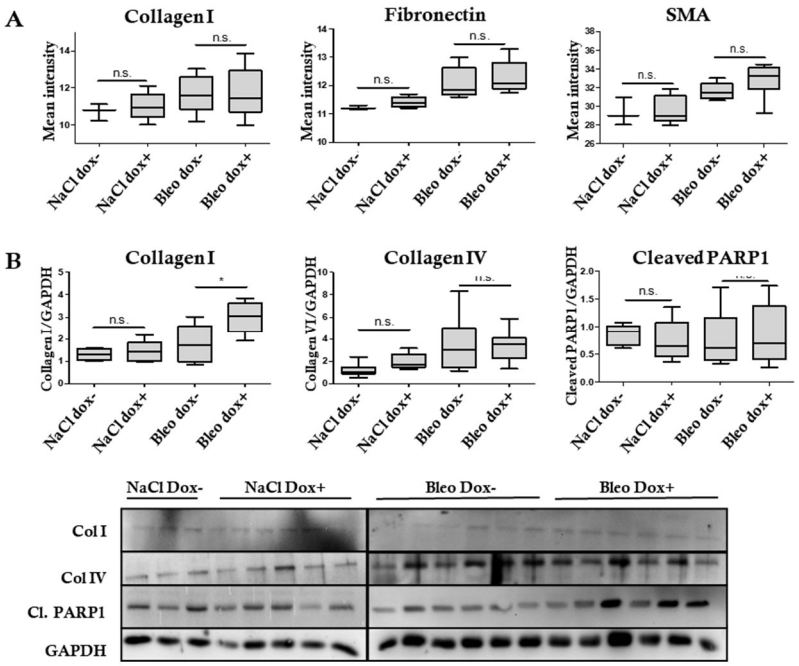

Figure 21. Impact of ATF6p50 on expression of ECM protein in bleomycin induced fibrosis

A. *Quantified IF signal in lung tissue staining with pro-fibrotic markers.* ***B.*** *Western blotting and densitometry quantification for Collagen I, Collagen IV and cleaved PARP1. All data are expressed as box plots where the horizontal lines represent 25th ,50th and 90th percentiles and the vertical lines represent min and max values, analyzed by Bonferroni's multiple comparison test. The number of biological replicates 3-6 in each treatment group, the number of technical replicates 3 per a mouse (whole sections or blots). *p< 0.05.*

4.1.3.4. Evaluation of respiratory mechanics of mice

Fibrosis leads to disturbances in lung function, and its examination is the first step in clinical diagnosis. Therefore, mouse lung function also was tested by FlexiVend and described by static compliance, inspiratory capacity, tissue elastance, and PV-loop. As shown in Figure 22, no significant difference was observed in any of these parameters between the Bleo dox- and Bleo dox+ groups. Therefore, and as shown before, ATF6p50 overexpression on top of bleomycin exposure did not seem to cause additional changes.

4.1.4. Impact of ATF6p50overexpression on influenza infection

Acute exacerbation (AE) of IPF is a severe deterioration and leads to a high one-year mortality level of patients. What causes AE is a theme of many debates, but viral and bacterial infections are considered as potential triggers. It is also well known that The UPR is upregulated in the infected cells as a part of innate antiviral immune response [Frabutt et al., 2018], and, at the same time, viruses can use UPR to support their needs [Phillips et al., 2017; Hebert et al., 1997; Hogue; Nayak, 1992; Choukhi et al., 1998]. Therefore, as ER stress markers already present in fibrotic lung tissue, it could affect viral infection one way or

another. To study this, I used 250µm precision-cut lung slices (PCLS) from ATF6 overexpressing mice. Animals (n=3-5) were fed with dox food to overexpress transgene for two days and sacrificed for isolation of lung and PCLS generation. PCLS were then immediately infected with influenza virus PR8 and incubated in a medium with or without dox regarding the experimental settings (Fig. 23). Samples were collected 48h p.i. for flow cytometry analysis. All epithelial cells ($EpCam^{pos}$, $CD45/CD31^{neg}$) were used to characterize the level of infection via nucleoprotein expression (NP) and apoptosis via cleaved caspase 3 expression. Dead cells were marked by Zombie fixable dye and cleaved caspase 3^{neg} $Zombie^{pos}$ cells were marked as necrotic cells. As shown in figure 24, there was no significant difference in infection level or the number of necrotic cells. But the number of apoptotic cells was significantly elevated in infected, dox-induced PCLS compared to infected PCLS without dox. It suggests that ATF6 overexpression did not affect the level of IV infection but increased the death level of the epithelial cells after the viral infection.

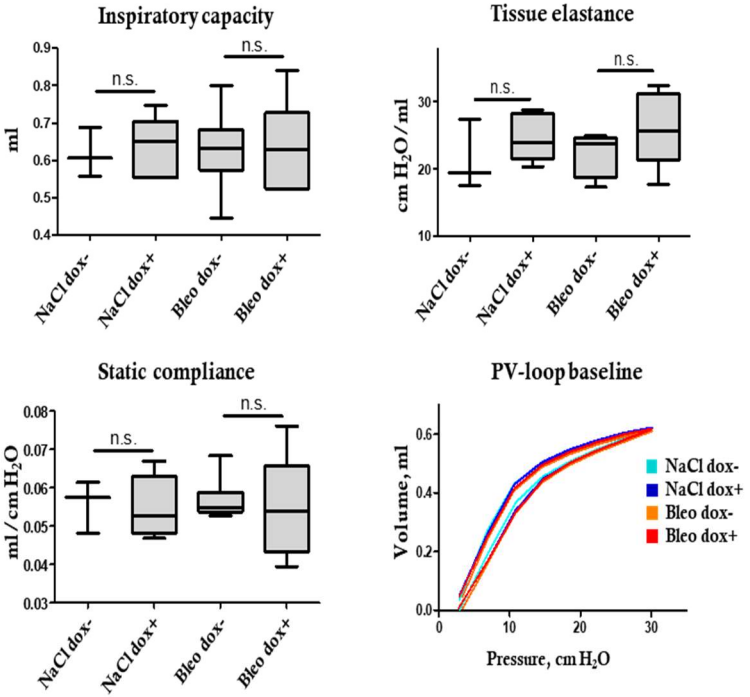

Figure 22. Mechanical function of lung from inducible rtTA/tetO7-ATF6p50 transgenic mice after bleomycin treatment

*Lung mechanical function and mechanical properties. Data are expressed as box plots where the horizontal lines represent 25th ,50th and 90th percentiles and the vertical lines represent min and max values, analyzed by Bonferroni's multiple comparison test. The number of biological replicates was 3-6 in each treatment group *p< 0.05, ** p<0.01, *** p<0.001.*

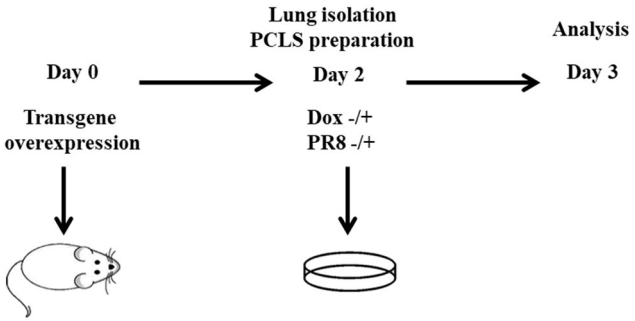

Figure 23. Experiment overview

After 2 days of transgene expression mice were sacrificed and one lobe was cut with a chopper to make PCLS for following infection. Cells from PCLS were analyzed at 48h p.i. by flow cytometry.

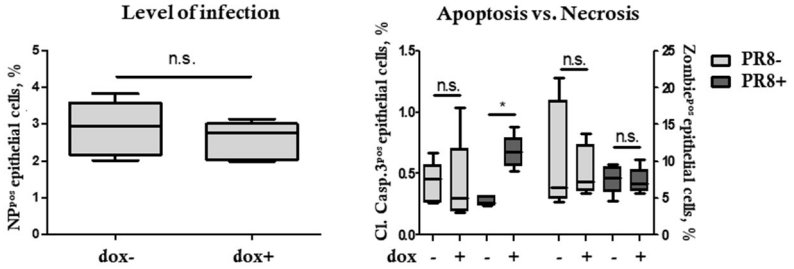

Figure 24. Impact of ATF6p50 on influenza virus infection

*Epithelial cells (CD45/31^{neg} EpCam^{pos}) from PCLS were analyzed for IV infection by Nucleoprotein (NP) and apoptosis by Cleaved caspase 3. Necrotic cells are defined as Cleaved caspase 3^{neg} Zombie^{pos} cells. Data are expressed as box plots where the horizontal lines represent 25th ,50th and 90th percentiles and the vertical lines represent min and max values, analyzed by unpaired Student's t test or Bonferroni's multiple comparison test. *p< 0.05, the number of biological replicates 3-5 in each treatment group.*

4.2. XBP1 branch of UPR

4.2.1. Inducible XBP1s overexpressing transgenic mice

To investigate the impact of the XBP1 pathway on lung fibrosis development, a SP-C rtTA/tetO7-XBP1s (referred to as XBP1 from here on) mouse line was created. The generation of this transgenic mouse line was described by Dr. Hühn in his doctoral thesis [Martin Hühn, 2012]. Briefly, transgenic mice expressing XBP1s and luciferase under the bi-directional Tet-On promoter were crossed with driver mice expressing rtTA transgene under the SP-C promoter [Perl et al., 2009]. Furthermore, the same work strategy as for ATF6 overexpressing mice was applied for XBP1s overexpressing mice. And the first step was the analysis of transgene efficiency in AECII during different time points.

4.2.1.1. Efficiency of XBP1s overexpression

To determine the short- and long-term consequences of XBP1 *in vivo* overexpression, XBP1 overexpressing mice were exposed to dox for 1, 28, 168, and 365 days. At each time point, mouse lungs (n=4-5) were analyzed for XBP1 protein expression and luciferase activity. Three sections of lung tissue from each mouse were stained with anti-XBP1s and anti-SP-C antibodies (Fig. 25D). Double positive cells

were counted as transgene overexpressing AECII using the following equation:

$$\textit{\% of transgene overexpressing AECII} = (N_{XBP1s^{pos}\,SP\text{-}C^{pos}\,cells} * 100) / N_{SP\text{-}C^{pos}\,cells}$$

As shown in figure 25A, the highest number of XBP1s overexpressing AECII were observed on day 1. At the same time, the level of luciferase expression was still strong at day 28 of dox induction (Fig 25B). It probably can be explained by a very short half-life of XBP1 protein compared to luciferase (less than 1 hour vs. 50 hours). The same as for ATF6 overexpressing mice, XBP1 overexpressing mice have a time-dependent decrease in transgene expression. Since no change in the number of AECII or level of proliferation and apoptosis was observed in ATF6 mice lungs, I wanted to know if the same occurred in XBP1 mice lungs. To answer this question, the number of AECII ($CD45^{neg}$ $CD31^{neg}$ $EpCAM^{pos}$ $proSPC^{pos}$) at day 1 and 28 of dox exposure was determined by flow cytometry (Fig. 25C), proliferation level by immunofluorescence staining for Ki67 (Fig. 26B), and apoptosis level by western blot analysis for Cleaved PARP1 (Fig. 26C). None of these parameters were changed at any studied time points. Thus, similar to ATF6, the decrease in XBP1s expression can be a result of epigenetic changes.

4.2.1.2. Expression of downstream targets of XBP1

Previous data suggested that the highest level of transgene expression was during the first four weeks. Therefore, XBP1 downstream targets were determined on day 28. IF staining showed the upregulation of chaperons BiP and HSP70 and transcription factor ATF6 but not ATF4 (Fig. 26A). These data are consistent with published literature.

4.2.1.3. Pro-fibrotic markers in the lungs of XBP1 overexpressing mice

The Masson-Goldner's staining was performed to determine the consequences of XBP1s overexpression at all-time points on lung structure. No obvious fibrotic phenotype was observed following transgene induction. These data support the results of Dr. M. Hühn and suggest that XBP1 overexpression alone is not enough to induce fibrotic tissue alterations.

Nevertheless, XBP1 overexpression could induce a pro-fibrotic phenotype. To determine this, I performed immunofluorescence analysis of ECM proteins in lungs of 1 day, 28 days, 6 months, and 12 months dox treated or untreated mice (n=3-5). From each mouse, whole three

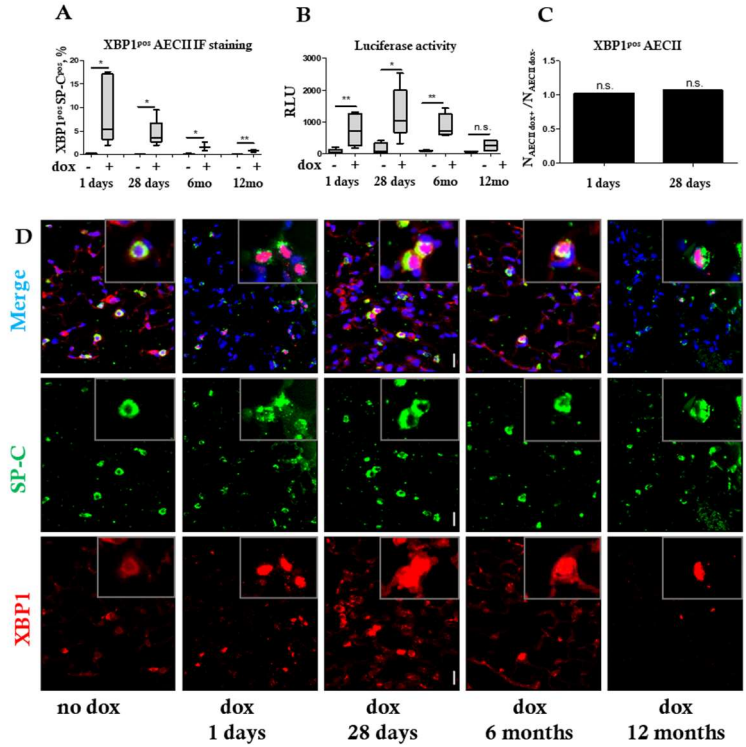

Figure 25. Transgene expression efficiency in lungs of SP-C rtTA/tetO7-XBP1s transgenic mice

A. *Quantification of XBP1s^{pos} AECII cells (SP-C^{pos}) in IF staining of lung tissue.* ***B.*** *Luciferase activity in response to dox food. RLU, relative luciferase units. For A and B data are expressed as box plots where the horizontal lines represent 25th ,50th and 90th percentiles and the vertical lines represent min and max values, analyzed by unpaired Student's t test. The number of biological replicates 4-5 in each treatment group, the number of technical replicates 3 per a mouse (whole sections or probes). *p< 0.05, ** p<0.01, *** p<0.001.* ***C.*** *Flow cytometry analysis of the number of AECIIs (CD45^{neg} CD31^{neg} EpCAM^{pos} proSPC^{pos}) in the lungs of 1 day and 28 days induced compared to non-induced controls (n=4-5).* ***D.*** *Representative pictures of IF staining of lung tissue with anti-XBP1s and anti-proSP-C antibodies.*

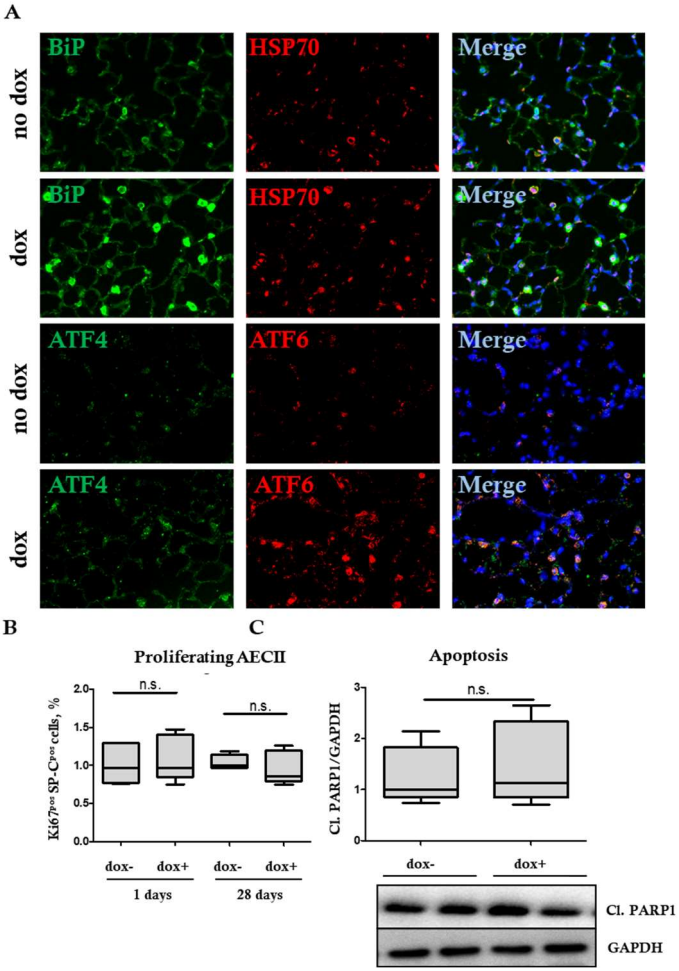

Figure 26. Analysis of inducible rtTA/tetO7-XBP1s transgenic mice

A. *Representative pictures of IF staining with anti-BiP, anti-HSP70, anti-ATF4 and anti-ATF6 antibodies.* ***B.*** *Quantification of Ki67^{pos} AECII cells in IF staining of lung tissue. The number of biological replicates 4-5 in each treatment group, the number of technical replicates 3 per a mouse (whole sections).* ***C.*** *Expression of cleaved PARP 1 in lung tissue from mice after 28 days of dox feeding was analysed by western blot. Data are expressed as box plots where the horizontal lines represent 25th ,50th and 90th percentiles and the vertical lines represent min and max values, analyzed by unpaired Student's t test, n=4-5.*

sections of lung tissue were used to quantify the immunofluorescence signal.

The analysis revealed no significant changes in collagen I, SMA, or fibronectin (Fig. 27). Hence, *in vivo* AECII specific overexpression of XBP1 is not sufficient to induce pro-fibrotic phenotype in mice lung.

4.2.2. Impact of XBP1 on bleomycin induced lung fibrosis

To explore the impact of XBP1 overexpression on lung fibrosis development, 4 days dox-induced and non-induced mice were additionally treated with bleomycin or NaCl and sacrificed on day 28 for analysis (Fig. 28). Because XBP1 can behave as a pro-apoptotic factor, it was expected that its overexpression could exacerbate bleomycin-induced lung fibrosis. Therefore, a mild dose of bleomycin was used for this experiment (2.5U/kg). The number of mice per group was five to six.

4.2.2.1. Evaluation of lung injury

To evaluate the level of injury after bleomycin treatment, mice were scored and weighed every day of the experiment. No difference was observed between Bleo dox- and Bleo dox+ groups, and, thus, XBP1 overexpression did not seem to affect health scores of mice. (Fig. 29C).

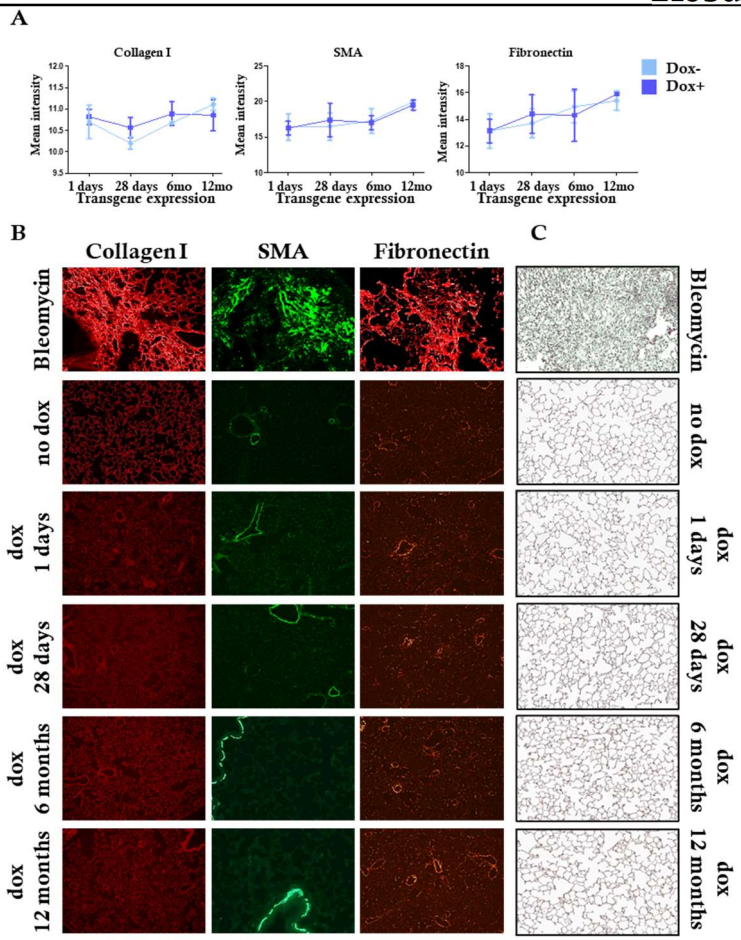

Figure 27. Pro-fibrotic markers in lung tissue from inducible rtTA/tetO7-XBP1s transgenic mice

A*. Quantification of IF staining as integrated density. The number of biological replicates 4-5 in each treatment group, the number of technical replicates 3 per a mouse (whole sections). Data are expressed as mean values ± SD and analyzed by unpaired Student's t test.* ***B.*** *Representative images of IF staining for fibrotic ECM markers at various time points of transgene expression.* ***C.*** *Representative images of Masson-Goldner's trichrome staining at various time points of transgene expression. Lung tissue from a bleomycin treated mouse was used as a positive control.*

Figure 28. Experiment overview

Briefly, 4 days dox treated and dox untreated mice were additionally

As mentioned in chapter 3.1.3.1, patches of cytokeratin 5 positive ($CK5^{pos}$) epithelial cells arise in the lung parenchyma during tissue regeneration and re-epithelization after injury, and their size is proportional to the injury level. $CK5^{pos}$ cells pods appeared in the mouse lungs of both bleomycin-treated groups. Nevertheless, the Bleo dox+ group had a mild, but non-significant, increase of immunofluorescence signal compared to the Bleo dox- group (Fig. 29A, B).

Additionally, apoptosis level was measured by western blot analysis for the late apoptotic marker PARP1. Also, no difference was observed in Bleo dox+ mice compared to Bleo dox- (Fig. 32B). These data suggested that XBP1s dox induced mice were not more sensitive to bleomycin injury than non-induced mice.

4.2.2.2. Evaluation of morphological and structural changes in lung tissue

Fibroblasts accumulation and extracellular matrix deposition are typical hallmarks of fibrosis. Therefore, I performed Masson-Goldner's trichrome staining to evaluate these tissue alterations. Although fibrotic areas presented in most samples from both Bleo dox- and Bleo dox+ groups, tissue evaluation by light microscopy did not show obvious differences between the groups (Fig. 30)

Bleo dox+ mice were not higher than in Bleo dox- mice. At the same time, there was no significant change in alveolar linear intercept between all Bleo and NaCl groups (Fig. 31A, B).

Additionally, kernel density estimation was applied to see the distribution of the septal thickness and alveolar size values. It demonstrated a shift in septal thickness towards higher values and a shift in alveolar size toward smaller values in both Bleo groups, but there was no difference between Bleo dox+ and Bleo dox- mice (Fig. 31D).

Hence, XBP1 overexpression did not affect the morphology of the bleomycin-treated mouse lung tissue.

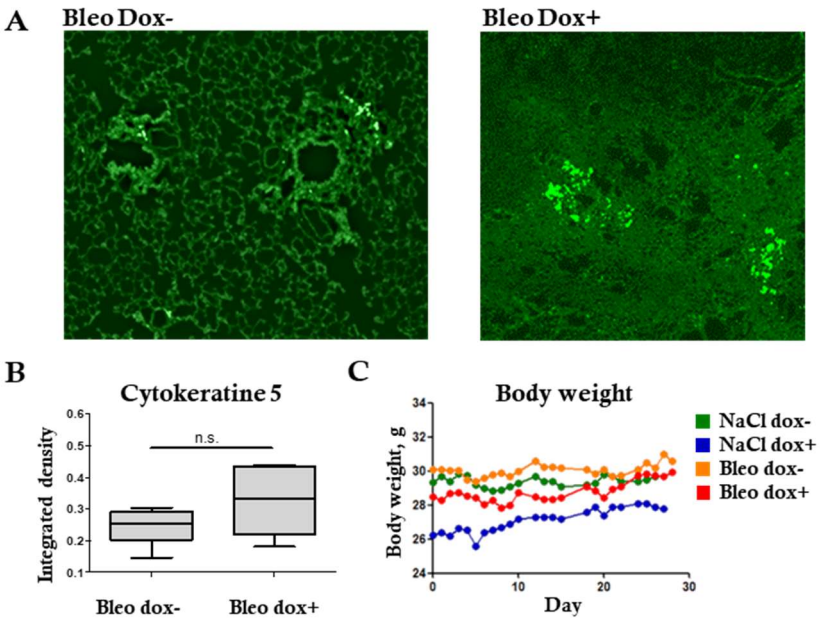

Figure 29. Evaluation of injury in lung tissue from inducible rtTA/tetO7-XBP1s transgenic mice after bleomycin treatment

A. *Representative pictures of IF staining of lung tissue with anti-CK5 antibodies.* ***B.*** *Quantification of anti-CK5 antibodies fluorescence signal as integrated density. Data are expressed as box plots where the horizontal lines represent 25th ,50th and 90th percentiles and the vertical lines represent min and max values, analyzed by unpaired Student's t test. The number of biological replicates 5-6 in each treatment group, the number of technical replicates 3 per a mouse (whole sections).* ***C.*** *Dynamic of mice body weight after bleomycin treatment. Data are expressed as a mean of group (n=5-6).*

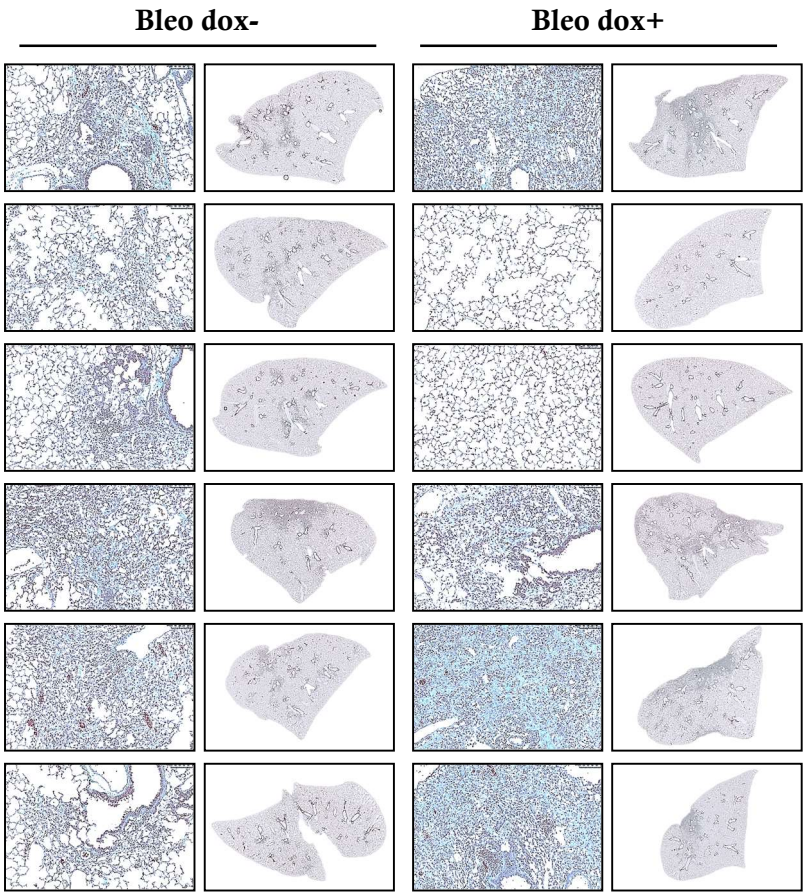

Figure 30. Impact of XBP1 on bleomycin induced fibrosis

Representative pictures of Masson-Goldner's trichrome staining of lung tissue from inducible rtTA/tetO7-XBP1s transgenic mice after bleomycin treatment (N=6)

4.2.2.3. Evaluation of pro-fibrotic ECM markers in lung tissue

Immunofluorescence (IF) and western blotting were used to analyze the level of fibrotic ECM markers in the mouse lungs after bleomycin administration. Three sections from each mouse were used for Collagen I, SMA, and fibronectin IF staining. The fluorescence signal was scanned using the EVOS imaging system and quantified by ImageJ software. As shown in Figure 32A, the level of ECM proteins was increased in all Bleo mice. Nevertheless, there was no difference between dox-induced and non-induced mice. The western blotting analyzes for Collagen I and Collagen IV also showed similar results. There was an increase of Collagens in both Bleo groups, but no difference between Bleo dox+ and Bleo dox- mice was observed (Fig. 32B).

4.2.2.4. Evaluation of respiratory mechanics of mice

The decline in lung function is one of the symptoms of IPF. Therefore, a lung function test is an important measure in clinical diagnosis and can reflect the severity of the disease. For this reason, mouse lung function was tested by FlexiVend and was assessed by static compliance, inspiratory capacity, tissue elastance, and PV-loop values. As shown in Figure 31C, no significant difference was observed in any of these

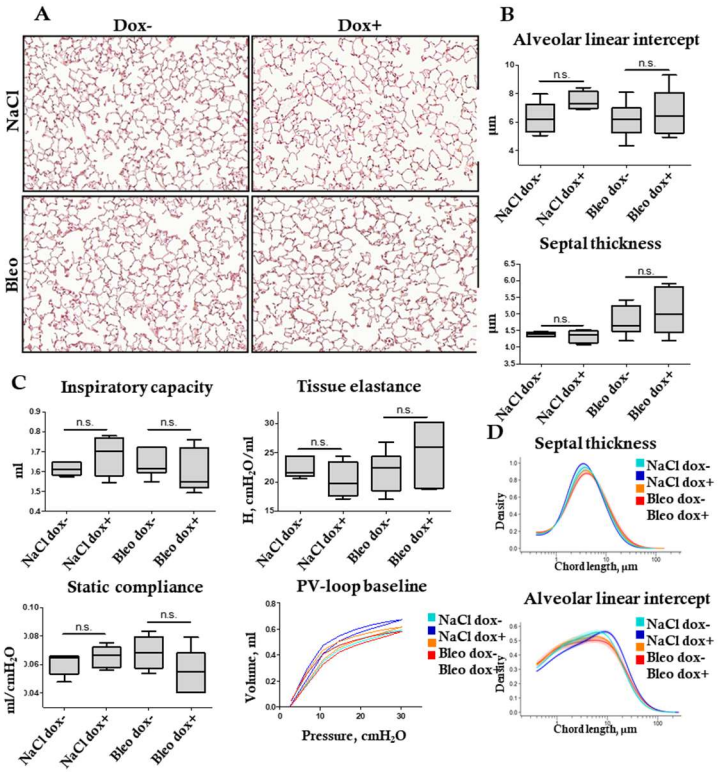

Figure 31. Morphometry and mechanical function of lung from inducible rtTA/tetO7-XBP1s transgenic mice after bleomycin treatment

A. *Representative pictures of H&E staining of alveolar region in lung tissue.* ***B.*** *Morphometric analysis of septal thickness and alveolar mean linear intercept.* ***C.*** *Lung mechanical function and mechanical properties. Data for B and C are expressed as box plots where the horizontal lines represent 25th ,50th and 90th percentiles and the vertical lines represent min and max values, analyzed by Bonferroni's multiple comparison test. The number of biological replicates was 5-6 in each treatment group, the number of technical replicates in B was 3 per a mouse (whole sections).* ***D.*** *Morphometric analysis of septal thickness and alveolar mean linear intercept. Data are shown as a probability density estimate function. The displayed curves represent point-wise mean values from individual densities within a group, and the shaded area indicates the standard errors.*

parameters between dox-induced and non-induced mice. Nevertheless, there is a clear tendency of worsening lung function in Bleo dox+ mice compared to Bleo dox- mice.

4.2.3. Influence of XBP1 on influenza virus infection

UPR is known to be upregulated in both lung tissue of IPF patients and lung epithelial cells infected with the influenza virus (IV). At the same time, viral infections are considered a potential risk factor of acute exacerbation of IPF. Thus, activated UPR in fibrotic tissue could affect a viral infection by either boosting or reducing it. To test this theory and evaluate XBP1s impact on IV infection, I used 250µm precision-cut lung slices (PCLS). For this, XBP1 overexpressing mice (n=3-5) were fed with dox food for two days and then sacrificed for isolation of lung and preparation of PCLS. PCLS were then immediately infected with influenza virus PR8 and incubated in medium with or without dox regarding the experimental settings (Fig. 33A). Samples were collected after 48h p.i. for flow cytometry analysis. All epithelial cells ($EpCam^{pos}$, $CD45/CD31^{neg}$) were used to evaluate the level of infection by nucleoprotein (NP) and apoptosis by cleaved caspase 3. Dead cells were marked by Zombie fixable dye.

As shown in Figure 33B, the level of infection was the same in dox-induced and non-induced PCLS. At the same time, the level of apoptosis was elevated in all infected PCLS, but no difference was observed between dox + and dox- PCLS. Also, there was no significant difference in necrosis level (Fig. 33B). Thus, XBP1 overexpression did not affect the level of IV infection or epithelial cell apoptosis.

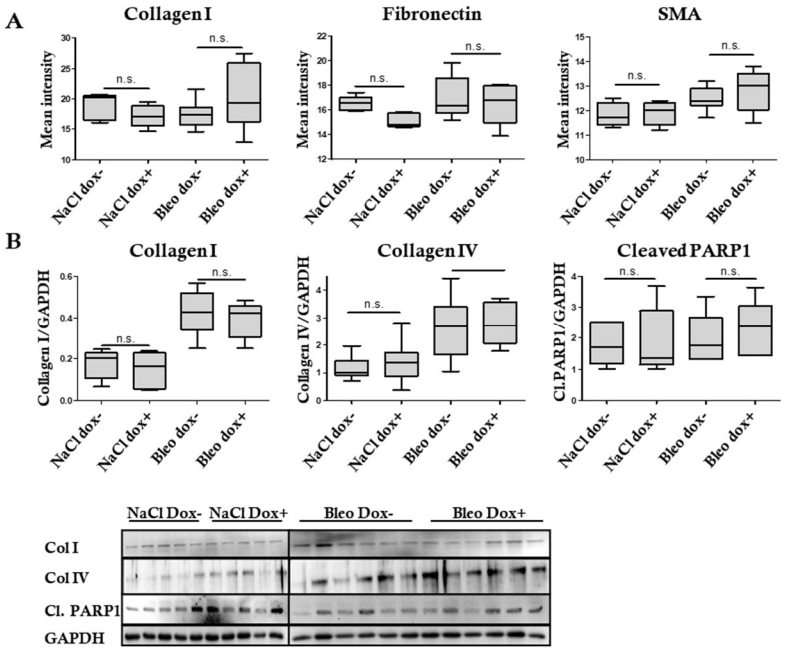

Figure 32. Impact of XBP1s on bleomycin induced fibrosis

A. *Quantified IF signal in lung tissue staining with pro-fibrotic markers.* ***B.*** *Western blotting for Collagen I, Collagen IV and cleaved PARP1 and densitometry quantification. All data are expressed as box plots where the horizontal lines represent 25th ,50th and 90th percentiles and the vertical lines represent min and max values, analyzed by Bonferroni's multiple comparison test. The number of biological replicates 5-6 in each treatment group, the number of technical replicates 3 per a mouse (whole sections).*

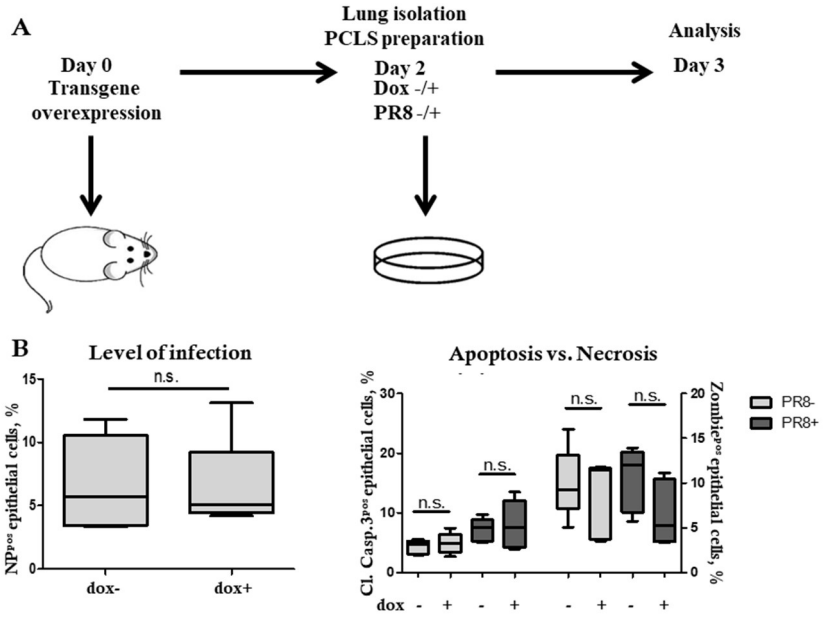

Figure 33. Impact of XBP1s on influenza virus infection

A. *Experiment overview. After 2 days of transgene activation mice were sacrificed and one lobe were cut with a chopper to make PCLS for following infection. Cells from PCLS were analyzed after 48h p.i. by flow cytometry.* ***B.*** *Epithelial cells (CD45/31^{neg} EpCam^{pos}) from PCLS were analyzed for IV infection by Nucleoprotein (NP) and apoptosis by Cleaved caspase 3. Necrotic cells are defined as Cleaved caspase 3^{neg} Zombie^{pos} cells. Data are expressed as box plots where the horizontal lines represent 25th ,50th and 90th percentiles and the vertical lines represent min and max values, analyzed by unpaired Student's t test or Bonferroni's multiple comparison test. The number of biological replicates was 3-5 in each treatment group.*

4.3. UPR downstream target CHOP

Activation of XBP1 and ATF6 during ER stress has adaptive character and is supposed to help cells to overcome the accumulation of unfolded and misfolded proteins by chaperon production [Lee, 1992; Määttänen et al., 2010; Hammond et al., 1994], translational attenuation [Trusina; Tang, 2010; Starr et al., 2018; Harding et al., 2000c; Harding et al., 1999] and ERAD machinery [Shen et al., 2007; Belmont et al., 2010].

At the same time, when alveolar epithelial cells are continuously injured, it may cause overwhelming ER stress and, together with other factors or alone, lead to cell death via CHOP-mediated apoptosis [Delbrel et al., 2018; Klymenko et al., 2019; Ma et al., 2002; McCullough et al., 2001]. This change in lung homeostasis is considered one of the first events in fibrosis development.

To test this theory and establish a possible role of CHOP in lung fibrosis development, Dr. M. Korfei and Dr. O. Klymenko created inducible rtTA/tetO7-CHOP transgenic mice. The generation of the mice and their phenotype were described in Dr. Klymenko's doctoral dissertation [Klymenko, 2016a]. The transgenic system to induce CHOP overexpression was the same as for ATF6 and

XBP1 overexpressing mice. Briefly, CHOP and luciferase reporter genes are expressed under the same bi-directional promoter that is activated by rt-TA binding in the presence of doxycycline.

4.3.1. Efficiency of transgene overexpression in CHOP mice

I used luciferase assay and IF staining to evaluate transgene efficiency in CHOP overexpressing mice after 1 day, 28 days, 6 months, and 1 year of dox+/- feeding (n=3-5). For IF analysis, three sections from each mouse were stained with anti-CHOP and anti-SP-C antibodies. Double-positive cells were counted as transgene overexpressing AECII, and their number was calculated using the following equation:

$$\textit{\% of transgene overexpressing AECII} = (N_{CHOP^{pos}SP\text{-}C^{pos}\ cells} * 100) / N_{SP\text{-}C^{pos}}\ \textit{cells}$$

As shown in Figure 34A, the peak of transgene expression was on day 1, followed by a time-dependent decrease after day 28. Luciferase activity level was also the highest on day 1 and day 28 (Fig. 34B). To explain the transgene efficiency reduction over a lifetime in CHOP overexpressing mice, I analyzed the number of AECII, their

proliferation, and apoptosis levels. Interestingly, the flow cytometry analysis showed a decrease in number of AECII in dox-induced mice (Fig. 34C). Although on day 1 of dox feeding, this reduction was not high enough in all mice to be statistically significant, on day 28, the number of AECII dramatically decreased up to 40 percent.

Western blotting analysis with anti-cleaved PARP1 antibody showed enhanced apoptosis in lung tissue from dox-induced mice, but, at the same time, the AECII proliferation level did not change (Fig. 34D, E).

Since the genetic construct for all three analyzed mouse lines was the same, it is reasonable to assume that similar epigenetic changes, if any, could have occurred in the lung tissue from all of them, causing the transgene's shut down. Nevertheless, in the CHOP mice, CHOP overexpression clearly promoted the AECII death, which was also previously described in detail by Dr. Klymenko in his thesis. Thus, CHOP-induced apoptosis presumably caused AECII number reduction in the lungs from dox-induced mice. This outcome differs from ATF6 and XBP1 overexpression, which did not affect the AECII number and level of apoptosis in mice lungs.

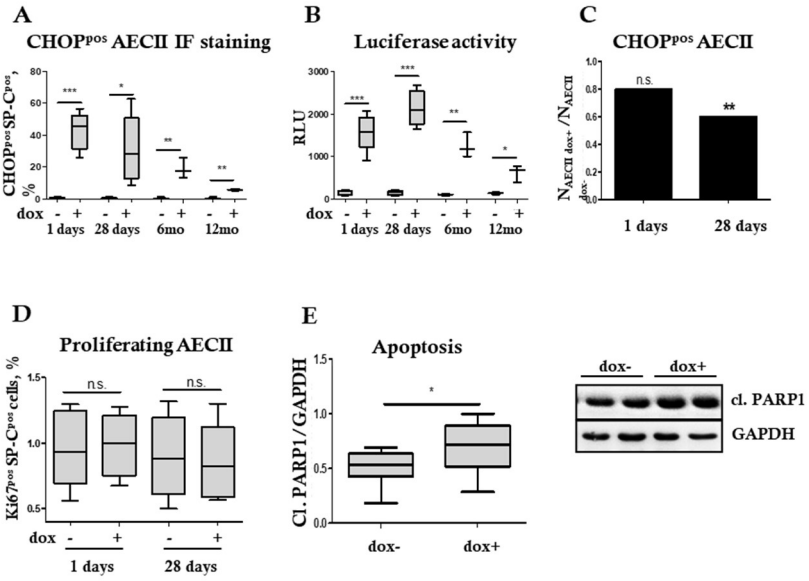

Figure 34. Transgene expression efficiency in lungs of SP-C rtTA/tetO7-CHOP transgenic mice

***A**. Quantification of CHOP^{pos} AECII cells (SP-C^{pos}) in IF staining of lung tissue. **B.** Luciferase activity in response to dox food. n=3-5. RLU, relative luciferase units. **C.** Flow cytometry analysis of the number of AECIIs (CD45^{neg} CD31^{neg} EpCAM^{pos} proSPC^{pos}) in the lungs of 1 day and 28 days induced compared to non-induced controls. **D.** Quantification of Ki67pos AECII cells in IF staining of lung tissue. **E.** Expression of cleaved PARP 1 in lung tissue from mice after 28 days of dox feeding was analysed by western blot. In A, B, D and E data are expressed as box plots, where the horizontal lines represent 25th ,50th and 90th percentiles and the vertical lines represent min and max values, analyzed by unpaired Student's t test. The number of biological replicates 3-5 in each treatment group, the number of technical replicates 3 per a mouse (whole sections or probes). *p< 0.05, ** p<0.01, *** p<0.001.*

4.3.2. Impact of CHOP on bleomycin induced lung fibrosis

To explore the impact of CHOP overexpression on lung fibrosis development, dox-induced and non-induced mice were treated with bleomycin or NaCl and sacrificed at day 28 for further analysis. As was described in chapter 3.3.1., CHOP overexpression induced AECII apoptosis. Consequently, its overexpression could exacerbate bleomycin-induced lung fibrosis and lead to a high mouse mortality rate. Therefore, a mild dose of bleomycin was used in this experiment (2.5U/kg) (Fig. 35). The number of mice per group was five to six.

4.3.2.1. Evaluation of lung injury

The same strategy as for ATF6 and XBP1 overexpressing mice was used to evaluate the severity of the injury in CHOP overexpressing mice after bleomycin treatment. Mice were scored and weighted every day of the experiment, but no difference was observed between Bleo dox+ and Bleo dox- mice (Fig. 36C).

The analysis of $CK5^{pos}$ cell patches did not reveal any significant difference between dox-induced and non-induced mice (Fig.36A, B). Nevertheless, there was a tendency to the

Figure 35. Experiment overview

Briefly, 4 days dox treated and dox untreated mice were additionally treated with bleomycin or NaCl and sacrificed on day 28 for analysis.

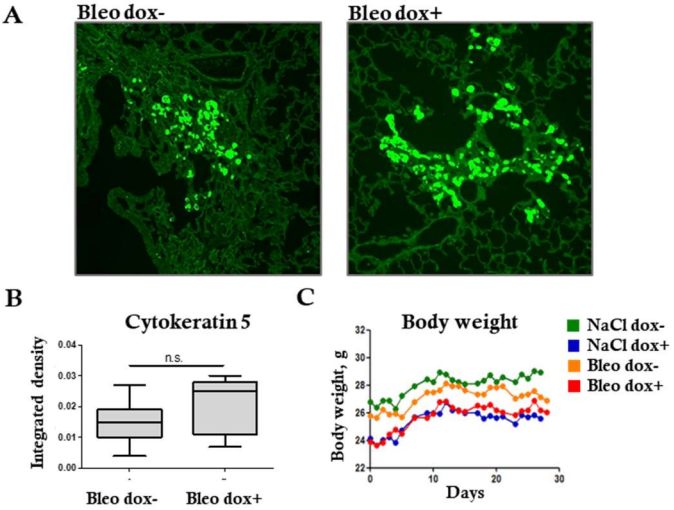

Figure 36. Evaluation of injury in lung tissue from inducible rtTA/tetO7-CHOP transgenic mice after bleomycin treatment

A. *Representative pictures of IF staining of lung tissue with anti-CK5 antibodies.* ***B.*** *Quantification of anti-CK5 antibodies fluorescence signal as integrated density. Data are expressed as box plots where the horizontal lines represent 25th ,50th and 90th percentiles and the vertical lines represent min and max values, analyzed by unpaired Student's t test. The number of biological replicates 6-7 in each treatment group, the number of technical replicates 3 per a mouse (whole sections).* ***C.*** *Dynamic of mice body weight after bleomycin treatment. Data are expressed as a mean of a group (5-6 mice per group).*

larger $CK5^{pos}$ cell areas in the Bleo dox+ group compared to the Bleo dox- group.

Additionally, mouse tissue was analyzed by western blotting for cleaved PARP1. Although apoptosis was increased in the NaCl dox+ group compared to the NaCl dox- group, no significant difference was observed between Bleo dox- and Bleo dox+ mice (Fig. 39B). Thus, against expectations, CHOP overexpression did not exacerbate bleomycin injury of mouse lung tissue.

4.3.2.2. Evaluation of morphological and structural changes in lung tissue

Lung fibrotic tissue is characterized by fibroblasts accumulation, extracellular matrix deposition, an increase of alveolar septa thickness, and a decrease of alveolar size. To evaluate these changes, I performed Masson-Goldner's trichrome staining.

Surprisingly, lung tissue of all bleomycin-treated mice was very mildly affected by fibrotic areas, and no obvious differences were observed between the groups using light microscopy (Fig. 37).

Also, morphometric analysis using mean linear intercept did not reveal any significant change in alveolar linear intercept or septal thickness values in Bleo dox+ mice

compared to Bleo dox- mice (Fig. 38 A, B). Additional kernel density estimation was applied to see the distribution of the septal thickness and alveolar linear intercept values. It showed a shift in alveolar size toward lower values in Bleo dox+ mice. At the same time, the septal thickness values did not change between the groups (Fig. 38D).

Thus, CHOP overexpression did not or barely affect the morphology of the bleomycin-treated mouse lung tissue.

4.3.2.3. Evaluation of pro-fibrotic ECM markers in lung tissue

Western blotting and immunofluorescence staining were performed to evaluate the level of ECM proteins in the lungs after bleomycin administration. Thus, for IF analysis, three sections from each mouse were stained for Collagen I, smooth muscle actin, and fibronectin. The fluorescence signal was scanned by the EVOS imaging system, and its intensity was quantified by ImageJ software. As shown in Figure 39A and B, ECM proteins were slightly increased in all Bleo mice, but there was no difference between induced and non-induced mice.

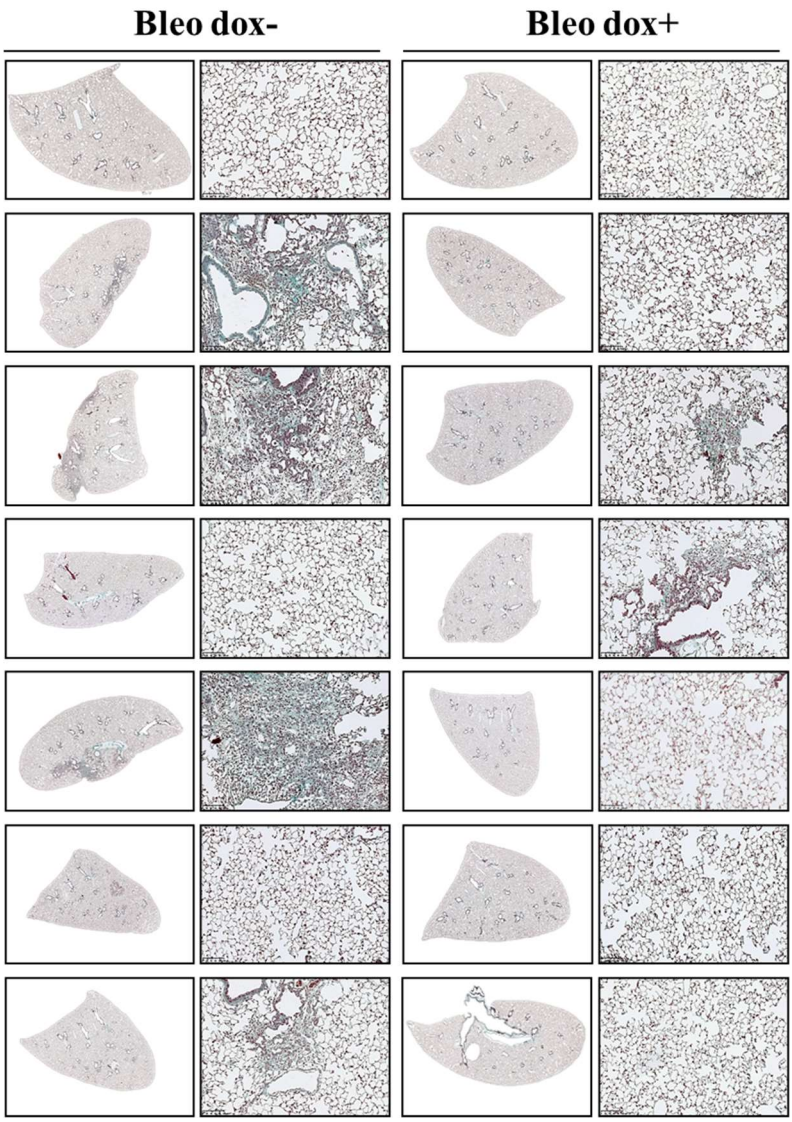

Figure 37. Impact of CHOP on bleomycin induced fibrosis

Representative pictures of Masson-Goldner's trichrome staining of lung tissue from inducible rtTA/tetO7-CHOP transgenic mice after bleomycin treatment (N=6)

The level of Collagen I and Collagen IV in the western blotting analysis was also elevated in all bleomycin-treated mice. Nevertheless, there was no significant difference between Bleo dox+ and Bleo dox- groups. This data indicates that CHOP overexpression did not influence the level of pro-fibrotic markers in mouse lung tissue after bleomycin administration.

4.3.2.4. Evaluation of respiratory mechanics of mice

Evaluation of lung function of IPF patients is one of the main parts of clinical diagnostic and can reflect the severity of the disease. Similarly, it can be applied to the mice fibrosis model. Therefore, the lung capacity of mice after bleomycin administration was measured by FlexiVend and evaluated using static compliance, inspiratory capacity, elastance, and PV-loop values. Although none of the parameters significantly changed, a clear worsening tendency was observed in Bleo dox+ mice compared to Bleo dox- (Fig. 38C).

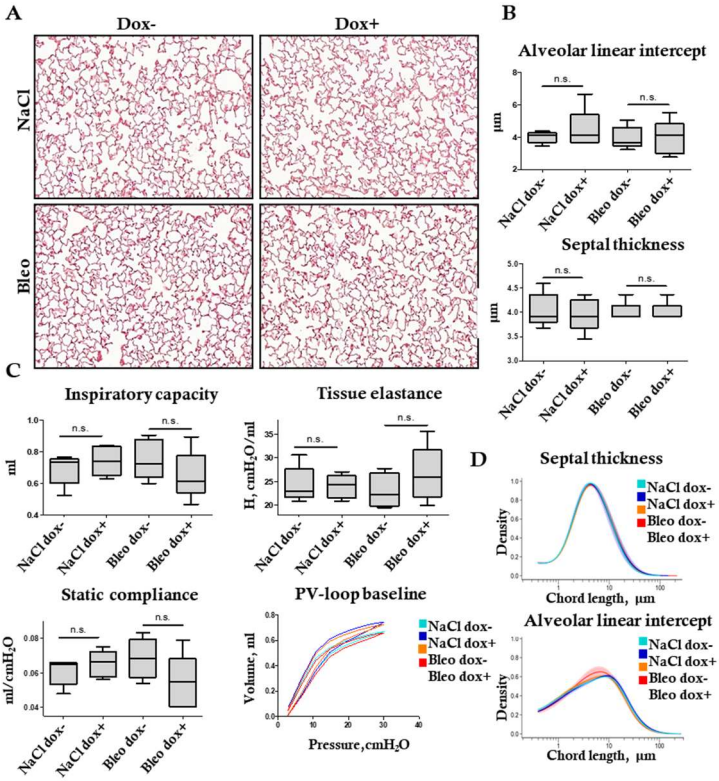

Figure 38. Morphometry and mechanical function of lung from inducible rtTA/tetO7-CHOP transgenic mice after bleomycin treatment

A. *Representative pictures of H&E staining of alveolar region of lung tissue.* ***B.*** *Morphometric analysis of septal thickness and alveolar mean linear intercept.* ***C.*** *Lung mechanical function and mechanical properties. Data in B and C are expressed as box plots where the horizontal lines represent 25th ,50th and 90th percentiles and the vertical lines represent min and max values, analyzed by Bonferroni's multiple comparison test. The number of biological replicates was 5-6 in each treatment group, the number of technical replicates in B was 3 per a mouse (whole sections).* ***D.*** *Morphometric analysis of septal thickness and alveolar mean linear intercept. Data are shown as a probability density estimate function. The displayed curves represent point-wise mean values from individual densities within a group, and the shaded area indicates the standard errors.*

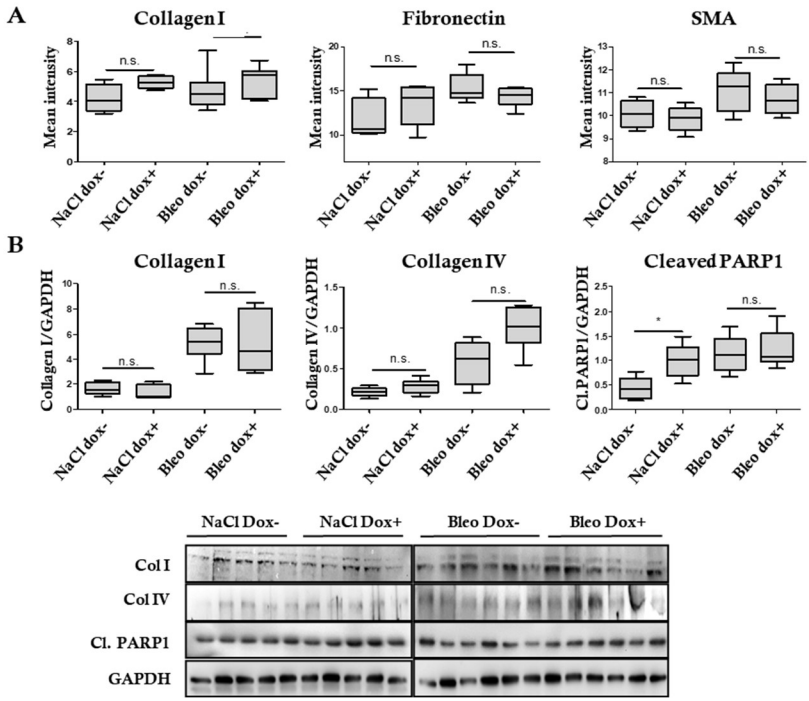

Figure 39. Impact of CHOP on regulation of fibrotic markers in bleomycin model

A. *Quantified IF signal in lung tissue staining with pro-fibrotic markers*
B. *Western blotting for Collagen I, Collagen IV and cleaved PARP1 and densitometry quantification. Data are expressed as box plots where the horizontal lines represent 25th ,50th and 90th percentiles and the vertical lines represent min and max values, analyzed by Bonferroni's multiple comparison test. The number of biological replicates was 5-6 mice in each treatment group, the number of technical replicates was 3 per a mouse (whole sections). *p< 0.05.*

4.3.3. Influence of CHOP on influenza virus infection

Activated UPR in lung tissue from IPF patients potentially could play an essential role in the viral infection process. It could either boost it and trigger acute exacerbation or activate apoptosis in infected cells and suppress the spreading of the virus. To test this theory, I used 250µm PCLS from CHOP overexpressing mice. For this, animals (n=3-5) were fed with dox food for one day and sacrificed for lung uptake and further PCLS preparation. Ready PCLS were immediately infected with influenza virus PR8 (IV) and incubated in a medium with or without dox regarding the experimental settings (Fig. 40A). Samples were collected after 48h p.i. for flow cytometry analysis. All epithelial cells ($EpCam^{pos}$, $CD45/CD31^{neg}$) were used to evaluate the level of infection by Nucleoprotein (NP) and apoptosis by cleaved caspase 3 (Cl. $casp.3^{pos}$ $Zombie^{neg}$). Dead cells were marked by Zombie fixable dye and Cl. $casp.3^{neg}$ $Zombie^{pos}$ cells were counted as necrotic.

Flow cytometry analysis showed an elevated level of infection in dox-activated PCLS compared to non-induced PCLS (Fig. 40B). Moreover, although the level of apoptosis was increased in all infected PCLS, dox+ IV+ PCLS had a significantly higher level of apoptosis than dox- IV+ PCLS. Therefore, a short-term CHOP overexpression had an

amplifying impact on IV infection and increased epithelial cell death. Interestingly, the necrosis and apoptosis levels were increased in both dox-induced infected and non-infected PCLS, additionally verifying the presence of CHOP-induced apoptosis in AECs in CHOP overexpressing mice lungs after dox activation.

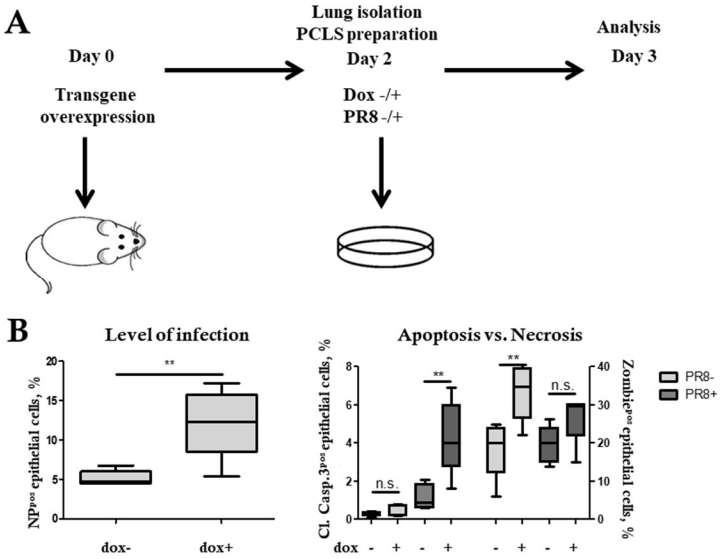

Figure 40 Impact of CHOP on influenza virus infection

A. *Experiment overview. After 2 days of transgene activation mice were sacrificed and one lobe were cut with a chopper to make PCLS for following infection. Cells from PCLS were analyzed after 48h p.i. by flow cytometry.* ***B.*** *Epithelial cells (CD45/31^{neg} EpCam^{pos}) from PCLS were analyzed for IV infection by Nucleoprotein (NP) and apoptosis by Cleaved caspase 3. Necrotic cells are defined as Cleaved caspase 3^{neg} Zombie^{pos} cells. Data are expressed as box plots where the horizontal lines represent 25th ,50th and 90th percentiles and the vertical lines represent min and max values, analyzed by Bonferroni's multiple comparison test. The number of biological replicates was 3-5 mice in each treatment group ** p< 0.01.*

5. Discussion

5.1. Regeneration capacity of the lung and possible impact of ER stress and apoptosis in AECII on lung tissue susceptibility to injury

Endoplasmic reticulum stress (ER stress) results from accumulation of unfolded or misfolded proteins in ER. It can be induced by disrupted Ca^{2+} homeostasis, oxidative stress, lipid imbalance, improper protein folding, etc. [Lepock, 2005; Schultz; Oroszlan, 1979; Sehgal et al., 2017; Zeeshan et al., 2016; Choi et al., 2013]. These factors can appear in response to cell injury caused by chemicals, viruses, mutations, or physical damage. To cope with ER stress, cells activate the unfolded protein response (UPR). UPR has three arms with different mediators and partly overlapping functions and cellular effect. As a first response to the stress, the UPR results in chaperone production to help protein folding, attenuation of translation to reduce the pressure on the protein production machinery, and induction of the ER-associated degradation (ERAD) to help to discard misfolded or unfolded proteins [Lee et al., 2003; Hollien; Weissman, 2006; Yamamoto et al., 2007; Yamamoto et al., 2004; Harding et al., 2000b]. These mechanisms help cells to

stabilize and to regain cellular homeostasis. If cells can overcome ER stress at this stage, one would talk about adaptive ER stress. However, sometimes the stress becomes too strong and prolonged, and cells cannot recover their normal function through ER stress activation. In this case, UPR, as a second measure, activates apoptosis [Allagnat et al., 2010; Chen et al., 2016; Choi et al., 2013]. In this case, it is called maladaptive ERS.

Since UPR is one of the most basic and conservative cellular surveillance mechanisms, it is not surprising that it is involved in the pathology of many different chronic and acute diseases, including lung fibrosis (LF). A variety of factors were shown to be able to activate ER stress in epithelial lung cells. For instance, the mutated surfactant proteins cannot be correctly folded and accumulate in the endoplasmic reticulum, thus, inducing ER stress [Maitra et al., 2010; Ono et al., 2011]. Different chemicals, like asbestos, cause ER stress by disruption of $Ca2^{+}$ homeostasis [Ryan et al., 2014]. Viruses can promote ER expansion to support their protein production and maturation, thereby inducing upregulation of UPR mediators [Gao et al., 2019; Li et al., 2007; Mulvey et al., 2007; Schmoldt et al., 2019].

Several studies showed that induced ER stress enhanced the severity of injury or disease outcome, including LF [Abdullahi et al., 2020; Lawson et al., 2011; Heindryckx et al., 2016; Li et al., 2021]. Intratracheal application of tunicamycin intensified fibrosis after bleomycin treatment. The same effect was observed genetically modified mice carrying the L188Q SFTPC mutation. It induced ER stress in epithelial cells, and together with lower bleomycin dose, it had a synergistic effect causing enhanced fibrosis [Lawson et al., 2011].

Thus, there is clear evidence that ER stress makes tissue more vulnerable to injury. Nevertheless, downstream pathways of the three UPR arms can be different and probably depend on the kind of stimuli and cell type. For these reasons, it is crucial to investigate the precise function of each arm of UPR, UPR proteins, and their communication. This knowledge will give a better understanding of lung fibrosis development mechanisms, and it will uncover possible targets for its treatment and ideas for early preventive measures. To answer these questions, ATF6p50, XBP1s, and CHOP overexpressing transgenic mouse lines were generated in our laboratory. Previously, Dr. Hühn and Dr. Klymenko already showed that none of

these mouse lines develop spontaneous fibrosis [Hühn, 2013; Klymenko, 2016b]. Nevertheless, the activation of downstream targets was observed in AECIIs of these transgenic mice. This study gives additional insight into the role of ER stress in the increased susceptibility of lung tissue to injury and lung tissue fibrotic remodeling.

Different factors can play a role in increasing tissue susceptibility to injury. Since this research is focused on the lung epithelium, such parameters as AECIIs proliferation, apoptosis, and cell number were used to evaluate possible tissue damage and recovery capacity, and thus, to conclude about ER stress mediators influence on epithelial susceptibility to the injury.

Analysis of transgenic mice overexpressing early ER stress markers XBP1s and ATF6p50 showed no change in AECIIs number, proliferation, and apoptosis. Thus, despite the upregulation of downstream targets, no morphological alterations suggestive of lung fibrosis were observed in either mouse line even after one year of transgene expression. Two factors should be taken into consideration, though. The first one is the transgene expression efficiency. One possible explanation is that the number of transgene overexpressing cells or/and the transgene expression level per each cell was

too low to induce tissue morphology disruption. This seems indeed to be the case of the XBP1 mice, where the number of transgene positive cells reached only around 17%. I hypothesize that stressed and apoptotic AECIIs must reach a critical quorum to induce disturbance of tissue homeostasis. Until this threshold value, the capacity to recover and/or regenerate together with other possible mechanisms that help to maintain tissue homeostasis will compensate or abolish any transgene effect. A second condition may stem from the fact that overexpression of only one key UPR protein may not be sufficient to induce severe, if any, changes in the lung tissue. A lack of phenotype may thus be possible even in the case of 100% transgene expression efficiency. However, overexpression of the late the ER stress marker CHOP led to apoptosis and reduced the number of AECIIs in the mice lungs by 40 % at day 28 of transgene induction. Nevertheless, even such significant increase in apoptotic AECII did not result in spontaneous fibrosis or disruption of lung tissue morphology.

The concepts discussed above are consistent with some published data. T.H. Sisson and colleagues investigated targeted AECIIs injury and whether it may induce fibrosis. For this purpose, they used SP-C DTR mice [Sisson et al.,

2010], which express the diphtheria toxin receptor (DTR) under control of the murine SP-C promoter. Thus, exogenously administered diphtheria toxin (DT) binds to DTR expressing cells inducing cell death. Interestingly, a single dose of the toxin did not lead to a phenotypic change in transgenic mice. Because of this, researchers used daily administrations of DT for two weeks to induce fibrotic changes in the lung tissue, such as collagen deposition, alveolar contraction, and appearance of the scar areas. At the same time, another research group used SP-C CreER; Rosa-DTA/RosaTM mice and failed to induce lung fibrosis despite a four-time tamoxifen injection and 52% AECIIs loss [Barkauskas et al., 2013]. Such differences in results can be explained by the different toxicity strengths due to various levels of transgenes expression. But regardless of the reasons, it indicates a broad "buffer zone" in the timeline of the epithelial damage. Apparently, AECIIs from our CHOP mice were also in this zone since they were affected without causing following lung tissue disturbance similar to the case in the Barkauskas´s work. I assume that within this "twilight zone", the epithelial cell apoptosis or injury does not lead to severe consequences because it is in the balance with the tissue recovery capacity. However, multiple injury events

may overcome this capacity in the long term like in Sisson´s work. Therefore, duration of injury is important in fibrosis development. Presumably, if CHOP overexpression in our mice was more consistent over time, it would possibly also lead to the fibrotic change like in SP-C DTR mice in Sisson´s work.

Besides the duration, the strength of injury also plays an essential role, which was shown in the experiments of O. Garcia and colleagues [Garcia et al., 2016]. They established a dose dependent AECII targeted injury mouse model (SPCTK mice) using mutant SR39TK Herpes simplex thymidine kinase. These mice converted intraperitoneally administered ganciclovir (GCV) to a toxic metabolite in SP-C-expressing AECIIs. This, in turn, caused targeted cell injury and death. Interestingly, both lower and middle doses of GCV induced up to 50% AECIIs loss followed by complete restoration after 60 days and did not induce fibrosis. Nevertheless, the middle dose induced significant collagen upregulation and foci of alveolar collapse at days 14 and 28 post-injury. Administration of a high GCV dose, in turn, caused 82 % of AECIIs loss and severe lung pathology, with a fatal outcome within two weeks after injury. Therefore, these data also point to high regenerative capacity of the lung

tissue and importance of the strength of injury and the extent of epithelial cell loss for fibrosis development.

Another indirect evidence showing the dependence of fibrogenesis from injury intensity and duration is the pathogenesis of different fibrosis-associated diseases. For example, IPF needs years to develop, and it is associated with multiple mild injuries during the lifetime. At the same time, viral infections like influenza or coronavirus can induce often fibrosis within weeks due to massive lung tissue destruction [Polak et al., 2020; Zou et al., 2021; Mineo et al., 2012]. Thus, the imbalance between strength/duration of injury and recovery capacity is the crucial factor for lung fibrosis development (Fig. 41).

Applying this theory for my research outcome, I can conclude that single overexpression of key UPR mediators does not seem to overcome the regenerative capacity of the lung even in combination with a low bleomycin dose. ATF6, XBP1, or CHOP overexpression did not promote more severe injury (cell death level, $CK5^{pos}$ areas) in transgenic mice after a mild bleomycin dose compared with non-induced control mice. It again confirms that lung tissue has a high regenerative capacity. Nevertheless, I speculate that a combined overexpression of several ER stress factors

alongside with exposure to higher bleomycin doses may exceed the regeneration capacity of the lungs and will induce more severe injury and exacerbate fibrosis.

I observed this enhanced effect in my experiments with influenza virus (IV) infected PCLS from transgenic mice. In IV infected, dox-induced PCLS, additional CHOP overexpression increased the fraction of dead cells in the infected AECs population. Two factors could explain this result. The first is different AECII infection level in dox- and dox+ PCLS. As discussed above, CHOP overexpression induces AECIIs apoptosis and reduces their number in lung tissue. Thus, dox+ PCLS had a smaller number of AECs per viral particle, which increased the percentage of infected cells. The second factor is the possibility that a faster cell death of AECII in dox+ PCLS could result in enhanced release of live viral particles, which could promote the further spreading of the infection. Thus, the late ER stress mediator CHOP overexpression made mouse lung tissue more vulnerable to IV infection. This can also explain development of acute exacerbation in IPF patients during viral and bacterial infections. One could speculate that IV upregulates UPR and enhances the ER stress pressure on already

weakened epithelial cells in fibrotic lungs, which will further increase cell apoptosis, injury, and fibrogenesis.

In their turn, ATF6 and XBP1 overexpression did not influence the level of influenza infection or tissue injury. However, our previous collaborative experiments with Dr. Susanne Herold's laboratory showed that XBP1 overexpressing PCLS had a high infection level [Schmoldt et al., 2019]. These different results can be explained by the low number of transgene overexpressing AECII in the lungs of mice that were used for the current research.

Taken together, the regenerative capacity of healthy lungs is high enough to cope with UPR and epithelial cell

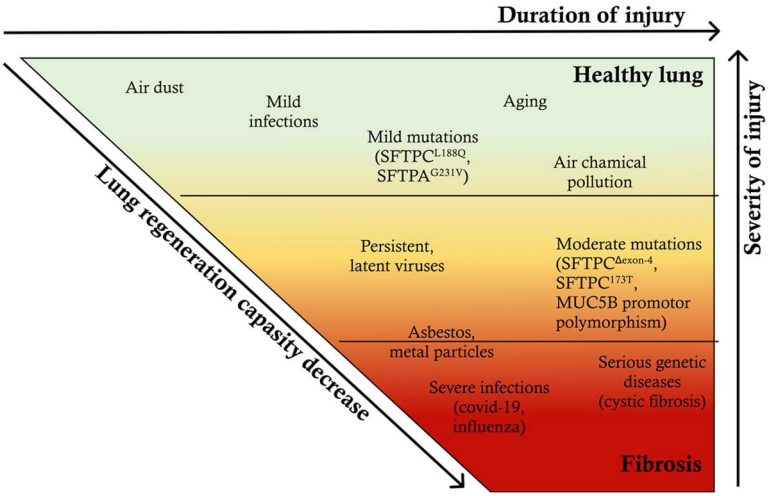

Figure 41. Relationship between strength and duration of injury and regeneration capacity of the lungs

death even in the presence of an additional mild second hit. Nevertheless, when the second hit or/and initial injury are severe or prolonged, UPR and apoptosis of AECIIs seem to act as accelerators and may enhance tissue damage and induce fibrotic remodeling.

5.2. UPR and pro-fibrotic pathway crosstalk

The disturbed epithelial-mesenchymal crosstalk plays a pivotal role in the development of lung fibrosis. It was shown that injured epithelial cells express and release cytokines and growth factors that activate fibroblasts [Morishima et al., 2001; Khalil et al., 1996; Pan et al., 2001], which is consistent with the data from our laboratory. We showed that the culture medium from CHOP overexpressing epithelial cells induced fibroblast activation and ECM protein expression [Klymenko et al., 2019]. As CHOP is a pro-apoptotic protein, the results showed a clear connection between apoptosis in epithelial cells and activation of fibroblasts. It is essential to mention that activated fibroblasts can also promote epithelial injury [Uhal et al., 1995], thus creating a positive feedback loop and promoting fibrogenesis. Nevertheless, in my *in vivo* experiments, the level of CHOP overexpression in AECIIs was not enough to promote overt fibroblast activation and lung fibrosis.

A similar experiment with ATF6p50 overexpressing epithelial MLE12 in my research did not show any increase in fibroblasts proliferation or change in ECM protein expression level. This suggests that activation of the ATF6 arm of UPR in epithelial cells was not sufficient to induce

fibroblasts activation. It is likely that epithelial cells need to initiate first the apoptotic pathway to induce fibroblast activation, which was not the case in my ATF6 overexpressing MLE12 cells. In healthy tissue, fibroblast activation is considered is a normal part of the repair response following epithelial cell injury. In my experiments, ATF6 overexpressing cells could not activate fibroblasts since they did not experience apoptosis and, thus, there was no need for repair.

Data from my *in vivo* experiments showed similar results. ATF6p50 overexpression in mouse AECIIs did not induce lung fibrosis, as well as it did not influence ECM protein deposition even after a year of the transgene activation. At the same time, after a mild dose of bleomycin administration, ATF6 overexpression showed a potential for fibrosis enhancement. Some morphological changes and the increase in collagen I were observed in ATF6 overexpressing mice, although the pulmonary function test did not show a significant difference between dox+ and dox- mice. Hence, in healthy lungs, activation of the ATF6 in AECII did not induce fibroblast activation. Nevertheless, it may have the potential to worsen fibrosis in the case of injury. More experiments with different bleomycin doses and different

duration of transgene activation are needed to make a clear statement.

In vivo experiments with XBP1 overexpressing mice also did not show a significant difference between dox-activated and not activated mice after bleomycin administration despite the tendency for an increased tissue elastance and a decrease in lung compliance in the dox+ mice. The lack of phenotype in this case can be explained by the very low level of transgene expression efficiency (below 17% of AECIIs), which may not be enough to induce a noticeable phenotype in the presence or absence of a further injurious stimulus. Further experiments will clarify the role of XBP1s expression in AECII on fibrosis development.

In the experiments involving the CHOP overexpressing mice, I expected a severe outcome for the dox-induced mice after a low dose of bleomycin, but the results were surprisingly opposite. CHOP overexpression did not worsen bleomycin-induced fibrosis, although there was a clear trend toward a decline in lung function in doxycycline treated mice. One possibility explaining this result is the short dox induction period that preceded bleomycin administration. It is likely that the four-day induction was not enough to induce overt AECII apoptosis, and therefore to alter the bleomycin

response. It would therefore be very important to determine in future experiments the effect of bleomycin injury on 28 days induced CHOP overexpressing mice, where the level of AECIIs injury reached up to 40%. Thus, further experiments with different transgene expression times and higher bleomycin doses will clarify how and to what degree CHOP expression in AECII can affect the course of fibrosis development. In summary, I can conclude that early UPR mediators have little influence on lung tissue homeostasis and do not seem to have much impact on lung vulnerability to injury. At the same time, it appears that the late UPR mediator CHOP has a higher potential to increase the mouse lung susceptibility to injury and enhance fibrotic remodeling due to induced cellular apoptosis.

These data in the context of the already published literature help to understand the process of fibrosis development and its possible etiology. In the case of IPF, the disease usually develops slower, and very likely, a combination of very different causative factors play an important role. One of such crucial factors probably is the presence of UPR and especially late UPR mediators in alveolar epithelial cells, which may predispose the lung to injury and trigger a fibrotic response when the injury

overcomes the recovery capacity (Fig. 42). At the same time, IPF is a complex disease affecting a variety of cells (epithelial cells, fibroblasts, macrophages). In each cell type involved in fibrosis pathology, UPR probably plays a crucial role through its different branches to activate or change a cell status or induce apoptosis.

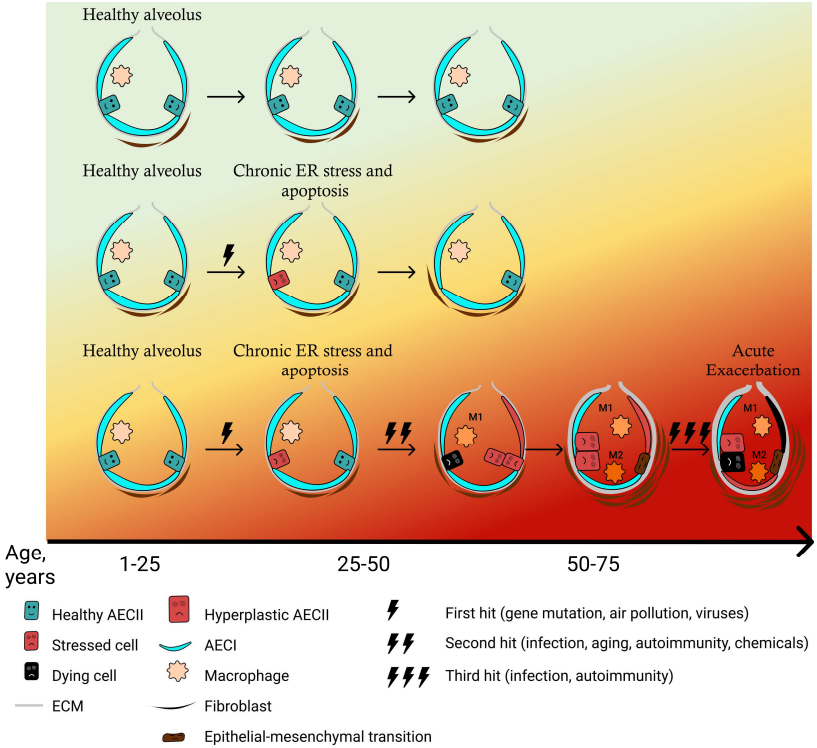

Figure 42. Schematic representation of the potential consequences of injury in the human lung over a lifetime

A. *An alveolus in the lung without an injury during the lifetime.* ***B.*** *An alveolus in the lung that experienced mild or short-term injury (e.g., a surfactant-related mutation, an infection). Despite increased levels of ER stress and AECII apoptosis, the regeneration capacity of the lung is still high enough to overcome the damage.* ***C.*** *An alveolus in the lung that experienced several injuries during the lifetime (e.g., surfactant-related mutation, infection, autoimmunity, etc.). The level of apoptosis and loss of AECII is very high and exceeds the ability of lung tissue to regenerate. This disbalance leads to alveolar dysfunction and morphological changes. To repair the damage, macrophages and fibroblasts are activated and recruited. This induces changes in tissue morphology and deterioration in lung function. Another injury at this stage can cause an acute exacerbation and accelerate deaths.*

6. Summary

Idiopathic pulmonary fibrosis (IPF) is a rare lung disease with no cure. Despite much research, the precise pathomechanism of this disease remains uncovered. Nevertheless, according to the central paradigm, apoptosis of alveolar epithelial cells type II (AECIIs) plays a crucial role in triggering the event cascade that leads to fibrosis. Several publications confirmed this hypothesis, showing that dramatic loss of AECIIs in mice leads to lung fibrosis. However, the reason for the high level of apoptosis and AECII loss in IPF lungs remains unclear. One of the mechanisms involved in fibrosis pathology that can cause cell death is the unfolded protein response (UPR) triggered by endoplasmic reticulum (ER) stress. Therefore, this thesis aimed to decipher the role of the activation of different UPR branches in AECII in the development of pulmonary fibrosis.

To that end, three UPR mediators, XBP1s, ATF6p50, and CHOP, were conditionally overexpressed in the AECIIs of mouse lungs. Western blotting, immunofluorescence (IF) staining, and flow cytometry analysis showed that overexpression of XBP1s and ATF6p50 did not induce AECII apoptosis and did not change the ECM protein level (smooth muscle actin, collagen I, fibronectin) even after 12

months of the transgene overexpression. At the same time, the overexpression of CHOP induced cell death and led to reduced AECIIs number up to 40 % on the 28th day of transgene expression. Thus, CHOP may be a possible link between maladaptive ER stress and apoptosis, leading to the loss of AECIIs.

We also analyzed the influence of overexpression of UPR mediators on mouse lung morphology and mechanics in the bleomycin-induced fibrosis model. According to IF staining, Masson-Goldner staining, and western blot analysis, neither XBP1s, ATF6p50, nor CHOP overexpression induced significant changes in the level of injury (CK5pos patches, apoptosis level) and ECM proteins (smooth muscle actin, fibronectin, and collagen I) after bleomycin treatment. Interestingly, tissue morphometric analysis showed a significant decrease in septal thickness and alveolar mean linear intercept in ATF6p50 overexpressing mice after bleomycin application. At the same time, no significant change in these parameters was observed in the lungs of XBP1s and CHOP overexpressing mice. Nevertheless, despite the absence of substantial morphological changes, XBP1s and CHOP overexpressing mice showed a clear trend toward worsening lung mechanics.

Tissue elastance was increased, and inspiratory capacity and static compliance were decreased. Such changes can possibly indicate early pro-fibrotic alterations in the lungs.

In addition, since viral infections are considered a potential trigger for acute exacerbations in IPF, and viruses can also activate UPR to their advantage, it is essential to know how the presence of the activated UPR may influence the level of infection and alveolar epithelial cell (AEC) death during this infection. To this end, we infected precision-cut lung slices (PCLS) from ATF6p50, XBP1s, and CHOP overexpressing mice with Influenza virus and analyzed the infection level and epithelial apoptosis by flow cytometry. Interestingly, ATF6p50 and XBP1 overexpression had no significant effect on influenza infection or AEC death. At the same time, CHOP overexpression positively affected the number of infected and apoptotic AEC. This fact may also explain the acute exacerbations in patients with IPF after infection.

Altogether, our findings demonstrate that 1. Overexpression of ATF6p50 and XBP1s in the AECII of mouse lungs does not affect the number of AECII, does not induce their apoptosis, and does not upregulate pro-fibrotic markers. At the same time, overexpression of CHOP leads to

a 40% reduction of AECII. 2. When using a low dose of bleomycin and short-term activation of the transgene, overexpression of UPR mediators does not change lung morphology but tends to worsen respiratory mechanics. 3. CHOP overexpression can increase the level of influenza virus infection and the number of apoptotic AEC during the infection.

7. Zusammenfassung

Die idiopathische Lungenfibrose (IPF) ist eine seltene, unheilbare Lungenerkrankung. Trotz intensiver Forschung ist der genaue Pathomechanismus dieser Krankheit noch immer nicht geklärt. Das zentrale Paradigma besagt jedoch, dass die Apoptose der Alveolar Epithelzellen vom Typ II (AECIIs) eine entscheidende Rolle bei der Auslösung der Ereigniskaskade spielt, die zur Fibrose führt. Mehrere Veröffentlichungen bestätigten diese Hypothese und zeigten, dass der dramatische Verlust von AECIIs bei Mäusen zu Lungenfibrose führt. Der Grund für das hohe Maß an Apoptose und dem AECII-Verlust in IPF-Lungen bleibt jedoch unklar. Einer der an der Fibrose Pathologie beteiligten Mechanismen, der zum Zelltod führen kann, ist die durch Stress des endoplasmatischen Retikulums (ER) ausgelöste Unfolded Protein Response (UPR). Ziel dieser Arbeit war es daher, die Rolle der Aktivierung verschiedener UPR-Zweige in AECII bei der Entwicklung von Lungenfibrose zu entschlüsseln.

Zu diesem Zweck wurden drei UPR-Vermittler, XBP1s, ATF6p50 und CHOP, in den AECIIs der Mauslunge bedingt überexprimiert. Western Blotting, Immunfluoreszenzfärbung (IF) und Durchflusszytometrie-

Analysen zeigten, dass die Überexpression von XBP1s und ATF6p50 keine AECII-Apoptose auslöste und den ECM-Proteinspiegel (Aktin der glatten Muskulatur, Kollagen I, Fibronektin) auch nach 12 Monaten der Transgen-Überexpression nicht veränderte. Gleichzeitig induzierte die Überexpression von CHOP den Zelltod und führte am 28. Tag der Transgenexpression zu einer Verringerung der AECII-Anzahl um bis zu 40 %. Somit könnte CHOP ein mögliches Bindeglied zwischen maladaptivem ER-Stress und Apoptose sein, das zum Verlust von AECIIs führt.

Wir analysierten auch den Einfluss der Überexpression von UPR-Mediatoren auf die Morphologie und Mechanik der Mauslunge im Bleomycin-induzierten Fibrosemodell. Laut IF-Färbung, Masson-Goldner-Färbung und Western-Blot-Analyse führte weder die Überexpression von XBP1s, ATF6p50 noch von CHOP zu signifikanten Veränderungen des Verletzungsniveaus (CK5pos-Flecken, Apoptose-Niveau) und der ECM-Proteine (Aktin der glatten Muskulatur, Fibronektin und Kollagen I) nach Bleomycin-Behandlung. Interessanterweise zeigte die morphometrische Analyse des Gewebes eine signifikante Abnahme der Septumdicke und des mittleren linearen Abschnitts der Alveolen bei ATF6p50-überexprimierenden Mäusen nach

der Bleomycin-Anwendung. Gleichzeitig wurde in der Lunge von XBP1s und CHOP überexprimierenden Mäusen keine signifikante Veränderung dieser Parameter beobachtet. Trotz des Fehlens wesentlicher morphologischer Veränderungen zeigten XBP1s und CHOP-überexprimierende Mäuse jedoch einen klaren Trend zur Verschlechterung der Lungenmechanik. Die Gewebeelastizität war erhöht, und die Inspirationskapazität und die statische Compliance waren verringert. Solche Veränderungen können möglicherweise auf frühe pro-fibrotische Veränderungen in der Lunge hinweisen.

Da Virusinfektionen als potenzieller Auslöser für akute Exazerbationen bei IPF gelten und Viren auch die UPR zu ihrem Vorteil aktivieren können, ist es wichtig zu wissen, wie die UPR das Ausmaß der Infektion und den Tod von Alveolar Epithelzellen (AEC) während dieser Infektion beeinflussen kann. Zu diesem Zweck infizierten wir präzisions-geschnittene Lungenschnitte (PCLS) von ATF6p50-, XBP1s- und CHOP-überexprimierenden Mäusen mit dem Influenzavirus und analysierten das Infektionsniveau und die epitheliale Apoptose mittels Durchflusszytometrie. Interessanterweise hatte die Überexpression von ATF6p50 und XBP1 keine signifikante

Auswirkung auf die Influenza-Infektion oder den AEC-Tod. Gleichzeitig wirkte sich die Überexpression von CHOP positiv auf die Anzahl der infizierten und apoptotischen AEC aus. Diese Tatsache könnte auch die akute Exazerbation bei Patienten mit IPF nach einer Infektion erklären.

Insgesamt zeigen unsere Ergebnisse, dass 1. die Überexpression von ATF6p50 und XBP1s in den AECII der Mauslunge die Anzahl der AECII nicht beeinflusst, ihre Apoptose nicht induziert und keine pro-fibrotischen Marker hochreguliert. Gleichzeitig führt die Überexpression von CHOP zu einer 40 %igen Verringerung der AECII. 2. Bei Verwendung einer niedrigen Bleomycin-Dosis und einer kurzzeitigen Aktivierung des Transgens führt die Überexpression von UPR-Mediatoren nicht zu einer Veränderung der Lungenmorphologie, sondern eher zu einer Verschlechterung der Atmungsmechanik. 3. Die Überexpression von CHOP kann das Niveau der Influenzavirusinfektion und die Anzahl der apoptotischen AEC während der Infektion erhöhen

8. Publication bibliography

Abdullahi A, Barayan D, Vinaik R, Diao L, Yu N, Jeschke MG. 2020. Activation of ER stress signalling increases mortality after a major trauma. Journal of cellular and molecular medicine 24:9764–9773.

Acloque H, Adams MS, Fishwick K, Bronner-Fraser M, Nieto MA. 2009. Epithelial-mesenchymal transitions: the importance of changing cell state in development and disease. The Journal of clinical investigation 119:1438–1449.

Acosta-Alvear D, Zhou Y, Blais A, Tsikitis M, Lents NH, Arias C, Lennon CJ, Kluger Y, Dynlacht BD. 2007. XBP1 controls diverse cell type- and condition-specific transcriptional regulatory networks. Molecular Cell 27:53–66.

Aguirre V, Uchida T, Yenush L, Davis R, White MF. 2000. The c-Jun NH(2)-terminal kinase promotes insulin resistance during association with insulin receptor substrate-1 and phosphorylation of Ser(307). The Journal of biological chemistry 275:9047–9054.

Akiyama M, Liew CW, Lu S, Hu J, Martinez R, Hambro B, Kennedy RT, Kulkarni RN. 2013. X-box binding protein 1 is essential for insulin regulation of pancreatic α-cell function. Diabetes 62:2439–2449.

Albera C, Costabel U, Fagan EA, Glassberg MK, Gorina E, Lancaster L, Lederer DJ, Nathan SD, Spirig D, Swigris JJ. 2016. Efficacy of pirfenidone in patients with idiopathic pulmonary fibrosis with more preserved lung function. The European respiratory journal 48:843–851.

Alder JK, Chen JJ-L, Lancaster L, Danoff S, Su S, Cogan JD, Vulto I, Xie M, Qi X, Tuder RM, Phillips JA, Lansdorp PM, Loyd JE, Armanios MY. 2008. Short telomeres are a risk factor for idiopathic pulmonary fibrosis. Proceedings of the National Academy of Sciences of the United States of America 105:13051–13056.

Allagnat F, Christulia F, Ortis F, Pirot P, Lortz S, Lenzen S, Eizirik DL, Cardozo AK. 2010. Sustained production of spliced X-box binding protein 1 (XBP1) induces pancreatic beta cell dysfunction and apoptosis. Diabetologia 53:1120–1130.

Allden SJ, Ogger PP, Ghai P, McErlean P, Hewitt R, Toshner R, Walker SA, Saunders P, Kingston S, Molyneaux PL, Maher TM, Lloyd CM, Byrne AJ. 2019. The Transferrin Receptor CD71 Delineates Functionally Distinct Airway Macrophage Subsets during Idiopathic Pulmonary Fibrosis. American journal of respiratory and critical care medicine 200:209–219.

Amodio G, Margarucci L, Moltedo O, Casapullo A, Remondelli P. 2017. Identification of Cysteine Ubiquitylation Sites on the Sec23A Protein of the COPII Complex Required for Vesicle Formation from the ER. The open biochemistry journal 11:36–46.

Azfer A, Niu J, Rogers LM, Adamski FM, Kolattukudy PE. 2006. Activation of endoplasmic reticulum stress response during the development of ischemic heart disease. American journal of physiology. Heart and circulatory physiology 291:H1411-20.

Azuma A, Nukiwa T, Tsuboi E, Suga M, Abe S, Nakata K, Taguchi Y, Nagai S, Itoh H, Ohi M, Sato A, Kudoh S. 2005. Double-blind, placebo-controlled trial of pirfenidone in patients with idiopathic pulmonary fibrosis. American journal of respiratory and critical care medicine 171:1040–1047.

Baek J-H, Whitfield D, Howlett D, Francis P, Bereczki E, Ballard C, Hortobágyi T, Attems J, Aarsland D. 2016. Unfolded protein response is activated in Lewy body dementias. Neuropathology and applied neurobiology 42:352–365.

Bando M, Ohno S, Hosono T, Yanase K, Sato Y, Sohara Y, Hironaka M, Sugiyama Y. 2009. Risk of Acute Exacerbation After Video-assisted Thoracoscopic Lung Biopsy for Interstitial Lung Disease. Journal of bronchology & interventional pulmonology 16:229–235.

Banerjee ER, Laflamme MA, Papayannopoulou T, Kahn M, Murry CE, Henderson WR. 2012. Human embryonic stem cells differentiated to lung lineage-specific cells ameliorate pulmonary fibrosis in a xenograft transplant mouse model. PloS one 7:e33165.

Barabutis N. 2019. Unfolded Protein Response supports endothelial barrier function. Biochimie 165:206–209.

Barkauskas CE, Cronce MJ, Rackley CR, Bowie EJ, Keene DR, Stripp BR, Randell SH, Noble PW, Hogan BLM. 2013. Type 2 alveolar cells are stem cells in adult lung. The Journal of clinical investigation 123:3025–3036.

Bartoszewski R, Rab A, Jurkuvenaite A, Mazur M, Wakefield J, Collawn JF, Bebok Z. 2008. Activation of the

unfolded protein response by deltaF508 CFTR. American journal of respiratory cell and molecular biology 39:448–457.

Batista A, Rodvold JJ, Xian S, Searles SC, Lew A, Iwawaki T, Almanza G, Waller TC, Lin J, Jepsen K, Carter H, Zanetti M. 2020. IRE1α regulates macrophage polarization, PD-L1 expression, and tumor survival. PLoS biology 18:e3000687.

Baumgartner KB, Samet JM, Stidley CA, Colby TV, Waldron JA. 1997. Cigarette smoking: a risk factor for idiopathic pulmonary fibrosis. American journal of respiratory and critical care medicine 155:242–248.

BD Life Sciences. FlowJo™ Software: Ashland, OR: Becton, Dickinson and Company; 2021.

Behr J, Günther A, Bonella F, Dinkel J, Fink L, Geiser T, Geissler K, Gläser S, Handzhiev S, Jonigk D, Koschel D, Kreuter M, Leuschner G, Markart P, Prasse A, Schönfeld N, Schupp JC, Sitter H, Müller-Quernheim J, Costabel U. 2021. S2K Guideline for Diagnosis of Idiopathic Pulmonary Fibrosis. Respiration; international review of thoracic diseases 100:238–271.

Belmont PJ, Chen WJ, San Pedro MN, Thuerauf DJ, Gellings Lowe N, Gude N, Hilton B, Wolkowicz R, Sussman MA, Glembotski CC. 2010. Roles for endoplasmic reticulum-associated degradation and the novel endoplasmic reticulum stress response gene Derlin-3 in the ischemic heart. Circulation research 106:307–316.

Beri R, Liu G, Mueller A, Trejo HE, Kamp DW. 2010. Asbestos induces an endoplasmic reticulum stress response

in alveolar epithelial cells. American journal of respiratory and critical care medicine:A4930-A4930.

Bernard GR, Artigas A, Brigham KL, Carlet J, Falke K, Hudson L, Lamy M, Legall JR, Morris A, Spragg R. 1994. The American-European Consensus Conference on ARDS. Definitions, mechanisms, relevant outcomes, and clinical trial coordination. American journal of respiratory and critical care medicine 149:818–824.

Bertolotti A, Wang X, Novoa I, Jungreis R, Schlessinger K, Cho JH, West AB, Ron D. 2001. Increased sensitivity to dextran sodium sulfate colitis in IRE1beta-deficient mice. The Journal of clinical investigation 107:585–593.

Bertolotti A, Zhang Y, Hendershot LM, Harding HP, Ron D. 2000. Dynamic interaction of BiP and ER stress transducers in the unfolded-protein response. Nature cell biology 2:326–332.

Blackwood EA, Azizi K, Thuerauf DJ, Paxman RJ, Plate L, Kelly JW, Wiseman RL, Glembotski CC. 2019. Pharmacologic ATF6 activation confers global protection in widespread disease models by reprograming cellular proteostasis. Nature communications 10:187.

Boesgaard TW, Pruhova S, Andersson EA, Cinek O, Obermannova B, Lauenborg J, Damm P, Bergholdt R, Pociot F, Pisinger C, Barbetti F, Lebl J, Pedersen O, Hansen T. 2010. Further evidence that mutations in INS can be a rare cause of Maturity-Onset Diabetes of the Young (MODY). BMC medical genetics 11:42.

Bogatkevich GS, Tourkina E, Silver RM, Ludwicka-Bradley A. 2001. Thrombin differentiates normal lung fibroblasts to

a myofibroblast phenotype via the proteolytically activated receptor-1 and a protein kinase C-dependent pathway. The Journal of biological chemistry 276:45184–45192.

Bogorad AM, Lin KY, Marintchev A. 2017. Novel mechanisms of eIF2B action and regulation by eIF2α phosphorylation. Nucleic acids research 45:11962–11979.

Bommiasamy H, Back SH, Fagone P, Lee K, Meshinchi S, Vink E, Sriburi R, Frank M, Jackowski S, Kaufman RJ, Brewer JW. 2009. ATF6alpha induces XBP1-independent expansion of the endoplasmic reticulum. Journal of cell science 122:1626–1636.

Bou M, Montfort J, Le Cam A, Rallière C, Lebret V, Gabillard J-C, Weil C, Gutiérrez J, Rescan P-Y, Capilla E, Navarro I. 2017. Gene expression profile during proliferation and differentiation of rainbow trout adipocyte precursor cells. BMC genomics 18:347.

Braakman I, Bulleid NJ. 2011. Protein folding and modification in the mammalian endoplasmic reticulum. Annual review of biochemistry 80:71–99.

Bridges JP, Wert SE, Nogee LM, Weaver TE. 2003. Expression of a human surfactant protein C mutation associated with interstitial lung disease disrupts lung development in transgenic mice. The Journal of biological chemistry 278:52739–52746.

Bromati CR, Lellis-Santos C, Yamanaka TS, Nogueira TCA, Leonelli M, Caperuto LC, Gorjão R, Leite AR, Anhê GF, Bordin S. 2011. UPR induces transient burst of apoptosis in islets of early lactating rats through reduced AKT phosphorylation via ATF4/CHOP stimulation of TRB3

expression. American journal of physiology. Regulatory, integrative and comparative physiology 300:R92-100.

Brown MS, Goldstein JL. 1999. A proteolytic pathway that controls the cholesterol content of membranes, cells, and blood. Proceedings of the National Academy of Sciences of the United States of America 96:11041–11048.

Bruen KJ, Campbell CA, Schooler WG, deSerres S, Cairns BA, Hultman CS, Meyer AA, Randell SH. 2004. Real-time monitoring of keratin 5 expression during burn re-epithelialization. The Journal of surgical research 120:12–20.

Bucala R, Spiegel LA, Chesney J, Hogan M, Cerami A. 1994. Circulating fibrocytes define a new leukocyte subpopulation that mediates tissue repair. Molecular Medicine 1:71–81.

Calfon M, Zeng H, Urano F, Till JH, Hubbard SR, Harding HP, Clark SG, Ron D. 2002. IRE1 couples endoplasmic reticulum load to secretory capacity by processing the XBP-1 mRNA. Nature 415:92–96.

Campo I, Zorzetto M, Mariani F, Kadija Z, Morbini P, Dore R, Kaltenborn E, Frixel S, Zarbock R, Liebisch G, Hegermann J, Wrede C, Griese M, Luisetti M. 2014. A large kindred of pulmonary fibrosis associated with a novel ABCA3 gene variant. Respiratory research 15:43.

Cao X, He Y, Li X, Xu Y, Liu X. 2019. The IRE1α-XBP1 pathway function in hypoxia-induced pulmonary vascular remodeling, is upregulated by quercetin, inhibits apoptosis and partially reverses the effect of quercetin in PASMCs. American Journal of Translational Research 11:641–654.

Carrasco DR, Sukhdeo K, Protopopova M, Sinha R, Enos M, Carrasco DE, Zheng M, Mani M, Henderson J, Pinkus GS, Munshi N, Horner J, Ivanova EV, Protopopov A, Anderson KC, Tonon G, DePinho RA. 2007. The differentiation and stress response factor XBP-1 drives multiple myeloma pathogenesis. Cancer cell 11:349–360.

Chan JY, Luzuriaga J, Maxwell EL, West PK, Bensellam M, Laybutt DR. 2015. The balance between adaptive and apoptotic unfolded protein responses regulates β-cell death under ER stress conditions through XBP1, CHOP and JNK. Molecular and cellular endocrinology 413:189–201.

Chaudhary NI, Roth GJ, Hilberg F, Müller-Quernheim J, Prasse A, Zissel G, Schnapp A, Park JE. 2007. Inhibition of PDGF, VEGF and FGF signalling attenuates fibrosis. The European respiratory journal 29:976–985.

Chen BL, Sheu ML, Tsai KS, Lan KC, Guan SS, Wu CT, Chen LP, Hung KY, Huang JW, Chiang CK, Liu SH. 2015. CCAAT-Enhancer-Binding Protein Homologous Protein Deficiency Attenuates Oxidative Stress and Renal Ischemia-Reperfusion Injury. Antioxidants & redox signaling 23:1233–1245.

Chen P, Hu T, Liang Y, Li P, Chen X, Zhang J, Ma Y, Hao Q, Wang J, Zhang P, Zhang Y, Zhao H, Yang S, Yu J, Jeong LS, Qi H, Yang M, Hoffman RM, Dong Z, Jia L. 2016. Neddylation Inhibition Activates the Extrinsic Apoptosis Pathway through ATF4-CHOP-DR5 Axis in Human Esophageal Cancer Cells. Clinical cancer research : an official journal of the American Association for Cancer Research 22:4145–4157.

Chen X, Iliopoulos D, Zhang Q, Tang Q, Greenblatt MB, Hatziapostolou M, Lim E, Tam WL, Ni M, Chen Y, Mai J, Shen H, Hu DZ, Adoro S, Hu B, Song M, Tan C, Landis MD, Ferrari M, Shin SJ, Brown M, Chang JC, Liu XS, Glimcher LH. 2014. XBP1 promotes triple-negative breast cancer by controlling the HIF1α pathway. Nature 508:103–107.

Chilosi M, Poletti V, Zamò A, Lestani M, Montagna L, Piccoli P, Pedron S, Bertaso M, Scarpa A, Murer B, Cancellieri A, Maestro R, Semenzato G, Doglioni C. 2003. Aberrant Wnt/β-Catenin Pathway Activation in Idiopathic Pulmonary Fibrosis. The American Journal of Pathology 162:1495–1502.

Choi J-A, Lim Y-J, Cho S-N, Lee J-H, Jeong JA, Kim EJ, Park JB, Kim SH, Park HS, Kim H-J, Song C-H. 2013. Mycobacterial HBHA induces endoplasmic reticulum stress-mediated apoptosis through the generation of reactive oxygen species and cytosolic Ca2+ in murine macrophage RAW 264.7 cells. Cell death & disease 4:e957.

Choukhi A, Ung S, Wychowski C, Dubuisson J. 1998. Involvement of Endoplasmic Reticulum Chaperones in the Folding of Hepatitis C Virus Glycoproteins. Journal of virology 72:3851–3858.

Choy MS, Yusoff P, Lee IC, Newton JC, Goh CW, Page R, Shenolikar S, Peti W. 2015. Structural and Functional Analysis of the GADD34:PP1 eIF2α Phosphatase. Cell reports 11:1885–1891.

Chujo S, Shirasaki F, Kondo-Miyazaki M, Ikawa Y, Takehara K. 2009. Role of connective tissue growth factor

and its interaction with basic fibroblast growth factor and macrophage chemoattractant protein-1 in skin fibrosis. Journal of cellular physiology 220:189–195.

Collard HR, Moore BB, Flaherty KR, Brown KK, Kaner RJ, King TE, Lasky JA, Loyd JE, Noth I, Olman MA, Raghu G, Roman J, Ryu JH, Zisman DA, Hunninghake GW, Colby TV, Egan JJ, Hansell DM, Johkoh T, Kaminski N, Kim DS, Kondoh Y, Lynch DA, Müller-Quernheim J, Myers JL, Nicholson AG, Selman M, Toews GB, Wells AU, Martinez FJ. 2007. Acute exacerbations of idiopathic pulmonary fibrosis. American journal of respiratory and critical care medicine 176:636–643.

Connor JH, Weiser DC, Li S, Hallenbeck JM, Shenolikar S. 2001. Growth arrest and DNA damage-inducible protein GADD34 assembles a novel signaling complex containing protein phosphatase 1 and inhibitor 1. Molecular and Cellular Biology 21:6841–6850.

Cook KL, Shajahan AN, Wärri A, Jin L, Hilakivi-Clarke LA, Clarke R. 2012. Glucose-regulated protein 78 controls cross-talk between apoptosis and autophagy to determine antiestrogen responsiveness. Cancer research 72:3337–3349.

Coope A, Milanski M, Arruda AP, Ignacio-Souza LM, Saad MJ, Anhê GF, Velloso LA. 2012. Chaperone insufficiency links TLR4 protein signaling to endoplasmic reticulum stress. The Journal of biological chemistry 287:15580–15589.

Corazzari M, Rapino F, Ciccosanti F, Giglio P, Antonioli M, Conti B, Fimia GM, Lovat PE, Piacentini M. 2015.

Oncogenic BRAF induces chronic ER stress condition resulting in increased basal autophagy and apoptotic resistance of cutaneous melanoma. Cell death and differentiation 22:946–958.

Costabel U, Richeldi L, Azuma A, Inoue Y, Collard HR, Tschoepe I, Stowasser S, Selman M. 2015. Pre-specified subgroup analyses of pooled data from the INPULSIS™ trials of nintedanib in idiopathic pulmonary fibrosis. Pneumologie 69.

Coward WR, Saini G, Jenkins G. 2010. The pathogenesis of idiopathic pulmonary fibrosis. Therapeutic advances in respiratory disease 4:367–388.

Croft A, Tay KH, Boyd SC, Guo ST, Jiang CC, Lai F, Tseng H-Y, Jin L, Rizos H, Hersey P, Zhang XD. 2014. Oncogenic activation of MEK/ERK primes melanoma cells for adaptation to endoplasmic reticulum stress. The Journal of investigative dermatology 134:488–497.

Darwish I, Mubareka S, Liles WC. 2011. Immunomodulatory therapy for severe influenza. Expert review of anti-infective therapy 9:807–822.

Delbrel E, Soumare A, Naguez A, Label R, Bernard O, Bruhat A, Fafournoux P, Tremblais G, Marchant D, Gille T, Bernaudin J-F, Callard P, Kambouchner M, Martinod E, Valeyre D, Uzunhan Y, Planès C, Boncoeur E. 2018. HIF-1α triggers ER stress and CHOP-mediated apoptosis in alveolar epithelial cells, a key event in pulmonary fibrosis. Scientific reports 8:17939.

Derynck R, Akhurst RJ, Balmain A. 2001. TGF-beta signaling in tumor suppression and cancer progression. Nature genetics 29:117–129.

Díaz-Bulnes P, Saiz ML, López-Larrea C, Rodríguez RM. 2019. Crosstalk Between Hypoxia and ER Stress Response: A Key Regulator of Macrophage Polarization. Frontiers in immunology 10:2951.

Doroudgar S, Thuerauf DJ, Marcinko MC, Belmont PJ, Glembotski CC. 2009. Ischemia activates the ATF6 branch of the endoplasmic reticulum stress response. The Journal of biological chemistry 284:29735–29745.

Egan JJ, Stewart JP, Hasleton PS, Arrand JR, Carroll KB, Woodcock AA. 1995. Epstein-Barr virus replication within pulmonary epithelial cells in cryptogenic fibrosing alveolitis. Thorax 50:1234–1239.

Eisenberg-Lerner A, Kimchi A. 2012. PKD is a kinase of Vps34 that mediates ROS-induced autophagy downstream of DAPk. Cell death and differentiation 19:788–797.

Esposito V, Grosjean F, Tan J, Huang L, Zhu L, Chen J, Xiong H, Striker GE, Zheng F. 2013. CHOP deficiency results in elevated lipopolysaccharide-induced inflammation and kidney injury. American journal of physiology. Renal physiology 304:F440-50.

Federti E, Matté A, Ghigo A, Andolfo I, James C, Siciliano A, Leboeuf C, Janin A, Manna F, Choi SY, Iolascon A, Beneduce E, Melisi D, Kim DW, Levi S, Franceschi L de. 2017. Peroxiredoxin-2 plays a pivotal role as multimodal cytoprotector in the early phase of pulmonary

hypertension. Free radical biology & medicine 112:376–386.

Fehrenbach H. 2001. Alveolar epithelial type II cell: defender of the alveolus revisited. Respiratory research 2:33–46.

Fields BN, Knipe DM, Howley PM. 2001. Fields virology. Philadelphia, London: Lippincott Williams & Wilkins.

Fingerlin TE, Murphy E, Zhang W, Peljto AL, Brown KK, Steele MP, Loyd JE, Cosgrove GP, Lynch D, Groshong S, Collard HR, Wolters PJ, Bradford WZ, Kossen K, Seiwert SD, Du Bois RM, Garcia CK, Devine MS, Gudmundsson G, Isaksson HJ, Kaminski N, Zhang Y, Gibson KF, Lancaster LH, Cogan JD, Mason WR, Maher TM, Molyneaux PL, Wells AU, Moffatt MF, Selman M, Pardo A, Kim DS, Crapo JD, Make BJ, Regan EA, Walek DS, Daniel JJ, Kamatani Y, Zelenika D, Smith K, McKean D, Pedersen BS, Talbert J, Kidd RN, Markin CR, Beckman KB, Lathrop M, Schwarz MI, Schwartz DA. 2013. Genome-wide association study identifies multiple susceptibility loci for pulmonary fibrosis. Nature genetics 45:613–620.

Frabutt DA, Wang B, Riaz S, Schwartz RC, Zheng Y-H. 2018. Innate Sensing of Influenza A Virus Hemagglutinin Glycoproteins by the Host Endoplasmic Reticulum (ER) Stress Pathway Triggers a Potent Antiviral Response via ER-Associated Protein Degradation. Journal of virology 92.

Fu HY, Okada K, Liao Y, Tsukamoto O, Isomura T, Asai M, Sawada T, Okuda K, Asano Y, Sanada S, Asanuma H, Asakura M, Takashima S, Komuro I, Kitakaze M,

Minamino T. 2010. Ablation of C/EBP homologous protein attenuates endoplasmic reticulum-mediated apoptosis and cardiac dysfunction induced by pressure overload. Circulation 122:361–369.

Gade P, Ramachandran G, Maachani UB, Rizzo MA, Okada T, Prywes R, Cross AS, Mori K, Kalvakolanu DV. 2012. An IFN-γ-stimulated ATF6-C/EBP-β-signaling pathway critical for the expression of Death Associated Protein Kinase 1 and induction of autophagy. Proceedings of the National Academy of Sciences of the United States of America 109:10316–10321.

Gao P, Chai Y, Song J, Liu T, Chen P, Zhou L, Ge X, Guo X, Han J, Yang H. 2019. Reprogramming the unfolded protein response for replication by porcine reproductive and respiratory syndrome virus. PLoS pathogens 15:e1008169.

Garcia O, Hiatt MJ, Lundin A, Lee J, Reddy R, Navarro S, Kikuchi A, Driscoll B. 2016. Targeted Type 2 Alveolar Cell Depletion. A Dynamic Functional Model for Lung Injury Repair. American journal of respiratory cell and molecular biology 54:319–330.

Ghatol A, Ruhl AP, Danoff SK. 2012. Exacerbations in idiopathic pulmonary fibrosis triggered by pulmonary and nonpulmonary surgery: a case series and comprehensive review of the literature. Lung 190:373–380.

Ghavami S, Yeganeh B, Zeki AA, Shojaei S, Kenyon NJ, Ott S, Samali A, Patterson J, Alizadeh J, Moghadam AR, Dixon IMC, Unruh H, Knight DA, Post M, Klonisch T, Halayko AJ. 2018. Autophagy and the unfolded protein

response promote profibrotic effects of TGF-β1 in human lung fibroblasts. American journal of physiology. Lung cellular and molecular physiology 314:L493-L504.

Ghosh R, Colon-Negron K, Papa FR. 2019. Endoplasmic reticulum stress, degeneration of pancreatic islet β-cells, and therapeutic modulation of the unfolded protein response in diabetes. Molecular metabolism 27S:S60-S68.

Glembotski CC. 2008. The role of the unfolded protein response in the heart. Journal of molecular and cellular cardiology 44:453–459.

Go D, Lee J, Choi J-A, Cho S-N, Kim S-H, Son S-H, Song C-H. 2019. Reactive oxygen species-mediated endoplasmic reticulum stress response induces apoptosis of Mycobacterium avium-infected macrophages by activating regulated IRE1-dependent decay pathway. Cellular microbiology 21:e13094.

Gribbin J, Hubbard R, Smith C. 2009. Role of diabetes mellitus and gastro-oesophageal reflux in the aetiology of idiopathic pulmonary fibrosis. Respiratory medicine 103:927–931.

Guillamat-Prats R, Gay-Jordi G, Xaubet A, Peinado VI, Serrano-Mollar A. 2014. Alveolar type II cell transplantation restores pulmonary surfactant protein levels in lung fibrosis. The Journal of heart and lung transplantation : the official publication of the International Society for Heart Transplantation 33:758–765.

Guo F-J, Xiong Z, Lu X, Ye M, Han X, Jiang R. 2014. ATF6 upregulates XBP1S and inhibits ER stress-mediated

apoptosis in osteoarthritis cartilage. Cellular signalling 26:332–342.

Hagimoto N, Kuwano K, Inoshima I, Yoshimi M, Nakamura N, Fujita M, Maeyama T, Hara N. 2002. TGF-beta 1 as an enhancer of Fas-mediated apoptosis of lung epithelial cells. Journal of immunology (Baltimore, Md. : 1950) 168:6470–6478.

Hammond C, Braakman I, Helenius A. 1994. Role of N-linked oligosaccharide recognition, glucose trimming, and calnexin in glycoprotein folding and quality control. Proceedings of the National Academy of Sciences of the United States of America 91:913–917.

Hamos JE, Oblas B, Pulaski-Salo D, Welch WJ, Bole DG, Drachman DA. 1991. Expression of heat shock proteins in Alzheimer's disease. Neurology 41:345–350.

Han J, Back SH, Hur J, Lin Y-H, Gildersleeve R, Shan J, Yuan CL, Krokowski D, Wang S, Hatzoglou M, Kilberg MS, Sartor MA, Kaufman RJ. 2013. ER-stress-induced transcriptional regulation increases protein synthesis leading to cell death. Nature cell biology 15:481–490.

Han MS, Jung DY, Morel C, Lakhani SA, Kim JK, Flavell RA, Davis RJ. 2012. JNK Expression by Macrophages Promotes Obesity-induced Insulin Resistance and Inflammation. Science (New York, N.Y.) 339.

Hancock A, Armstrong L, Gama R, Millar A. 1998. Production of interleukin 13 by alveolar macrophages from normal and fibrotic lung. American journal of respiratory cell and molecular biology 18:60–65.

Harding HP, Novoa I, Zhang Y, Zeng H, Wek R, Schapira M, Ron D. 2000a. Regulated Translation Initiation Controls Stress-Induced Gene Expression in Mammalian Cells. Molecular Cell 6:1099–1108.

Harding HP, Zeng H, Zhang Y, Jungries R, Chung P, Plesken H, Sabatini DD, Ron D. 2001. Diabetes Mellitus and Exocrine Pancreatic Dysfunction in Perk−/− Mice Reveals a Role for Translational Control in Secretory Cell Survival. Molecular Cell 7:1153–1163.

Harding HP, Zhang Y, Bertolotti A, Zeng H, Ron D. 2000b. Perk Is Essential for Translational Regulation and Cell Survival during the Unfolded Protein Response. Molecular Cell 5:897–904.

Harding HP, Zhang Y, Bertolotti A, Zeng H, Ron D. 2000c. Perk Is Essential for Translational Regulation and Cell Survival during the Unfolded Protein Response. Molecular Cell 5:897–904.

Harding HP, Zhang Y, Ron D. 1999. Protein translation and folding are coupled by an endoplasmic-reticulum-resident kinase. Nature 397:271–274.

Harnoss JM, Le Thomas A, Reichelt M, Guttman O, Wu TD, Marsters SA, Shemorry A, Lawrence DA, Kan D, Segal E, Merchant M, Totpal K, Crocker LM, Mesh K, Dohse M, Solon M, Modrusan Z, Rudolph J, Koeppen H, Walter P, Ashkenazi A. 2020. IRE1α Disruption in Triple-Negative Breast Cancer Cooperates with Antiangiogenic Therapy by Reversing ER Stress Adaptation and Remodeling the Tumor Microenvironment. Cancer research 80:2368–2379.

Hassan IH, Zhang MS, Powers LS, Shao JQ, Baltrusaitis J, Rutkowski DT, Legge K, Monick MM. 2012. Influenza A viral replication is blocked by inhibition of the inositol-requiring enzyme 1 (IRE1) stress pathway. The Journal of biological chemistry 287:4679–4689.

Hawkins A, Guttentag SH, Deterding R, Funkhouser WK, Goralski JL, Chatterjee S, Mulugeta S, Beers MF. 2015. A non-BRICHOS SFTPC mutant (SP-CI73T) linked to interstitial lung disease promotes a late block in macroautophagy disrupting cellular proteostasis and mitophagy. American journal of physiology. Lung cellular and molecular physiology 308:L33-47.

Haze K, Yoshida H, Yanagi H, Yura T, Mori K. 1999. Mammalian transcription factor ATF6 is synthesized as a transmembrane protein and activated by proteolysis in response to endoplasmic reticulum stress. Molecular biology of the cell 10:3787–3799.

He B, Zhang W, Qiao J, Peng Z, Chai X. 2019. Melatonin protects against COPD by attenuating apoptosis and endoplasmic reticulum stress via upregulating SIRT1 expression in rats. Canadian journal of physiology and pharmacology 97:386–391.

Hebert DN, Foellmer B, Helenius A. 1996. Calnexin and calreticulin promote folding, delay oligomerization and suppress degradation of influenza hemagglutinin in microsomes. The EMBO journal 15:2961–2968.

Hebert DN, Molinari M. 2007. In and out of the ER: protein folding, quality control, degradation, and related human diseases. Physiological reviews 87:1377–1408.

Hebert DN, Zhang JX, Chen W, Foellmer B, Helenius A. 1997. The number and location of glycans on influenza hemagglutinin determine folding and association with calnexin and calreticulin. The Journal of cell biology 139:613–623.

Heindryckx F, Binet F, Ponticos M, Rombouts K, Lau J, Kreuger J, Gerwins P. 2016. Endoplasmic reticulum stress enhances fibrosis through IRE1α-mediated degradation of miR-150 and XBP-1 splicing. EMBO molecular medicine 8:729–744.

Higa A, Taouji S, Lhomond S, Jensen D, Fernandez-Zapico ME, Simpson JC, Pasquet J-M, Schekman R, Chevet E. 2014. Endoplasmic reticulum stress-activated transcription factor ATF6α requires the disulfide isomerase PDIA5 to modulate chemoresistance. Molecular and Cellular Biology 34:1839–1849.

Hilberg F, Roth GJ, Krssak M, Kautschitsch S, Sommergruber W, Tontsch-Grunt U, Garin-Chesa P, Bader G, Zoephel A, Quant J, Heckel A, Rettig WJ. 2008. BIBF 1120: triple angiokinase inhibitor with sustained receptor blockade and good antitumor efficacy. Cancer research 68:4774–4782.

Hinnebusch AG. 2014. The scanning mechanism of eukaryotic translation initiation. Annual review of biochemistry 83:779–812.

Hinte F, van Anken E, Tirosh B, Brune W. 2020. Repression of viral gene expression and replication by the unfolded protein response effector XBP1u. eLife 9.

Hinz B, Phan SH, Thannickal VJ, Galli A, Bochaton-Piallat M-L, Gabbiani G. 2007. The myofibroblast: one function, multiple origins. The American Journal of Pathology 170:1807–1816.

Hiramatsu N, Messah C, Han J, LaVail MM, Kaufman RJ, Lin JH. 2014. Translational and posttranslational regulation of XIAP by eIF2α and ATF4 promotes ER stress–induced cell death during the unfolded protein response. Molecular biology of the cell 25:1411–1420.

Hogue BG, Nayak DP. 1992. Synthesis and processing of the influenza virus neuraminidase, a type II transmembrane glycoprotein. Virology 188:510–517.

Hollien J, Weissman JS. 2006. Decay of endoplasmic reticulum-localized mRNAs during the unfolded protein response. Science (New York, N.Y.) 313:104–107.

Hoozemans JJM, van Haastert ES, Eikelenboom P, Vos RAI de, Rozemuller JM, Scheper W. 2007. Activation of the unfolded protein response in Parkinson's disease. Biochemical and biophysical research communications 354:707–711.

Hoozemans JJM, van Haastert ES, Nijholt DAT, Rozemuller AJM, Eikelenboom P, Scheper W. 2009. The unfolded protein response is activated in pretangle neurons in Alzheimer's disease hippocampus. The American Journal of Pathology 174:1241–1251.

Hoozemans JJM, Veerhuis R, van Haastert ES, Rozemuller JM, Baas F, Eikelenboom P, Scheper W. 2005. The unfolded protein response is activated in Alzheimer's disease. Acta neuropathologica 110:165–172.

Horiguchi M, Koyanagi S, Okamoto A, Suzuki SO, Matsunaga N, Ohdo S. 2012. Stress-regulated transcription factor ATF4 promotes neoplastic transformation by suppressing expression of the INK4a/ARF cell senescence factors. Cancer research 72:395–401.

Hsieh H-L, Wang H-H, Wu W-B, Chu P-J, Yang C-M. 2010. Transforming growth factor-β1 induces matrix metalloproteinase-9 and cell migration in astrocytes: roles of ROS-dependent ERK- and JNK-NF-κB pathways. Journal of neuroinflammation 7:88.

Hsu H-S, Liu C-C, Lin J-H, Hsu T-W, Hsu J-W, Su K, Hung S-C. 2017. Involvement of ER stress, PI3K/AKT activation, and lung fibroblast proliferation in bleomycin-induced pulmonary fibrosis. Scientific reports 7:14272.

Huang J, Wan L, Lu H, Li X. 2018. High expression of active ATF6 aggravates endoplasmic reticulum stress-induced vascular endothelial cell apoptosis through the mitochondrial apoptotic pathway. Molecular medicine reports 17:6483–6489.

Hubbard R, Cooper M, Antoniak M, Venn A, Khan S, Johnston I, Lewis S, Britton J. 2000. Risk of cryptogenic fibrosing alveolitis in metal workers. The Lancet 355:466–467.

Hubbard R, Lewis S, Richards K, Johnston I, Britton J. 1996. Occupational exposure to metal or wood dust and aetiology of cryptogenic fibrosing alveolitis. The Lancet 347:284–289.

Huh WJ, Esen E, Geahlen JH, Bredemeyer AJ, Lee A-H, Shi G, Konieczny SF, Glimcher LH, Mills JC. 2010. XBP1

controls maturation of gastric zymogenic cells by induction of MIST1 and expansion of the rough endoplasmic reticulum. Gastroenterology 139:2038–2049.

Hühn M. 2013. Endoplasmic Reticulum (ER)-stress signalling in the alveolar epithelium. Gießen.

Hunninghake GM, Hatabu H, Okajima Y, Gao W, Dupuis J, Latourelle JC, Nishino M, Araki T, Zazueta OE, Kurugol S, Ross JC, Estépar RSJ, Murphy E, Steele MP, Loyd JE, Schwarz MI, Fingerlin TE, Rosas IO, Washko GR, O'Connor GT, Schwartz DA. 2013. MUC5B Promoter Polymorphism and Interstitial Lung Abnormalities. The New England journal of medicine 368:2192–2200.

Imagawa Y, Hosoda A, Sasaka S-I, Tsuru A, Kohno K. 2008. RNase domains determine the functional difference between IRE1alpha and IRE1beta. FEBS letters 582:656–660.

Inbal B, Bialik S, Sabanay I, Shani G, Kimchi A. 2002. DAP kinase and DRP-1 mediate membrane blebbing and the formation of autophagic vesicles during programmed cell death. The Journal of cell biology 157:455–468.

Irving WL, Day S, Johnston ID. 1993. Idiopathic pulmonary fibrosis and hepatitis C virus infection. The American review of respiratory disease 148:1683–1684.

Ishikawa F, Miyoshi H, Nose K, Shibanuma M. 2010. Transcriptional induction of MMP-10 by TGF-beta, mediated by activation of MEF2A and downregulation of class IIa HDACs. Oncogene 29:909–919.

Iwawaki T, Akai R, Yamanaka S, Kohno K. 2009. Function of IRE1 alpha in the placenta is essential for placental development and embryonic viability. Proceedings of the National Academy of Sciences of the United States of America 106:16657–16662.

Iwawaki T, Hosoda A, Okuda T, Kamigori Y, Nomura-Furuwatari C, Kimata Y, Tsuru A, Kohno K. 2001. Translational control by the ER transmembrane kinase/ribonuclease IRE1 under ER stress. Nature cell biology 3:158–164.

Jackson RJ, Hellen CUT, Pestova TV. 2010. The mechanism of eukaryotic translation initiation and principles of its regulation. Nature reviews. Molecular cell biology 11:113–127.

Jang W-G, Kim E-J, Kim D-K, Ryoo H-M, Lee K-B, Kim S-H, Choi H-S, Koh J-T. 2012. BMP2 protein regulates osteocalcin expression via Runx2-mediated Atf6 gene transcription. The Journal of biological chemistry 287:905–915.

Jin J-K, Blackwood EA, Azizi K, Thuerauf DJ, Fahem AG, Hofmann C, Kaufman RJ, Doroudgar S, Glembotski CC. 2017. ATF6 Decreases Myocardial Ischemia/Reperfusion Damage and Links ER Stress and Oxidative Stress Signaling Pathways in the Heart. Circulation research 120:862–875.

Jolly L, Stavrou A, Vanderstoken G, Meliopoulos VA, Habgood A, Tatler AL, Porte J, Knox A, Weinreb P, Violette S, Hussell T, Kolb M, Stampfli MR, Schultz-Cherry S, Jenkins G. 2014. Influenza promotes collagen

deposition via αvβ6 integrin-mediated transforming growth factor β activation. The Journal of biological chemistry 289:35246–35263.

Kanegai CM, Xi Y, Donne ML, Gotts JE, Driver IH, Amidzic G, Lechner AJ, Jones KD, Vaughan AE, Chapman HA, Rock JR. 2016. Persistent Pathology in Influenza-Infected Mouse Lungs. American journal of respiratory cell and molecular biology 55:613–615.

Kapnadak SG, Raghu G. 2021. Lung transplantation for interstitial lung disease. European respiratory review : an official journal of the European Respiratory Society 30.

Katzen J, Wagner BD, Venosa A, Kopp M, Tomer Y, Russo SJ, Headen AC, Basil MC, Stark JM, Mulugeta S, Deterding RR, Beers MF. 2019. An SFTPC BRICHOS mutant links epithelial ER stress and spontaneous lung fibrosis. JCI insight 4.

Khalil N, O'Connor RN, Flanders KC, Unruh H. 1996. TGF-beta 1, but not TGF-beta 2 or TGF-beta 3, is differentially present in epithelial cells of advanced pulmonary fibrosis: an immunohistochemical study. American journal of respiratory cell and molecular biology 14:131–138.

Khan MM, Yang W-L, Brenner M, Bolognese AC, Wang P. 2017. Cold-inducible RNA-binding protein (CIRP) causes sepsis-associated acute lung injury via induction of endoplasmic reticulum stress. Scientific reports 7:41363.

Kim HJ, Jeong JS, Kim SR, Park SY, Chae HJ, Lee YC. 2013. Inhibition of endoplasmic reticulum stress alleviates lipopolysaccharide-induced lung inflammation through

modulation of NF-κB/HIF-1α signaling pathway. Scientific reports 3.

Kim HJ, Perlman D, Tomic R. 2015a. Natural history of idiopathic pulmonary fibrosis. Respiratory medicine 109:661–670.

Kim KK, Wei Y, Szekeres C, Kugler MC, Wolters PJ, Hill ML, Frank JA, Brumwell AN, Wheeler SE, Kreidberg JA, Chapman HA. 2009. Epithelial cell alpha3beta1 integrin links beta-catenin and Smad signaling to promote myofibroblast formation and pulmonary fibrosis. The Journal of clinical investigation 119:213–224.

Kim SR, Kim HJ, Im Kim D, Lee KB, Park HJ, Jeong JS, Cho SH, Lee YC. 2015b. Blockade of Interplay between IL-17A and Endoplasmic Reticulum Stress Attenuates LPS-Induced Lung Injury. Theranostics 5:1343–1362.

Kim Y-B, Yoon Y-S, Choi Y-H, Park E-M, Kang JL. 2017. Interaction of macrophages with apoptotic cells inhibits transdifferentiation and invasion of lung fibroblasts. Oncotarget 8:112297–112312.

Klymenko O. 2016a. Regulation and role of the pro-apoptotic transcription factor C/EBP homologous protein (CHOP) in type II cells apoptosis and Idiopathic Pulmonary Fibrosis (IPF). Giessen.

Klymenko O. 2016b. Regulation and role of the pro-apoptotic transcription factor C/EBP homologous protein (CHOP) in type II cells apoptosis and Idiopathic Pulmonary Fibrosis (IPF). Gießen.

Klymenko O, Huehn M, Wilhelm J, Wasnick R, Shalashova I, Ruppert C, Henneke I, Hezel S, Guenther K, Mahavadi

P, Samakovlis C, Seeger W, Guenther A, Korfei M. 2019. Regulation and role of the ER stress transcription factor CHOP in alveolar epithelial type-II cells. Journal of molecular medicine (Berlin, Germany) 97:973–990.

Königshoff M, Balsara N, Pfaff E-M, Kramer M, Chrobak I, Seeger W, Eickelberg O. 2008. Functional Wnt signaling is increased in idiopathic pulmonary fibrosis. PloS one 3:e2142.

Königshoff M, Eickelberg O. 2010. WNT signaling in lung disease: a failure or a regeneration signal? American journal of respiratory cell and molecular biology 42:21–31.

Königshoff M, Kramer M, Balsara N, Wilhelm J, Amarie OV, Jahn A, Rose F, Fink L, Seeger W, Schaefer L, Günther A, Eickelberg O. 2009. WNT1-inducible signaling protein-1 mediates pulmonary fibrosis in mice and is upregulated in humans with idiopathic pulmonary fibrosis. The Journal of clinical investigation 119:772–787.

Konishi K, Gibson KF, Lindell KO, Richards TJ, Zhang Y, Dhir R, Bisceglia M, Gilbert S, Yousem SA, Song JW, Kim DS, Kaminski N. 2009. Gene expression profiles of acute exacerbations of idiopathic pulmonary fibrosis. American journal of respiratory and critical care medicine 180:167–175.

Kopp MC, Nowak PR, Larburu N, Adams CJ, Ali MM. 2018. In vitro FRET analysis of IRE1 and BiP association and dissociation upon endoplasmic reticulum stress. eLife 7.

Korfei M, Ruppert C, Mahavadi P, Henneke I, Markart P, Koch M, Lang G, Fink L, Bohle R-M, Seeger W, Weaver

TE, Guenther A. 2008. Epithelial endoplasmic reticulum stress and apoptosis in sporadic idiopathic pulmonary fibrosis. American journal of respiratory and critical care medicine 178:838–846.

Koul PA, Mir H, Akram S, Potdar V, Chadha MS. 2017. Respiratory viruses in acute exacerbations of chronic obstructive pulmonary disease. Lung India : official organ of Indian Chest Society 34:29–33.

Kroeger H, Grimsey N, Paxman R, Chiang W-C, Plate L, Jones Y, Shaw PX, Trejo J, Tsang SH, Powers E, Kelly JW, Wiseman RL, Lin JH. 2018. The unfolded protein response regulator ATF6 promotes mesodermal differentiation. Science signaling 11.

Kulalert W, Sadeeshkumar H, Zhang YK, Schroeder FC, Kim DH. 2017. Molecular Determinants of the Regulation of Development and Metabolism by Neuronal eIF2α Phosphorylation in Caenorhabditis elegans. Genetics 206:251–263.

Kurata M, Yamazaki Y, Kanno Y, Ishibashi S, Takahara T, Kitagawa M, Nakamura T. 2011. Anti-apoptotic function of Xbp1 as an IL-3 signaling molecule in hematopoietic cells. Cell death & disease 2:e118.

Kuwano K, Nomoto Y, Kunitake R, Hagimoto N, Matsuba T, Nakanishi Y, Hara N. 1997. Detection of adenovirus E1A DNA in pulmonary fibrosis using nested polymerase chain reaction. The European respiratory journal 10:1445–1449.

Laporta Hernandez R, Aguilar Perez M, Lázaro Carrasco MT, Ussetti Gil P. 2018. Lung Transplantation in

Idiopathic Pulmonary Fibrosis. Medical sciences (Basel, Switzerland) 6.

Lara-Reyna S, Scambler T, Holbrook J, Wong C, Jarosz-Griffiths HH, Martinon F, Savic S, Peckham D, McDermott MF. 2019. Metabolic Reprograming of Cystic Fibrosis Macrophages via the IRE1α Arm of the Unfolded Protein Response Results in Exacerbated Inflammation. Frontiers in immunology 10:1789.

Lawson WE, Cheng D-S, Degryse AL, Tanjore H, Polosukhin VV, Xu XC, Newcomb DC, Jones BR, Roldan J, Lane KB, Morrisey EE, Beers MF, Yull FE, Blackwell TS. 2011. Endoplasmic reticulum stress enhances fibrotic remodeling in the lungs. Proceedings of the National Academy of Sciences of the United States of America 108:10562–10567.

Lawson WE, Crossno PF, Polosukhin VV, Roldan J, Cheng D-S, Lane KB, Blackwell TR, Xu C, Markin C, Ware LB, Miller GG, Loyd JE, Blackwell TS. 2008. Endoplasmic reticulum stress in alveolar epithelial cells is prominent in IPF: association with altered surfactant protein processing and herpesvirus infection. American journal of physiology. Lung cellular and molecular physiology 294:L1119-26.

Lawson WE, Grant SW, Ambrosini V, Womble KE, Dawson EP, Lane KB, Markin C, Renzoni E, Lympany P, Thomas AQ, Roldan J, Scott TA, Blackwell TS, Phillips JA, Loyd JE, Du Bois RM. 2004. Genetic mutations in surfactant protein C are a rare cause of sporadic cases of IPF. Thorax 59:977–980.

Lee A-H, Chu GC, Iwakoshi NN, Glimcher LH. 2005. XBP-1 is required for biogenesis of cellular secretory machinery of exocrine glands. The EMBO journal 24:4368–4380.

Lee A-H, Iwakoshi NN, Glimcher LH. 2003. XBP-1 regulates a subset of endoplasmic reticulum resident chaperone genes in the unfolded protein response. Molecular and Cellular Biology 23:7448–7459.

Lee AS. 1992. Mammalian stress response: induction of the glucose-regulated protein family. Current Opinion in Cell Biology 4:267–273.

Lee AS. 2007. GRP78 induction in cancer: therapeutic and prognostic implications. Cancer research 67:3496–3499.

Lee J, Sun C, Zhou Y, Lee J, Gokalp D, Herrema H, Park SW, Davis RJ, Ozcan U. 2011. p38 MAPK-mediated regulation of Xbp1s is crucial for glucose homeostasis. Nature medicine 17:1251–1260.

Lee JS, Collard HR, Anstrom KJ, Martinez FJ, Noth I, Roberts RS, Yow E, Raghu G. 2013. Anti-acid treatment and disease progression in idiopathic pulmonary fibrosis: an analysis of data from three randomised controlled trials. The Lancet. Respiratory medicine 1:369–376.

Lee M-S, Cherla RP, Leyva-Illades D, Tesh VL. 2009. Bcl-2 regulates the onset of shiga toxin 1-induced apoptosis in THP-1 cells. Infection and immunity 77:5233–5244.

Lee SH, Lee EJ, Lee SY, Kim JH, Shim JJ, Shin C, In KH, Kang KH, Uhm CS, Kim H-K, Yang K-S, Park S, Kim HS, Kim YM, Yoo TJ. 2014. The effect of adipose stem cell therapy on pulmonary fibrosis induced by repetitive

intratracheal bleomycin in mice. Experimental lung research 40:117–125.

Lee S-Y, Lee M-S, Cherla RP, Tesh VL. 2008. Shiga toxin 1 induces apoptosis through the endoplasmic reticulum stress response in human monocytic cells. Cellular microbiology 10:770–780.

Lee Y-J, Moon C, Lee SH, Park H-J, Seoh J-Y, Cho M-S, Kang JL. 2012. Apoptotic cell instillation after bleomycin attenuates lung injury through hepatocyte growth factor induction. The European respiratory journal 40:424–435.

Leonard A, Paton AW, El-Quadi M, Paton JC, Fazal F. 2014. Preconditioning with endoplasmic reticulum stress ameliorates endothelial cell inflammation. PloS one 9:e110949.

Lepock JR. 2005. How do cells respond to their thermal environment? International journal of hyperthermia : the official journal of European Society for Hyperthermic Oncology, North American Hyperthermia Group 21:681–687.

Ley B, Collard HR, King TE. 2011. Clinical course and prediction of survival in idiopathic pulmonary fibrosis. American journal of respiratory and critical care medicine 183:431–440.

Li B, Gao B, Ye L, Han X, Wang W, Kong L, Fang X, Zeng Y, Zheng H, Li S, Wu Z, Ye L. 2007. Hepatitis B virus X protein (HBx) activates ATF6 and IRE1-XBP1 pathways of unfolded protein response. Virus research 124:44–49.

Li G, Mongillo M, Chin K-T, Harding H, Ron D, Marks AR, Tabas I. 2009. Role of ERO1-alpha-mediated stimulation

of inositol 1,4,5-triphosphate receptor activity in endoplasmic reticulum stress-induced apoptosis. The Journal of cell biology 186:783–792.

Li H, Meng Q, Xiao F, Chen S, Du Y, Yu J, Wang C, Guo F. 2011. ATF4 deficiency protects mice from high-carbohydrate-diet-induced liver steatosis. The Biochemical journal 438:283–289.

Li M, Xie Y, Zhao K, Chen K, Cao Y, Zhang J, Han M, Hu L, He R, Wang D, Li H. 2021. Endoplasmic reticulum stress exacerbates inflammation in chronic rhinosinusitis with nasal polyps via the transcription factor XBP1. Clinical immunology (Orlando, Fla.) 223:108659.

Li P, Zhang L, Zhang M, Zhou C, Lin N. 2016. Uric acid enhances PKC-dependent eNOS phosphorylation and mediates cellular ER stress: A mechanism for uric acid-induced endothelial dysfunction. International journal of molecular medicine 37:989–997.

Lin F, Liao C, Sun Y, Zhang J, Lu W, Bai Y, Liao Y, Li M, Ni X, Hou Y, Qi Y, Chen Y. 2017. Hydrogen Sulfide Inhibits Cigarette Smoke-Induced Endoplasmic Reticulum Stress and Apoptosis in Bronchial Epithelial Cells. Frontiers in pharmacology 8:675.

Liu J-Q, Zhang L, Yao J, Yao S, Yuan T. 2018. AMPK alleviates endoplasmic reticulum stress by inducing the ER-chaperone ORP150 via FOXO1 to protect human bronchial cells from apoptosis. Biochemical and biophysical research communications 497:564–570.

Liu T, Los Santos FG de, Phan SH. 2017. The Bleomycin Model of Pulmonary Fibrosis. Methods in molecular biology (Clifton, N.J.) 1627:27–42.

Liu X, Kwak D, Lu Z, Xu X, Fassett J, Wang H, Wei Y, Cavener DR, Hu X, Hall J, Bache RJ, Chen Y. 2014. Endoplasmic reticulum stress sensor protein kinase R-like endoplasmic reticulum kinase (PERK) protects against pressure overload-induced heart failure and lung remodeling. Hypertension (Dallas, Tex. : 1979) 64:738–744.

Liu Z, Li C, Kang N, Malhi H, Shah VH, Maiers JL. 2019. Transforming growth factor β (TGFβ) cross-talk with the unfolded protein response is critical for hepatic stellate cell activation. The Journal of biological chemistry 294:3137–3151.

Lowe CE, Dennis RJ, Obi U, O'Rahilly S, Rochford JJ. 2012. Investigating the involvement of the ATF6α pathway of the unfolded protein response in adipogenesis. International journal of obesity (2005) 36:1248–1251.

Lu H-Y, Zhang J, Wang Q-X, Tang W, Zhang L-J. 2015. Activation of the endoplasmic reticulum stress pathway involving CHOP in the lungs of rats with hyperoxia-induced bronchopulmonary dysplasia. Molecular medicine reports 12:4494–4500.

Lu M, Lawrence DA, Marsters S, Acosta-Alvear D, Kimmig P, Mendez AS, Paton AW, Paton JC, Walter P, Ashkenazi A. 2014. Opposing unfolded-protein-response signals converge on death receptor 5 to control apoptosis. Science (New York, N.Y.) 345:98–101.

Lu PD, Jousse C, Marciniak SJ, Zhang Y, Novoa I, Scheuner D, Kaufman RJ, Ron D, Harding HP. 2004. Cytoprotection by pre-emptive conditional phosphorylation of translation initiation factor 2. The EMBO journal 23:169–179.

Ludwicka-Bradley A, Bogatkevich G, Silver RM. 2004. Thrombin-mediated cellular events in pulmonary fibrosis associated with systemic sclerosis (scleroderma). Clinical and experimental rheumatology 22:S38-46.

Ma Y, Brewer JW, Alan Diehl J, Hendershot LM. 2002. Two Distinct Stress Signaling Pathways Converge Upon the CHOP Promoter During the Mammalian Unfolded Protein Response. Journal of Molecular Biology 318:1351–1365.

Määttänen P, Gehring K, Bergeron JJM, Thomas DY. 2010. Protein quality control in the ER: the recognition of misfolded proteins. Seminars in cell & developmental biology 21:500–511.

Magadán JG, Pérez-Victoria FJ, Sougrat R, Ye Y, Strebel K, Bonifacino JS. 2010. Multilayered mechanism of CD4 downregulation by HIV-1 Vpu involving distinct ER retention and ERAD targeting steps. PLoS pathogens 6:e1000869.

Maharaj S, Shimbori C, Kolb M. 2013. Fibrocytes in pulmonary fibrosis: a brief synopsis. European respiratory review : an official journal of the European Respiratory Society 22:552–557.

Maitra M, Wang Y, Gerard RD, Mendelson CR, Garcia CK. 2010. Surfactant protein A2 mutations associated with

pulmonary fibrosis lead to protein instability and endoplasmic reticulum stress. The Journal of biological chemistry 285:22103–22113.

Maiuolo J, Bulotta S, Verderio C, Benfante R, Borgese N. 2011. Selective activation of the transcription factor ATF6 mediates endoplasmic reticulum proliferation triggered by a membrane protein. Proceedings of the National Academy of Sciences of the United States of America 108:7832–7837.

Makioka K, Yamazaki T, Fujita Y, Takatama M, Nakazato Y, Okamoto K. 2010. Involvement of endoplasmic reticulum stress defined by activated unfolded protein response in multiple system atrophy. Journal of the neurological sciences 297:60–65.

Mao C, Tai W-C, Bai Y, Poizat C, Lee AS. 2006. In vivo regulation of Grp78/BiP transcription in the embryonic heart: role of the endoplasmic reticulum stress response element and GATA-4. The Journal of biological chemistry 281:8877–8887.

Martin Hühn. 2012. Endoplasmic Reticulum (ER)-stress signalling in the alveolar epithelium. Giessen.

Martino MEB, Olsen JC, Fulcher NB, Wolfgang MC, O'Neal WK, Ribeiro CMP. 2009. Airway epithelial inflammation-induced endoplasmic reticulum Ca2+ store expansion is mediated by X-box binding protein-1. The Journal of biological chemistry 284:14904–14913.

McCullough KD, Martindale JL, Klotz LO, Aw TY, Holbrook NJ. 2001. Gadd153 sensitizes cells to endoplasmic reticulum stress by down-regulating Bcl2 and

perturbing the cellular redox state. Molecular and Cellular Biology 21:1249–1259.

Meltzer EB, Noble PW. 2008. Idiopathic pulmonary fibrosis. Orphanet journal of rare diseases 3:8.

Meur G, Simon A, Harun N, Virally M, Dechaume A, Bonnefond A, Fetita S, Tarasov AI, Guillausseau P-J, Boesgaard TW, Pedersen O, Hansen T, Polak M, Gautier J-F, Froguel P, Rutter GA, Vaxillaire M. 2010. Insulin gene mutations resulting in early-onset diabetes: marked differences in clinical presentation, metabolic status, and pathogenic effect through endoplasmic reticulum retention. Diabetes 59:653–661.

Meusser B, Hirsch C, Jarosch E, Sommer T. 2005. ERAD: the long road to destruction. Nature cell biology 7:766–772.

Min T, Bodas M, Mazur S, Vij N. 2011. Critical role of proteostasis-imbalance in pathogenesis of COPD and severe emphysema. Journal of molecular medicine (Berlin, Germany) 89:577–593.

Minagawa S, Araya J, Numata T, Nojiri S, Hara H, Yumino Y, Kawaishi M, Odaka M, Morikawa T, Nishimura SL, Nakayama K, Kuwano K. 2011. Accelerated epithelial cell senescence in IPF and the inhibitory role of SIRT6 in TGF-β-induced senescence of human bronchial epithelial cells. American journal of physiology. Lung cellular and molecular physiology 300:L391-401.

Minamino T, Komuro I, Kitakaze M. 2010. Endoplasmic reticulum stress as a therapeutic target in cardiovascular disease. Circulation research 107:1071–1082.

Mineo G, Ciccarese F, Modolon C, Landini MP, Valentino M, Zompatori M. 2012. Post-ARDS pulmonary fibrosis in patients with H1N1 pneumonia: role of follow-up CT. La Radiologia medica 117:185–200.

Miyake Y, Sasaki S, Yokoyama T, Chida K, Azuma A, Suda T, Kudoh S, Sakamoto N, Okamoto K, Kobashi G, Washio M, Inaba Y, Tanaka H. 2005. Occupational and environmental factors and idiopathic pulmonary fibrosis in Japan. The Annals of occupational hygiene 49:259–265.

Mizgerd JP. 2008. Acute lower respiratory tract infection. The New England journal of medicine 358:716–727.

Moeller A, Ask K, Warburton D, Gauldie J, Kolb M. 2008. The bleomycin animal model: a useful tool to investigate treatment options for idiopathic pulmonary fibrosis? The international journal of biochemistry & cell biology 40:362–382.

Moenner M, Pluquet O, Bouchecareilh M, Chevet E. 2007. Integrated endoplasmic reticulum stress responses in cancer. Cancer research 67:10631–10634.

Molina-Molina M, Planas-Cerezales L, Perona R. 2018. Telomere Shortening in Idiopathic Pulmonary Fibrosis. Archivos de Bronconeumología (English Edition) 54:3–4.

Molinari M, Calanca V, Galli C, Lucca P, Paganetti P. 2003. Role of EDEM in the release of misfolded glycoproteins from the calnexin cycle. Science (New York, N.Y.) 299:1397–1400.

Moore BB, Hogaboam CM. 2008. Murine models of pulmonary fibrosis. American journal of physiology. Lung cellular and molecular physiology 294:L152-60.

Morinaga N, Yahiro K, Matsuura G, Moss J, Noda M. 2008. Subtilase cytotoxin, produced by Shiga-toxigenic Escherichia coli, transiently inhibits protein synthesis of Vero cells via degradation of BiP and induces cell cycle arrest at G1 by downregulation of cyclin D1. Cellular microbiology 10:921–929.

Morishima N, Nakanishi K, Nakano A. 2011. Activating transcription factor-6 (ATF6) mediates apoptosis with reduction of myeloid cell leukemia sequence 1 (Mcl-1) protein via induction of WW domain binding protein 1. The Journal of biological chemistry 286:35227–35235.

Morishima Y, Nomura A, Uchida Y, Noguchi Y, Sakamoto T, Ishii Y, Goto Y, Masuyama K, Zhang MJ, Hirano K, Mochizuki M, Ohtsuka M, Sekizawa K. 2001. Triggering the induction of myofibroblast and fibrogenesis by airway epithelial shedding. American journal of respiratory cell and molecular biology 24:1–11.

Mughal W, Kirshenbaum LA. 2011. Cell death signalling mechanisms in heart failure. Experimental & Clinical Cardiology 16:102–108.

Mulvey M, Arias C, Mohr I. 2007. Maintenance of endoplasmic reticulum (ER) homeostasis in herpes simplex virus type 1-infected cells through the association of a viral glycoprotein with PERK, a cellular ER stress sensor. Journal of virology 81:3377–3390.

Murray LA, Chen Q, Kramer MS, Hesson DP, Argentieri RL, Peng X, Gulati M, Homer RJ, Russell T, van Rooijen N, Elias JA, Hogaboam CM, Herzog EL. 2011. TGF-beta driven lung fibrosis is macrophage dependent and blocked

by Serum amyloid P. The international journal of biochemistry & cell biology 43:154–162.

Murray LA, Rosada R, Moreira AP, Joshi A, Kramer MS, Hesson DP, Argentieri RL, Mathai S, Gulati M, Herzog EL, Hogaboam CM. 2010. Serum amyloid P therapeutically attenuates murine bleomycin-induced pulmonary fibrosis via its effects on macrophages. PloS one 5:e9683.

Nabhan A, Brownfield DG, Krasnow MA, Desai TJ. 2018. A single cell Wnt signaling niche maintains stemness of alveolar type 2 cells. Science (New York, N.Y.) 359:1118–1123.

Nadanaka S, Okada T, Yoshida H, Mori K. 2007. Role of disulfide bridges formed in the luminal domain of ATF6 in sensing endoplasmic reticulum stress. Molecular and Cellular Biology 27:1027–1043.

Nadanaka S, Yoshida H, Mori K. 2006. Reduction of disulfide bridges in the lumenal domain of ATF6 in response to glucose starvation. Cell structure and function 31:127–134.

Nagy P, Varga A, Pircs K, Hegedűs K, Juhász G. 2013. Myc-driven overgrowth requires unfolded protein response-mediated induction of autophagy and antioxidant responses in Drosophila melanogaster. PLoS genetics 9:e1003664.

Naik PK, Moore BB. 2010. Viral infection and aging as cofactors for the development of pulmonary fibrosis. Expert review of respiratory medicine 4:759–771.

Nguyen-Van-Tam JS, Openshaw PJM, Hashim A, Gadd EM, Lim WS, Semple MG, Read RC, Taylor BL, Brett SJ, McMenamin J, Enstone JE, Armstrong C, Nicholson KG. 2010. Risk factors for hospitalisation and poor outcome with pandemic A/H1N1 influenza: United Kingdom first wave (May-September 2009). Thorax 65:645–651.

Nijholt DAT, van Haastert ES, Rozemuller AJM, Scheper W, Hoozemans JJM. 2012. The unfolded protein response is associated with early tau pathology in the hippocampus of tauopathies. The Journal of pathology 226:693–702.

Nishitoh H. 2012. CHOP is a multifunctional transcription factor in the ER stress response. Journal of biochemistry 151:217–219.

Nogee LM, Dunbar AE, Wert SE, Askin F, Hamvas A, Whitsett JA. 2001. A mutation in the surfactant protein C gene associated with familial interstitial lung disease. The New England journal of medicine 344:573–579.

Noth I, Zhang Y, Ma S-F, Flores C, Barber M, Huang Y, Broderick SM, Wade MS, Hysi P, Scuirba J, Richards TJ, Juan-Guardela BM, Vij R, Han MK, Martinez FJ, Kossen K, Seiwert SD, Christie JD, Nicolae D, Kaminski N, Garcia JGN. 2013. Genetic variants associated with idiopathic pulmonary fibrosis susceptibility and mortality: a genome-wide association study. The Lancet Respiratory Medicine 1:309–317.

Novoa I, Zeng H, Harding HP, Ron D. 2001. Feedback inhibition of the unfolded protein response by GADD34-mediated dephosphorylation of eIF2alpha. The Journal of cell biology 153:1011–1022.

Oda K, Ishimoto H, Yamada S, Kushima H, Ishii H, Imanaga T, Harada T, Ishimatsu Y, Matsumoto N, Naito K, Yatera K, Nakazato M, Kadota J-I, Watanabe K, Kohno S, Mukae H. 2014. Autopsy analyses in acute exacerbation of idiopathic pulmonary fibrosis. Respiratory research 15:109.

Oda Y, Hosokawa N, Wada I, Nagata K. 2003. EDEM as an acceptor of terminally misfolded glycoproteins released from calnexin. Science (New York, N.Y.) 299:1394–1397.

Oda Y, Okada T, Yoshida H, Kaufman RJ, Nagata K, Mori K. 2006. Derlin-2 and Derlin-3 are regulated by the mammalian unfolded protein response and are required for ER-associated degradation. The Journal of cell biology 172:383–393.

Oh J, Riek AE, Weng S, Petty M, Kim D, Colonna M, Cella M, Bernal-Mizrachi C. 2012. Endoplasmic reticulum stress controls M2 macrophage differentiation and foam cell formation. The Journal of biological chemistry 287:11629–11641.

Okada K, Minamino T, Tsukamoto Y, Liao Y, Tsukamoto O, Takashima S, Hirata A, Fujita M, Nagamachi Y, Nakatani T, Yutani C, Ozawa K, Ogawa S, Tomoike H, Hori M, Kitakaze M. 2004. Prolonged endoplasmic reticulum stress in hypertrophic and failing heart after aortic constriction: possible contribution of endoplasmic reticulum stress to cardiac myocyte apoptosis. Circulation 110:705–712.

Ono S, Tanaka T, Ishida M, Kinoshita A, Fukuoka J, Takaki M, Sakamoto N, Ishimatsu Y, Kohno S, Hayashi T, Senba

M, Yasunami M, Kubo Y, Yoshida LM, Kubo H, Ariyoshi K, Yoshiura K, Morimoto K. 2011. Surfactant protein C G100S mutation causes familial pulmonary fibrosis in Japanese kindred. The European respiratory journal 38:861–869.

Oyadomari S, Harding HP, Zhang Y, Oyadomari M, Ron D. 2008. Dephosphorylation of translation initiation factor 2alpha enhances glucose tolerance and attenuates hepatosteatosis in mice. Cell metabolism 7:520–532.

Ozcan U, Cao Q, Yilmaz E, Lee A-H, Iwakoshi NN, Ozdelen E, Tuncman G, Görgün C, Glimcher LH, Hotamisligil GS. 2004. Endoplasmic reticulum stress links obesity, insulin action, and type 2 diabetes. Science (New York, N.Y.) 306:457–461.

Pain M, Bermudez O, Lacoste P, Royer P-J, Botturi K, Tissot A, Brouard S, Eickelberg O, Magnan A. 2014. Tissue remodelling in chronic bronchial diseases: from the epithelial to mesenchymal phenotype. European respiratory review : an official journal of the European Respiratory Society 23:118–130.

Pan LH, Yamauchi K, Uzuki M, Nakanishi T, Takigawa M, Inoue H, Sawai T. 2001. Type II alveolar epithelial cells and interstitial fibroblasts express connective tissue growth factor in IPF. The European respiratory journal 17:1220–1227.

Papa FR. 2012. Endoplasmic reticulum stress, pancreatic β-cell degeneration, and diabetes. Cold Spring Harbor perspectives in medicine 2:a007666.

Park SW, Herrema H, Salazar M, Cakir I, Cabi S, Basibuyuk Sahin F, Chiu Y-H, Cantley LC, Ozcan U. 2014. BRD7 regulates XBP1s' activity and glucose homeostasis through its interaction with the regulatory subunits of PI3K. Cell metabolism 20:73–84.

Parker MW, Rossi D, Peterson M, Smith K, Sikström K, White ES, Connett JE, Henke CA, Larsson O, Bitterman PB. 2014. Fibrotic extracellular matrix activates a profibrotic positive feedback loop. The Journal of clinical investigation 124:1622–1635.

Pechkovsky DV, Prasse A, Kollert F, Engel KMY, Dentler J, Luttmann W, Friedrich K, Müller-Quernheim J, Zissel G. 2010. Alternatively activated alveolar macrophages in pulmonary fibrosis-mediator production and intracellular signal transduction. Clinical immunology (Orlando, Fla.) 137:89–101.

Peljto AL, Zhang Y, Fingerlin TE, Ma S-F, Garcia JGN, Richards TJ, Silveira LJ, Lindell KO, Steele MP, Loyd JE, Gibson KF, Seibold MA, Brown KK, Talbert JL, Markin C, Kossen K, Seiwert SD, Murphy E, Noth I, Schwarz MI, Kaminski N, Schwartz DA. 2013. Association between the MUC5B promoter polymorphism and survival in patients with idiopathic pulmonary fibrosis. JAMA 309:2232–2239.

Perl A-K, Zhang L, Whitsett JA. 2009. Conditional expression of genes in the respiratory epithelium in transgenic mice: cautionary notes and toward building a better mouse trap. American journal of respiratory cell and molecular biology 40:1–3.

Phan SH. 2002. The myofibroblast in pulmonary fibrosis. Chest 122:286S-289S.

Phillips AM, Gonzalez LO, Nekongo EE, Ponomarenko AI, McHugh SM, Butty VL, Levine SS, Lin Y-S, Mirny LA, Shoulders MD. 2017. Host proteostasis modulates influenza evolution. eLife 6.

Pobre KFR, Poet GJ, Hendershot LM. 2019. The endoplasmic reticulum (ER) chaperone BiP is a master regulator of ER functions: Getting by with a little help from ERdj friends. The Journal of biological chemistry 294:2098–2108.

Polak SB, van Gool IC, Cohen D, Thüsen JH von der, van Paassen J. 2020. A systematic review of pathological findings in COVID-19: a pathophysiological timeline and possible mechanisms of disease progression. Modern pathology : an official journal of the United States and Canadian Academy of Pathology, Inc 33:2128–2138.

Prischi F, Nowak PR, Carrara M, Ali MMU. 2014. Phosphoregulation of Ire1 RNase splicing activity. Nature communications 5:3554.

Puthalakath H, O'Reilly LA, Gunn P, Lee L, Kelly PN, Huntington ND, Hughes PD, Michalak EM, McKimm-Breschkin J, Motoyama N, Gotoh T, Akira S, Bouillet P, Strasser A. 2007. ER stress triggers apoptosis by activating BH3-only protein Bim. Cell 129:1337–1349.

Qiao J, Zhang M, Bi J, Wang X, Deng G, He G, Luan Z, Lv N, Xu T, Zhao L. 2009. Pulmonary fibrosis induced by H5N1 viral infection in mice. Respiratory research 10:107.

Qing G, Li B, Vu A, Skuli N, Walton ZE, Liu X, Mayes PA, Wise DR, Thompson CB, Maris JM, Hogarty MD, Simon MC. 2012. ATF4 regulates MYC-mediated neuroblastoma cell death upon glutamine deprivation. Cancer cell 22:631–644.

Raghu G, Collard HR, Egan JJ, Martinez FJ, Behr J, Brown KK, Colby TV, Cordier J-F, Flaherty KR, Lasky JA, Lynch DA, Ryu JH, Swigris JJ, Wells AU, Ancochea J, Bouros D, Carvalho C, Costabel U, Ebina M, Hansell DM, Johkoh T, Kim DS, King TE, Kondoh Y, Myers J, Müller NL, Nicholson AG, Richeldi L, Selman M, Dudden RF, Griss BS, Protzko SL, Schünemann HJ. 2011. An official ATS/ERS/JRS/ALAT statement: idiopathic pulmonary fibrosis: evidence-based guidelines for diagnosis and management. American journal of respiratory and critical care medicine 183:788–824.

Rajdev K, Spanel AJ, McMillan S, Lahan S, Boer B, Birge J, Thi M. 2021. Pulmonary Barotrauma in COVID-19 Patients With ARDS on Invasive and Non-Invasive Positive Pressure Ventilation. Journal of intensive care medicine:8850666211019719.

Ramming T, Okumura M, Kanemura S, Baday S, Birk J, Moes S, Spiess M, Jenö P, Bernèche S, Inaba K, Appenzeller-Herzog C. 2015. A PDI-catalyzed thiol-disulfide switch regulates the production of hydrogen peroxide by human Ero1. Free radical biology & medicine 83:361–372.

Rao J, Zhang C, Wang P, Lu L, Qian X, Qin J, Pan X, Li G, Wang X, Zhang F. 2015. C/EBP homologous protein (CHOP) contributes to hepatocyte death via the promotion

of ERO1α signalling in acute liver failure. The Biochemical journal 466:369–378.

Rappolee DA, Mark D, Banda MJ, Werb Z. 1988. Wound macrophages express TGF-alpha and other growth factors in vivo: analysis by mRNA phenotyping. Science (New York, N.Y.) 241:708–712.

Reimold AM, Iwakoshi NN, Manis J, Vallabhajosyula P, Szomolanyi-Tsuda E, Gravallese EM, Friend D, Grusby MJ, Alt F, Glimcher LH. 2001. Plasma cell differentiation requires the transcription factor XBP-1. Nature 412:300–307.

Richeldi L, Costabel U, Selman M, Kim DS, Hansell DM, Nicholson AG, Brown KK, Flaherty KR, Noble PW, Raghu G, Brun M, Gupta A, Juhel N, Klüglich M, Du Bois RM. 2011. Efficacy of a tyrosine kinase inhibitor in idiopathic pulmonary fibrosis. The New England journal of medicine 365:1079–1087.

Richeldi L, Du Bois RM, Raghu G, Azuma A, Brown KK, Costabel U, Cottin V, Flaherty KR, Hansell DM, Inoue Y, Kim DS, Kolb M, Nicholson AG, Noble PW, Selman M, Taniguchi H, Brun M, Le Maulf F, Girard M, Stowasser S, Schlenker-Herceg R, Disse B, Collard HR. 2014. Efficacy and safety of nintedanib in idiopathic pulmonary fibrosis. The New England journal of medicine 370:2071–2082.

Rojas M, Vasconcelos G, Dever TE. 2015. An eIF2α-binding motif in protein phosphatase 1 subunit GADD34 and its viral orthologs is required to promote dephosphorylation of eIF2α. Proceedings of the National Academy of Sciences of the United States of America 112:E3466-75.

Rubenfeld GD, Caldwell E, Peabody E, Weaver J, Martin DP, Neff M, Stern EJ, Hudson LD. 2005. Incidence and outcomes of acute lung injury. The New England journal of medicine 353:1685–1693.

Rueden CT, Schindelin J, Hiner MC, DeZonia BE, Walter AE, Arena ET, Eliceiri KW. 2017. ImageJ2: ImageJ for the next generation of scientific image data.

Ryan AJ, Larson-Casey JL, He C, Murthy S, Carter AB. 2014. Asbestos-induced disruption of calcium homeostasis induces endoplasmic reticulum stress in macrophages. The Journal of biological chemistry 289:33391–33403.

Ryerson CJ, Cottin V, Brown KK, Collard HR. 2015. Acute exacerbation of idiopathic pulmonary fibrosis: shifting the paradigm. The European respiratory journal 46:512–520.

Ryerson CJ, Kolb M, Richeldi L, Lee J, Wachtlin D, Stowasser S, Poletti V. 2019. Effects of nintedanib in patients with idiopathic pulmonary fibrosis by GAP stage. ERJ open research 5.

Sabio G, Cavanagh-Kyros J, Barrett T, Jung DY, Ko HJ, Ong H, Morel C, Mora A, Reilly J, Kim JK, Davis RJ. 2010a. Role of the hypothalamic–pituitary–thyroid axis in metabolic regulation by JNK1. Genes & development 24:256–264.

Sabio G, Kennedy NJ, Cavanagh-Kyros J, Jung DY, Ko HJ, Ong H, Barrett T, Kim JK, Davis RJ. 2010b. Role of muscle c-Jun NH2-terminal kinase 1 in obesity-induced insulin resistance. Molecular and Cellular Biology 30:106–115.

Sakamoto K, Taniguchi H, Kondoh Y, Wakai K, Kimura T, Kataoka K, Hashimoto N, Nishiyama O, Hasegawa Y. 2012. Acute exacerbation of IPF following diagnostic bronchoalveolar lavage procedures. Respiratory medicine 106:436–442.

Sánchez-Elsner T, Botella LM, Velasco B, Corbí A, Attisano L, Bernabéu C. 2001. Synergistic cooperation between hypoxia and transforming growth factor-beta pathways on human vascular endothelial growth factor gene expression. The Journal of biological chemistry 276:38527–38535.

Sawada T, Minamino T, Fu HY, Asai M, Okuda K, Isomura T, Yamazaki S, Asano Y, Okada K, Tsukamoto O, Sanada S, Asanuma H, Asakura M, Takashima S, Kitakaze M, Komuro I. 2010. X-box binding protein 1 regulates brain natriuretic peptide through a novel AP1/CRE-like element in cardiomyocytes. Journal of molecular and cellular cardiology 48:1280–1289.

Scheuner D, Kaufman RJ. 2008. The unfolded protein response: a pathway that links insulin demand with beta-cell failure and diabetes. Endocrine reviews 29:317–333.

Scheuner D, Vander Mierde D, Song B, Flamez D, Creemers JWM, Tsukamoto K, Ribick M, Schuit FC, Kaufman RJ. 2005. Control of mRNA translation preserves endoplasmic reticulum function in beta cells and maintains glucose homeostasis. Nature medicine 11:757–764.

Schmoldt C, Vazquez-Armendariz AI, Shalashova I, Selvakumar B, Bremer CM, Peteranderl C, Wasnick R, Witte B, Gattenlöhner S, Fink L, Vadász I, Morty RE, Pleschka S, Seeger W, Günther A, Herold S. 2019. IRE1

Signaling As a Putative Therapeutic Target in Influenza Virus-induced Pneumonia. American journal of respiratory cell and molecular biology 61:537–540.

Schultz AM, Oroszlan S. 1979. Tunicamycin inhibits glycosylation of precursor polyprotein encoded by env gene of Rauscher murine leukemia virus. Biochemical and biophysical research communications 86:1206–1213.

Scotton CJ, Chambers RC. 2007. Molecular targets in pulmonary fibrosis: the myofibroblast in focus. Chest 132:1311–1321.

Segawa T, Nau ME, Xu LL, Chilukuri RN, Makarem M, Zhang W, Petrovics G, Sesterhenn IA, McLeod DG, Moul JW, Vahey M, Srivastava S. 2002. Androgen-induced expression of endoplasmic reticulum (ER) stress response genes in prostate cancer cells. Oncogene 21:8749–8758.

Sehgal P, Szalai P, Olesen C, Praetorius HA, Nissen P, Christensen SB, Engedal N, Møller JV. 2017. Inhibition of the sarco/endoplasmic reticulum (ER) Ca2+-ATPase by thapsigargin analogs induces cell death via ER Ca2+ depletion and the unfolded protein response. The Journal of biological chemistry 292:19656–19673.

Seibold MA, Wise AL, Speer MC, Steele MP, Brown KK, Loyd JE, Fingerlin TE, Zhang W, Gudmundsson G, Groshong SD, Evans CM, Garantziotis S, Adler KB, Dickey BF, Du Bois RM, Yang IV, Herron A, Kervitsky D, Talbert JL, Markin C, Park J, Crews AL, Slifer SH, Auerbach S, Roy MG, Lin J, Hennessy CE, Schwarz MI, Schwartz DA. 2011. A common MUC5B promoter

polymorphism and pulmonary fibrosis. The New England journal of medicine 364:1503–1512.

Serrano-Mollar A, Nacher M, Gay-Jordi G, Closa D, Xaubet A, Bulbena O. 2007. Intratracheal transplantation of alveolar type II cells reverses bleomycin-induced lung fibrosis. American journal of respiratory and critical care medicine 176:1261–1268.

Sevier CS, Qu H, Heldman N, Gross E, Fass D, Kaiser CA. 2007. Modulation of cellular disulfide-bond formation and the ER redox environment by feedback regulation of Ero1. Cell 129:333–344.

Sha H, He Y, Chen H, Wang C, Zenno A, Shi H, Yang X, Zhang X, Qi L. 2009. The IRE1alpha-XBP1 pathway of the unfolded protein response is required for adipogenesis. Cell metabolism 9:556–564.

Shan B, Wang X, Wu Y, Xu C, Xia Z, Dai J, Shao M, Zhao F, He S, Yang L, Zhang M, Nan F, Li J, Liu J, Liu J, Jia W, Qiu Y, Song B, Han J-DJ, Rui L, Duan S-Z, Liu Y. 2017. The metabolic ER stress sensor IRE1α suppresses alternative activation of macrophages and impairs energy expenditure in obesity. Nature immunology 18:519–529.

Shen J, Chen X, Hendershot L, Prywes R. 2002. ER Stress Regulation of ATF6 Localization by Dissociation of BiP/GRP78 Binding and Unmasking of Golgi Localization Signals. Developmental Cell 3:99–111.

Shen J, Snapp EL, Lippincott-Schwartz J, Prywes R. 2005. Stable binding of ATF6 to BiP in the endoplasmic reticulum stress response. Molecular and Cellular Biology 25:921–932.

Shen Y, Ballar P, Apostolou A, Doong H, Fang S. 2007. ER stress differentially regulates the stabilities of ERAD ubiquitin ligases and their substrates. Biochemical and biophysical research communications 352:919–924.

Shi Y, Vattem KM, Sood R, An J, Liang J, Stramm L, Wek RC. 1998. Identification and characterization of pancreatic eukaryotic initiation factor 2 alpha-subunit kinase, PEK, involved in translational control. Molecular and Cellular Biology 18:7499–7509.

Shimokado K. 1985. A significant part of macrophage-derived growth factor consists of at least two forms of PDGF. Cell 43:277–286.

Shruthi Sethuraman. April 2019. Macrophage and Fibroblast Interaction in the Setting of Idiopathic Pulmonary Fibrosis. Ohio.

Siddiqi S, Saleem U, Abumrad NA, Davidson NO, Storch J, Siddiqi SA, Mansbach CM. 2010. A novel multiprotein complex is required to generate the prechylomicron transport vesicle from intestinal ER. Journal of lipid research 51:1918–1928.

Sisson TH, Mendez M, Choi K, Subbotina N, Courey A, Cunningham A, Dave A, Engelhardt JF, Liu X, White ES, Thannickal VJ, Moore BB, Christensen PJ, Simon RH. 2010. Targeted injury of type II alveolar epithelial cells induces pulmonary fibrosis. American journal of respiratory and critical care medicine 181:254–263.

Solinas G, Vilcu C, Neels JG, Bandyopadhyay GK, Luo J-L, Naugler W, Grivennikov S, Wynshaw-Boris A, Scadeng M, Olefsky JM, Karin M. 2007. JNK1 in hematopoietically

derived cells contributes to diet-induced inflammation and insulin resistance without affecting obesity. Cell metabolism 6:386–397.

Soto-Pantoja DR, Wilson AS, Clear KY, Westwood B, Triozzi PL, Cook KL. 2017. Unfolded protein response signaling impacts macrophage polarity to modulate breast cancer cell clearance and melanoma immune checkpoint therapy responsiveness. Oncotarget 8:80545–80559.

Sowers CR, Wang R, Bourne RA, McGrath BC, Hu J, Bevilacqua SC, Paton JC, Paton AW, Collardeau-Frachon S, Nicolino M, Cavener DR. 2018. The protein kinase PERK/EIF2AK3 regulates proinsulin processing not via protein synthesis but by controlling endoplasmic reticulum chaperones. The Journal of biological chemistry 293:5134–5149.

Sriburi R, Jackowski S, Mori K, Brewer JW. 2004. XBP1: a link between the unfolded protein response, lipid biosynthesis, and biogenesis of the endoplasmic reticulum. The Journal of cell biology 167:35–41.

Starr CR, Pitale PM, Gorbatyuk M. 2018. Translational attenuation and retinal degeneration in mice with an active integrated stress response. Cell death & disease 9:484.

Stauffer WT, Blackwood EA, Azizi K, Kaufman RJ, Glembotski CC. 2020. The ER Unfolded Protein Response Effector, ATF6, Reduces Cardiac Fibrosis and Decreases Activation of Cardiac Fibroblasts. International journal of molecular sciences 21.

Stefan CJ, Manford AG, Baird D, Yamada-Hanff J, Mao Y, Emr SD. 2011. Osh proteins regulate phosphoinositide

metabolism at ER-plasma membrane contact sites. Cell 144:389–401.

Steinvall I, Bak Z, Sjoberg F. 2008. Acute respiratory distress syndrome is as important as inhalation injury for the development of respiratory dysfunction in major burns. Burns : journal of the International Society for Burn Injuries 34:441–451.

Støy J, Edghill EL, Flanagan SE, Ye H, Paz VP, Pluzhnikov A, Below JE, Hayes MG, Cox NJ, Lipkind GM, Lipton RB, Greeley SAW, Patch A-M, Ellard S, Steiner DF, Hattersley AT, Philipson LH, Bell GI. 2007. Insulin gene mutations as a cause of permanent neonatal diabetes. Proceedings of the National Academy of Sciences of the United States of America 104:15040–15044.

Tanaka K, Fujita T, Umezawa H, Namiki K, Yoshioka K, Hagihara M, Sudo T, Kimura S, Tatsumi K, Kasuya Y. 2014. Therapeutic effect of lung mixed culture-derived epithelial cells on lung fibrosis. Laboratory investigation; a journal of technical methods and pathology 94:1247–1259.

Tang X, Yu Q, Wen X, Di Qi, Peng J, He J, Deng W, Zhu T, Zhao Y, Wang D. 2020. Circulating Exosomes From Lipopolysaccharide-Induced Ards Mice Trigger Endoplasmic Reticulum Stress in Lung Tissue. Shock (Augusta, Ga.) 54:110–118.

Tang Y-W, Johnson JE, Browning PJ, Cruz-Gervis RA, Davis A, Graham BS, Brigham KL, Oates JA, Loyd JE, Stecenko AA. 2003. Herpesvirus DNA is consistently detected in lungs of patients with idiopathic pulmonary fibrosis. Journal of clinical microbiology 41:2633–2640.

Taniguchi H, Ebina M, Kondoh Y, Ogura T, Azuma A, Suga M, Taguchi Y, Takahashi H, Nakata K, Sato A, Takeuchi M, Raghu G, Kudoh S, Nukiwa T. 2010. Pirfenidone in idiopathic pulmonary fibrosis. The European respiratory journal 35:821–829.

Tashiro J, Rubio GA, Limper AH, Williams K, Elliot SJ, Ninou I, Aidinis V, Tzouvelekis A, Glassberg MK. 2017. Exploring Animal Models That Resemble Idiopathic Pulmonary Fibrosis. Frontiers in medicine 4:118.

Teng R-J, Jing X, Michalkiewicz T, Afolayan AJ, Wu T-J, Konduri GG. 2017. Attenuation of endoplasmic reticulum stress by caffeine ameliorates hyperoxia-induced lung injury. American journal of physiology. Lung cellular and molecular physiology 312:L586-L598.

Tersey SA, Nishiki Y, Templin AT, Cabrera SM, Stull ND, Colvin SC, Evans-Molina C, Rickus JL, Maier B, Mirmira RG. 2012. Islet β-cell endoplasmic reticulum stress precedes the onset of type 1 diabetes in the nonobese diabetic mouse model. Diabetes 61:818–827.

Thamsen M, Ghosh R, Auyeung VC, Brumwell A, Chapman HA, Backes BJ, Perara G, Maly DJ, Sheppard D, Papa FR. 2019. Small molecule inhibition of IRE1α kinase/RNase has anti-fibrotic effects in the lung. PloS one 14:e0209824.

Thomas AQ, Lane K, Phillips J, Prince M, Markin C, Speer M, Schwartz DA, Gaddipati R, Marney A, Johnson J, Roberts R, Haines J, Stahlman M, Loyd JE. 2002. Heterozygosity for a surfactant protein C gene mutation associated with usual interstitial pneumonitis and cellular nonspecific interstitial pneumonitis in one kindred.

American journal of respiratory and critical care medicine 165:1322–1328.

Thuerauf DJ, Marcinko M, Belmont PJ, Glembotski CC. 2007. Effects of the isoform-specific characteristics of ATF6 alpha and ATF6 beta on endoplasmic reticulum stress response gene expression and cell viability. The Journal of biological chemistry 282:22865–22878.

Tian X, Zhang J, Tan TK, Lyons JG, Zhao H, Niu B, Lee SR, Tsatralis T, Zhao Y, Wang Y, Cao Q, Wang C, Wang Y, Lee VWS, Kahn M, Zheng G, Harris DCH. 2013. Association of β-catenin with P-Smad3 but not LEF-1 dissociates in vitro profibrotic from anti-inflammatory effects of TGF-β1. Journal of cell science 126:67–76.

Tirasophon W, Welihinda AA, Kaufman RJ. 1998. A stress response pathway from the endoplasmic reticulum to the nucleus requires a novel bifunctional protein kinase/endoribonuclease (Ire1p) in mammalian cells. Genes & development 12:1812–1824.

Tiringer K, Treis A, Fucik P, Gona M, Gruber S, Renner S, Dehlink E, Nachbaur E, Horak F, Jaksch P, Döring G, Crameri R, Jung A, Rochat MK, Hörmann M, Spittler A, Klepetko W, Akdis CA, Szépfalusi Z, Frischer T, Eiwegger T. 2013. A Th17- and Th2-skewed cytokine profile in cystic fibrosis lungs represents a potential risk factor for Pseudomonas aeruginosa infection. American journal of respiratory and critical care medicine 187:621–629.

Tiringer K, Treis A, Kanolzer S, Witt C, Ghanim B, Gruber S, Schmidthaler K, Renner S, Dehlink E, Nachbaur E, Frischer T, Klepetko W, Akdis CA, Szépfalusi Z, Eiwegger

T. 2014. Differential expression of IL-33 and HMGB1 in the lungs of stable cystic fibrosis patients. The European respiratory journal 44:802–805.

Todd DJ, McHeyzer-Williams LJ, Kowal C, Lee A-H, Volpe BT, Diamond B, McHeyzer-Williams MG, Glimcher LH. 2009. XBP1 governs late events in plasma cell differentiation and is not required for antigen-specific memory B cell development. The Journal of experimental medicine 206:2151–2159.

Tong X, Li M, Liu N, Huang W, Xue X, Fu J. 2021. Hyperoxia induces endoplasmic reticulum stress-associated apoptosis via the IRE1α pathway in rats with bronchopulmonary dysplasia. Molecular medicine reports 23.

Travers KJ, Patil CK, Wodicka L, Lockhart DJ, Weissman JS, Walter P. 2000. Functional and Genomic Analyses Reveal an Essential Coordination between the Unfolded Protein Response and ER-Associated Degradation. Cell 101:249–258.

Trusina A, Tang C. 2010. The unfolded protein response and translation attenuation: a modelling approach. Diabetes, obesity & metabolism 12 Suppl 2:27–31.

Tsuru A, Imai Y, Saito M, Kohno K. 2016. Novel mechanism of enhancing IRE1α-XBP1 signalling via the PERK-ATF4 pathway. Scientific reports 6:24217.

Uhal BD, Joshi I, True AL, Mundle S, Raza A, Pardo A, Selman M. 1995. Fibroblasts isolated after fibrotic lung injury induce apoptosis of alveolar epithelial cells in vitro. The American journal of physiology 269:L819-28.

Umeda Y, Morikawa M, Anzai M, Sumida Y, Kadowaki M, Ameshima S, Ishizaki T. 2010. Acute exacerbation of idiopathic pulmonary fibrosis after pandemic influenza A (H1N1) vaccination. Internal medicine (Tokyo, Japan) 49:2333–2336.

Urano F, Wang X, Bertolotti A, Zhang Y, Chung P, Harding HP, Ron D. 2000. Coupling of stress in the ER to activation of JNK protein kinases by transmembrane protein kinase IRE1. Science (New York, N.Y.) 287:664–666.

Ushiki A, Yamazaki Y, Hama M, Yasuo M, Hanaoka M, Kubo K. 2014. Viral infections in patients with an acute exacerbation of idiopathic interstitial pneumonia. Respiratory investigation 52:65–70.

Vallée A, Lecarpentier Y, Guillevin R, Vallée J-N. 2017. Interactions between TGF-β1, canonical WNT/β-catenin pathway and PPAR γ in radiation-induced fibrosis. Oncotarget 8:90579–90604.

Vattem KM, Wek RC. 2004. Reinitiation involving upstream ORFs regulates ATF4 mRNA translation in mammalian cells. Proceedings of the National Academy of Sciences of the United States of America 101:11269–11274.

Vaughan AE, Brumwell AN, Xi Y, Gotts JE, Brownfield DG, Treutlein B, Tan K, Tan V, Liu FC, Looney MR, Matthay MA, Rock JR, Chapman HA. 2015. Lineage-negative progenitors mobilize to regenerate lung epithelium after major injury. Nature 517:621–625.

Vekich JA, Belmont PJ, Thuerauf DJ, Glembotski CC. 2012. Protein disulfide isomerase-associated 6 is an ATF6-inducible ER stress response protein that protects cardiac

myocytes from ischemia/reperfusion-mediated cell death. Journal of molecular and cellular cardiology 53:259–267.

Venosa A, Malaviya R, Choi H, Gow AJ, Laskin JD, Laskin DL. 2016. Characterization of Distinct Macrophage Subpopulations during Nitrogen Mustard-Induced Lung Injury and Fibrosis. American journal of respiratory cell and molecular biology 54:436–446.

Vernia S, Cavanagh-Kyros J, Garcia-Haro L, Sabio G, Barrett T, Jung DY, Kim JK, Xu J, Shulha HP, Garber M, Gao G, Davis RJ. 2014. The PPARα - FGF21 hormone axis contributes to metabolic regulation by the hepatic JNK signaling pathway. Cell metabolism 20:512–525.

Vitadello M, Penzo D, Petronilli V, Michieli G, Gomirato S, Menabò R, Di Lisa F, Gorza L. 2003. Overexpression of the stress protein Grp94 reduces cardiomyocyte necrosis due to calcium overload and simulated ischemia. FASEB journal : official publication of the Federation of American Societies for Experimental Biology 17:923–925.

Walters DM, Kleeberger SR. 2008. Mouse models of bleomycin-induced pulmonary fibrosis. Current protocols in pharmacology Chapter 5:Unit 5.46.

Wang J, Kang R, Huang H, Xi X, Wang B, Wang J, Zhao Z. 2014a. Hepatitis C virus core protein activates autophagy through EIF2AK3 and ATF6 UPR pathway-mediated MAP1LC3B and ATG12 expression. Autophagy 10:766–784.

Wang S, Chen Z, Lam V, Han J, Hassler J, Finck BN, Davidson NO, Kaufman RJ. 2012. IRE1α-XBP1s induces PDI expression to increase MTP activity for hepatic VLDL

assembly and lipid homeostasis. Cell metabolism 16:473–486.

Wang X, Herr RA, Chua W-J, Lybarger L, Wiertz EJHJ, Hansen TH. 2007. Ubiquitination of serine, threonine, or lysine residues on the cytoplasmic tail can induce ERAD of MHC-I by viral E3 ligase mK3. The Journal of cell biology 177:613–624.

Wang X, Karamariti E, Simpson R, Wang W, Xu Q. 2015a. Dickkopf Homolog 3 Induces Stem Cell Differentiation into Smooth Muscle Lineage via ATF6 Signalling. The Journal of biological chemistry 290:19844–19852.

Wang X, Ye Y, Lencer W, Hansen TH. 2006. The viral E3 ubiquitin ligase mK3 uses the Derlin/p97 endoplasmic reticulum-associated degradation pathway to mediate down-regulation of major histocompatibility complex class I proteins. The Journal of biological chemistry 281:8636–8644.

Wang X-C, Sun W-T, Yu C-M, Pun S-H, Underwood MJ, He G-W, Yang Q. 2015b. ER stress mediates homocysteine-induced endothelial dysfunction: Modulation of IKCa and SKCa channels. Atherosclerosis 242:191–198.

Wang ZV, Deng Y, Gao N, Pedrozo Z, Li DL, Morales CR, Criollo A, Luo X, Tan W, Jiang N, Lehrman MA, Rothermel BA, Lee A-H, Lavandero S, Mammen PPA, Ferdous A, Gillette TG, Scherer PE, Hill JA. 2014b. Spliced X-box binding protein 1 couples the unfolded protein response to hexosamine biosynthetic pathway. Cell 156:1179–1192.

Weng D, Chen X-Q, Qiu H, Zhang Y, Li Q-H, Zhao M-M, Wu Q, Chen T, Hu Y, Wang L-S, Wei Y-R, Du Y-K, Chen S-S, Zhou Y, Zhang F, Shen L, Su Y-L, Kolb M, Li H-P. 2019. The Role of Infection in Acute Exacerbation of Idiopathic Pulmonary Fibrosis. Mediators of inflammation 2019:5160694.

Wootton SC, Kim DS, Kondoh Y, Chen E, Lee JS, Song JW, Huh JW, Taniguchi H, Chiu C, Boushey H, Lancaster LH, Wolters PJ, DeRisi J, Ganem D, Collard HR. 2011. Viral infection in acute exacerbation of idiopathic pulmonary fibrosis. American journal of respiratory and critical care medicine 183:1698–1702.

Wynn TA, Vannella KM. 2016. Macrophages in Tissue Repair, Regeneration, and Fibrosis. Immunity 44:450–462.

Xiao G, Zhang T, Yu S, Lee S, Calabuig-Navarro V, Yamauchi J, Ringquist S, Dong HH. 2013. ATF4 protein deficiency protects against high fructose-induced hypertriglyceridemia in mice. The Journal of biological chemistry 288:25350–25361.

Xiong Z, Jiang R, Zhang P, Han X, Guo F-J. 2015. Transmission of ER stress response by ATF6 promotes endochondral bone growth. Journal of orthopaedic surgery and research 10:141.

Xu L, Cui W-H, Zhou W-C, Li D-L, Li L-C, Zhao P, Mo X-T, Zhang Z, Gao J. 2017. Activation of Wnt/β-catenin signalling is required for TGF-β/Smad2/3 signalling during myofibroblast proliferation. Journal of cellular and molecular medicine 21:1545–1554.

Yamaguchi H, Wang H-G. 2004. CHOP is involved in endoplasmic reticulum stress-induced apoptosis by enhancing DR5 expression in human carcinoma cells. The Journal of biological chemistry 279:45495–45502.

Yamamoto K, Sato T, Matsui T, Sato M, Okada T, Yoshida H, Harada A, Mori K. 2007. Transcriptional induction of mammalian ER quality control proteins is mediated by single or combined action of ATF6alpha and XBP1. Developmental Cell 13:365–376.

Yamamoto K, Yoshida H, Kokame K, Kaufman RJ, Mori K. 2004. Differential contributions of ATF6 and XBP1 to the activation of endoplasmic reticulum stress-responsive cis-acting elements ERSE, UPRE and ERSE-II. Journal of biochemistry 136:343–350.

Yanagitani K, Kimata Y, Kadokura H, Kohno K. 2011. Translational pausing ensures membrane targeting and cytoplasmic splicing of XBP1u mRNA. Science (New York, N.Y.) 331:586–589.

Yang F, Liu Y, Ren H, Zhou G, Yuan X, Shi X. 2019. ER-stress regulates macrophage polarization through pancreatic EIF-2alpha kinase. Cellular immunology 336:40–47.

Yang J, Wheeler SE, Velikoff M, Kleaveland KR, LaFemina MJ, Frank JA, Chapman HA, Christensen PJ, Kim KK. 2013. Activated alveolar epithelial cells initiate fibrosis through secretion of mesenchymal proteins. The American Journal of Pathology 183:1559–1570.

Yao Y, Wang Y, Zhang Z, He L, Zhu J, Zhang M, He X, Cheng Z, Ao Q, Cao Y, Yang P, Su Y, Zhao J, Zhang S,

Yu Q, Ning Q, Xiang X, Xiong W, Wang C-Y, Xu Y. 2016. Chop Deficiency Protects Mice Against Bleomycin-induced Pulmonary Fibrosis by Attenuating M2 Macrophage Production. Molecular therapy : the journal of the American Society of Gene Therapy 24:915–925.

Yen C-LE, Stone SJ, Koliwad S, Harris C, Farese RV. 2008. Thematic review series: glycerolipids. DGAT enzymes and triacylglycerol biosynthesis. Journal of lipid research 49:2283–2301.

Yoo J, Ghiassi M, Jirmanova L, Balliet AG, Hoffman B, Fornace AJ, Liebermann DA, Bottinger EP, Roberts AB. 2003. Transforming growth factor-beta-induced apoptosis is mediated by Smad-dependent expression of GADD45b through p38 activation. The Journal of biological chemistry 278:43001–43007.

Yoshida H, Haze K, Yanagi H, Yura T, Mori K. 1998. Identification of the cis-acting endoplasmic reticulum stress response element responsible for transcriptional induction of mammalian glucose-regulated proteins. Involvement of basic leucine zipper transcription factors. The Journal of biological chemistry 273:33741–33749.

Yoshida H, Matsui T, Yamamoto A, Okada T, Mori K. 2001. XBP1 mRNA Is Induced by ATF6 and Spliced by IRE1 in Response to ER Stress to Produce a Highly Active Transcription Factor. Cell 107:881–891.

Yoshida H, Oku M, Suzuki M, Mori K. 2006. pXBP1(U) encoded in XBP1 pre-mRNA negatively regulates unfolded protein response activator pXBP1(S) in mammalian ER stress response. The Journal of cell biology 172:565–575.

Yoshida H, Uemura A, Mori K. 2009. pXBP1(U), a negative regulator of the unfolded protein response activator pXBP1(S), targets ATF6 but not ATF4 in proteasome-mediated degradation. Cell structure and function 34:1–10.

Young LR, Nogee LM, Barnett B, Panos RJ, Colby TV, Deutsch GH. 2008. Usual interstitial pneumonia in an adolescent with ABCA3 mutations. Chest 134:192–195.

Zalckvar E, Berissi H, Mizrachy L, Idelchuk Y, Koren I, Eisenstein M, Sabanay H, Pinkas-Kramarski R, Kimchi A. 2009. DAP-kinase-mediated phosphorylation on the BH3 domain of beclin 1 promotes dissociation of beclin 1 from Bcl-XL and induction of autophagy. EMBO reports 10:285–292.

Zeeshan HMA, Lee GH, Kim H-R, Chae H-J. 2016. Endoplasmic Reticulum Stress and Associated ROS. International journal of molecular sciences 17:327.

Zeng L, Lu M, Mori K, Luo S, Lee AS, Zhu Y, Shyy JY-J. 2004. ATF6 modulates SREBP2-mediated lipogenesis. The EMBO journal 23:950–958.

Zeng L, Zampetaki A, Margariti A, Pepe AE, Alam S, Martin D, Xiao Q, Wang W, Jin Z-G, Cockerill G, Mori K, Li Y-SJ, Hu Y, Chien S, Xu Q. 2009. Sustained activation of XBP1 splicing leads to endothelial apoptosis and atherosclerosis development in response to disturbed flow. Proceedings of the National Academy of Sciences of the United States of America 106:8326–8331.

Zeng M, Sang W, Chen S, Chen R, Zhang H, Xue F, Li Z, Liu Y, Gong Y, Zhang H, Kong X. 2017. 4-PBA inhibits LPS-induced inflammation through regulating ER stress

and autophagy in acute lung injury models. Toxicology letters 271:26–37.

Zhang A, Lacy-Hulbert A, Anderton S, Haslett C, Savill J. 2020. Apoptotic Cell-Directed Resolution of Lung Inflammation Requires Myeloid αv Integrin-Mediated Induction of Regulatory T Lymphocytes. The American Journal of Pathology 190:1224–1235.

Zhang K, Rekhter MD, Gordon D, Phan SH. 1994. Myofibroblasts and their role in lung collagen gene expression during pulmonary fibrosis. A combined immunohistochemical and in situ hybridization study. The American Journal of Pathology 145:114–125.

Zhao Y, Jiang Y, Chen L, Zheng X, Zhu J, Song X, Shi J, Li Y, He W. 2020. Inhibition of the endoplasmic reticulum (ER) stress-associated IRE-1/XBP-1 pathway alleviates acute lung injury via modulation of macrophage activation. Journal of Thoracic Disease 12:284–295.

Zheng Y-Z, Cao Z-G, Hu X, Shao Z-M. 2014. The endoplasmic reticulum stress markers GRP78 and CHOP predict disease-free survival and responsiveness to chemotherapy in breast cancer. Breast cancer research and treatment 145:349–358.

Zhou Q, Ye X, Sun R, Matsumoto Y, Moriyama M, Asano Y, Ajioka Y, Saijo Y. 2014. Differentiation of mouse induced pluripotent stem cells into alveolar epithelial cells in vitro for use in vivo. Stem cells translational medicine 3:675–685.

Zhou Y, Lee J, Reno CM, Sun C, Park SW, Chung J, Lee J, Fisher SJ, White MF, Biddinger SB, Ozcan U. 2011.

Regulation of glucose homeostasis through a XBP-1-FoxO1 interaction. Nature medicine 17:356–365.

Zou J-N, Sun L, Wang B-R, Zou Y, Xu S, Ding Y-J, Shen L-J, Huang W-C, Jiang X-J, Chen S-M. 2021. The characteristics and evolution of pulmonary fibrosis in COVID-19 patients as assessed by AI-assisted chest HRCT. PloS one 16:e0248957.

Zuo W, Zhang T, Wu DZ, Guan SP, Liew A-A, Yamamoto Y, Wang X, Lim SJ, Vincent M, Lessard M, Crum CP, Xian W, McKeon F. 2015. p63(+)Krt5(+) distal airway stem cells are essential for lung regeneration. Nature 517:616–620.

9. Erklärung

„Ich erkläre: Ich habe die vorgelegte Dissertation selbstständig, ohne unerlaubte fremde Hilfe und nur mit den Hilfen angefertigt, die ich in der Dissertation angegeben habe. Alle Textstellen, die ich wörtlich oder sinngemäß aus veröffentlichten oder nicht veröffentlichten Schriften entnommen sind, und alle Angaben, die auf mündlichen Auskünften beruhen, sind als solche kenntlich gemacht. Bei den von mir durchgeführten und in der Dissertation erwähnten Untersuchungen habe ich die Grundsätze guter wissenschaftlicher Praxis wie sie in der „Satzung der Justus-Liebig-Universität Gießen zur Sicherung guter wissenschaftlicher Praxis“ niedergelegt sind, eingehalten.“

_____ _____

Datum Irina Shalashova

10.Acknowledgments

I would love to express my appreciation to all those who gave me the opportunity to make and complete my doctoral work.

First and foremost, I would like to express my gratitude to my supervisor, Prof. Dr. Andreas Günther, for the opportunity to make my doctoral dissertation in his laboratory and for providing scientific guidance and invaluable advice. In addition, I would like to gratitude all of the lab members, Dr. K. Piskulak, who got me started on the project, Dr. C. Ruppert, Dr. P. Mahavadi, Silke Händel, and Simone Becker for sharing their expertise. Special thanks to Dr. Martina Korfei, with whom we shared a laboratory room and had many scientific and not only conversations. Also, I want to thank Nicolai Smidt for making the laboratory routine more fun.

I must also acknowledge Prof. Dr. Werner Seeger, Prof. Dr. Rory Morty, and Prof. Dr. Elie El Agha for accepting me into the Molecular Biology and Medicine of the Lung program and providing excellent training that helped me to become a professional in my field. Also, I would like to thank my MBML classmates for the beautiful moments we shared and for cheering each other through the challenging times.

Acknowledgments

I am deeply grateful to Prof. Dr. Saverio Bellusci, Prof. Dr. Susanne Herold, and the members of their laboratories for an amazing opportunity to collaborate and learn from their robust expertise. It was a great experience that resulted in several valuable articles in peer reviewed journals.

Also, I want to thank my friends and family for their support and for being a great company during all my doctoral research time.

Finally, I want to thank three people without whom I could not have made it and who supported and believed in me the most. My mother, Anna Timofeeva, thank you for raising me as a person who bring what she started to the end, no matter what. Thanks to one of my best friends, Niko Schweifel, for being my rock all this time. And thanks to one of my dearest friends, the best colleague, and a mentor, Roxana Wasnick, for teaching and inspiring me to be a good researcher, sharing all your knowledge, and making me see myself as a worthy scientist. It was a long journey. Thank you all for always being by my side. To you, I dedicate my thesis.